SAPIENZA
UNIVERSITÀ DI ROMA

Enhanced Electromagnetic Wave Propagation in Lossy Media

Department of Information Engineering, Electronics and Telecommunications (DIET)

Ph.D. in Mathematical Models for Engineering, Electromagnetics and Nanosciences – XXIX Ciclo

Candidato

Patrizio Simeoni

Matricola 781595

Relatore

Prof. Fabrizio Frezza

Correlatore

Dr. Nicola Tedeschi

Coordinatore del corso di Dottorato
Prof. Daniele Andreucci

To my daughter Mya

Sommario

La profondità di penetrazione di onde elettromagnetiche in mezzi con perdita è un parametro fondamentale in molte applicazioni: dall'interazione con tessuti biologici, al GeoRadar (GPR), dalla comunicazione con mezzi sottomarini, all'analisi dei materiali. Questa dissertazione propone un metodo per raggiungere penetrazione profonda in mezzi con perdite attraverso l'uso di una particolare categoria di onde elettromagnetiche, dette inomogenee o non-uniformi. In particolare, viene studiato il comportamento di onde non omogenee all'interfaccia tra due mezzi, il primo, in cui è presente l'onda incidente, privo di perdite, e il secondo, in cui è presente l'onda trasmessa, con perdite. Le "consuete" onde elettromagnetiche omogenee, in questa situazione, provocano un'onda trasmessa che si attenua esponenzialmente nella direzione normale all'interfaccia tra i due mezzi, minimizzando la penetrazione. Al contrario, onde non omogenee possono provocare onde trasmesse che attenuano esponenzialmente, ma in direzioni diverse da quella normale all'interfaccia tra i due mezzi, per esempio tale direzione può essere parallela all'interfaccia con il mezzo con perdite oppure, il vettore di attenuazione può addirittura presentare un angolo superiore ai novanta gradi con la normale a tale superficie di separazione, risultando in un'amplificazione del segnale piuttosto che attenuazione nel mezzo con perdite. La tesi introduce dapprima i concetti di base riguardanti onde piane omogenee e inomogenee, fondamentali alla comprensione dello studio presentato in questa dissertazione, segue poi la trattazione delle soluzioni fisicamente accettabili per le onde inomogenee ed in particolare delle onde leaky, di conseguenza vengono introdotte le antenne leaky, che sono quelle strutture in grado di generare onde leaky. Quindi vengono illustrati i precedenti studi teorici, basati sullo studio di onde piane non uniformi. A questa fase introduttiva segue lo studio analitico effettuato in questa tesi, concernente i requisiti necessari per ottenere penetrazione profonda attraverso onde piane non omogenee; tale studio si pone a completamento degli studi precedenti. Le onde piane, non fisiche, vengono poi abbandonate per effettuare la verifica

della possibilità di ottenere penetrazione profonda, almeno in una limitata regione spaziale, con strutture realistiche: è pertanto progettata, e simulata attraverso un tool elettromagnetico commerciale (CST), un'antenna leaky con lo scopo di confrontare le caratteristiche di penetrazione ottenibile attraverso la radiazione generata dalla suddetta antenna con quello ottenibile da antenne altamente direttive comunemente utilizzate (antenne horn per esempio). La caratteristica di penetrazione profonda della radiazione generata da antenne leaky viene dimostrata, e i limiti di applicabilità vengono illustrati. Nella fase finale di questa tesi si descrive l'attuale ricerca, volta alla ricerca di strutture alternative per la generazione di onde leaky, e specificamente quella costituita dal prisma con perdite*. Si annunciano infine sviluppi futuri nella ricerca di penetrazione in mezzi con perdite.*

Introduzione ai risultati principali della ricerca

Introduzione

In questo capitolo, redatto in lingua italiana, si vuole fornire uno stringato riassunto degli argomenti affrontati nella dissertazione, introducendo i concetti generali relativi alla ricerca effettuata e i principali risultati ottenuti, la trattazione completa del fenomeno della penetrazione profonda, così come pure tutti i passaggi analitici o i diversi aspetti riscontrati durante la simulazione sono al di là dello scopo di questo capitolo, si rimanda pertanto il lettore al testo integrale della tesi, nella quale gli argomenti sono affrontati più dettagliatamente e più risultati sono riportati.

Questo capitolo, che non vuole essere esaustivo, è scritto con in mente il raggiungimento di due obiettivi: da una parte intende fornire un contesto alla dissertazione e, dall'altra, intende aiutare il lettore nell' individuazione dei contenuti innovativi che rappresentano il valore aggiunto che questa tesi porta all'indagine della penetrazione nei mezzi con perdite.

La prima parte di questo capitolo è dedicata ai concetti fondamentali che riguardano onde omogenee e onde non omogenee, segue poi una presentazione dei risultati teorico-analitico e infine di tipo numerico, dove simulazioni verranno presentate per mostrare potenzialità e limiti del metodo adottato.

Contesto teorico di riferimento

Le due equazioni di Maxwell con il rotore, descritte di seguito per un mezzo omogeneo, isotropo, non dispersivo nello spazio e nel tempo e generalmente dissipativo, sono differenziali del primo ordine accoppiate:

$$\begin{cases} \nabla \times \underline{E} = -\underline{J}_{mi} - j\omega\mu\underline{H} \\ \nabla \times \underline{H} = \underline{J}_i + (\sigma + j\omega\varepsilon)\,\underline{E} \end{cases} \tag{1}$$

dove $\underline{H}$ rappresenta il campo magnetico, $\underline{E}$ il campo elettrico, $\underline{J}_{mi}$ e $\underline{J}_i$ densità di correnti magnetiche ed elettriche impresse, μ la permeabilità magnetica, ε la costante dielettrica assoluta, e, infine, σ e conducibilità elettrica.

Spesso, piuttosto che utilizzare tale sistema di equazioni si preferisce lavorare con una equazione differenziale del secondo ordine ma in una sola variabile, $\underline{E}$ o $\underline{H}$, tale equazione prende il nome di equazione di Helmotz, che nel caso omogeneo (assenza di grandezze impresse) prende la forma:

$$\nabla^2\underline{E} + k^2\underline{E} = 0; \tag{2}$$

k è detto numero d'onda, e, introducendo la costante dielettrica complessa $\varepsilon_c = \varepsilon - j\sigma/\omega$, si può scrivere $k = \omega\sqrt{\mu\varepsilon_c}$ [1].

L'onda piana:

$$\underline{E} = \underline{E}_0 e^{-j\underline{k}\cdot\underline{r}}\ , \tag{3}$$

è soluzione dell'equazione di Helmotz omogenea ed è anche soluzione delle equazioni di Maxwell se $\underline{k}\cdot\underline{E} = 0$, dove la quantità complessa $\underline{k}$, è detto vettore d'onda, ed è esprimibile come differenza complessa di due vettori reali:

$$\underline{k} = \underline{\beta} - j\underline{\alpha} \tag{4}$$

$\underline{\beta}$ è detto vettore di fase, e $\underline{\alpha}$ è detto, invece, vettore di attenuazione.

Un'onda piana si dice omogenea se $\underline{\beta}$ e $\underline{\alpha}$ sono paralleli o se $\underline{\alpha} = 0$, negli altri casi si parla di onda non omogenea.

In un mezzo con perdite, $\underline{\beta}$ e $\underline{\alpha}$ formano un angolo θ strettamente minore di 90^o e il vettore di attenuazione deve esistere mandatoriamente, la soluzione omogenea è data pertanto da $\underline{\alpha}//\underline{\beta}$. In un mezzo senza perdite, due soluzioni sono possibili, una soluzione omogenea data da $\alpha = |\underline{\alpha}| = 0$ e una soluzione inomogenea individuata da $\underline{\alpha} \perp \underline{\beta}$.

Una proprietà fondamentale dei campi elettromagnetici è la conservazione della componente tangenziale del campo elettrico e magnetico all'interfaccia planare tra due mezzi, tale proprietà è verificata per tutti i mezzi realistici, caratterizzati cioè da conduttività finita. Da detta proprietà discende chiaramente che un'onda omogenea proveniente da un mezzo senza perdite provoca un'onda in un mezzo con perdite in cui l'attenuazione è esponenziale e normale all'interfaccia di separazione, rendendo minima la penetrazione, mentre, se l'onda incidente è inomogenea, esiste un vettore di attenuazione nel mezzo senza perdite la cui componente tangenziale all'interfaccia di separazione deve necessariamente conservarsi, ne segue che l'attenuazione non può mai essere diretta normalmente alla superficie di separazione.

La parte teorica di questa tesi si basa sullo sfruttamento di tale proprietà per verificare condizioni e caratteristiche della penetrazione che rendono possibile un vettore di attenuazione al limite parallelo alla superficie con perdite.

Un prima importante analisi sull'argomento è dovuto a Holmes [2] che studiò il caso dell'incidenza di un'onda piana omogenea su una superficie piana di separazione tra due mezzi con perdite trovando espressioni per l'ampiezza di vettore di fase e di attenuazione per l'onda trasmessa.

Radcliff [3] estese lo studio di Holmes considerando un'onda incidente qualsiasi, tuttavia egli fece uso delle espressioni intrinseche delle costanti di attenuazione [4] e di fase invece che le ampiezze dei rispettivi vettori, pertanto la sua soluzione risulta valida solo in approssimazione di angoli piccoli formati da vettore di fase e di attenuazione dell'onda incidente.

Roy, in [5], corresse la soluzione di Radcliff studiando il caso più generale di incidenza di un'onda piana tra due mezzi omogenei e dissipativi. Tuttavia,

la soluzione fece uso di formule per α e β valide solo per mezzi con perdita. In particolare, Roy, per trovare le soluzioni al proprio problema, fece uso di un metodo numerico di ricerca di radici. Detti $\underline{\beta}_2$ e $\underline{\alpha}_2$ i vettori di fase e di attenuazione nel mezzo con perdite ed indicati rispettivamente con ξ_2 e ζ_2 gli angoli che questi formano con la normale alla superficie di separazione, Roy fu il primo a notare la possibilità di avere un'onda trasmessa tale che $\zeta_2 > 90^o$ oppure $\xi_2 > 90^o$. Roy non indicò tuttavia le conseguenze in termini di penetrazione profonda dovute alla condizione $\zeta_2 \geq 90^o$.

Infine Frezza-Tedeschi in [6] approcciarono il problema in modo completamente analitico trovando una condizione valida per l'onda inomogenea proveniente da un mezzo senza perdite e incidente sull'interfaccia piana infinita di separazione con un mezzo con perdite, trovando una soluzione tale che $\zeta_2 = 90^o$.

La parte teorica di questa dissertazione consiste nell'estensione e completamento dei risultati dimostrati in [6].

Penetrazione profonda attraverso onde piane

Consideriamo la figura 1 in cui un'onda piana inomogenea proviene da un mezzo senza perdite, che indichiamo come mezzo 1, e incide sull'interfaccia piana di separazione, assunta infinita, con un mezzo con perdite, che indichiamo come mezzo 2, entrambi i mezzi sono omogenei, isotropi e non magnetici. L'onda incidente è caratterizzata da un vettore di fase $\underline{\beta}_1$ che forma un angolo ξ_1 con la normale all'interfaccia e da un vettore di attenuazione $\underline{\alpha}_1$ che forma un angolo ζ_1 con la normale all'interfaccia. L'onda trasmessa possiede un vettore di fase $\underline{\beta}_2$ e $\underline{\alpha}_2$ che formano angoli ξ_2 e ζ_2, rispettivamente, con la normale alla superficie di separazione.

In [7] viene trovato che l'angolo ξ_1 che permette $\zeta_2 = 90^o$ è soluzione della seguente equazione:

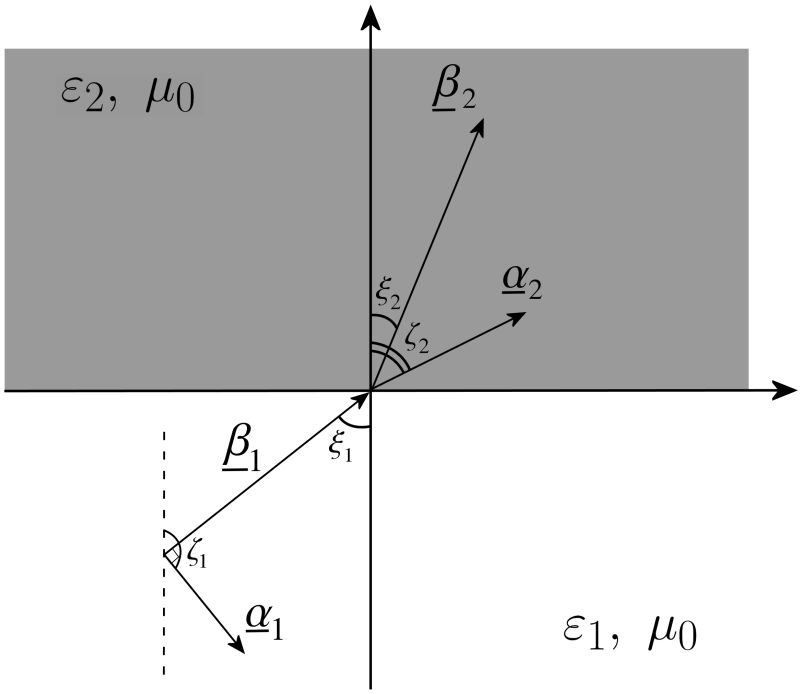

Figura 1. Geometria del problema: onda non omogenea incidente sull'interfaccia piana di separazione tra un mezzo senza perdite ed uno con perdite.

$$\beta_1 \alpha_1 \sin(2\xi_1) = \mathrm{Im}(k_2^2) \tag{5}$$

dove β_1 e α_1 rappresentano le ampiezze di $\underline{\beta}_1$ e $\underline{\alpha}_1$, rispettivamente. La soluzione individuata è:

$$\xi_1 = \frac{1}{2} \arcsin \left[\frac{\mathrm{Im}(k_2^2)}{\beta_1 \alpha_1} \right] \tag{6}$$

di conseguenza il minimo β_1 che permette penetrazione profonda è dato da β_{1c} è:

$$\beta_{1c} = \frac{k_1}{\sqrt{2}} \sqrt{1 + \sqrt{1 + \left[\frac{2\ \mathrm{Im}\,(k_2^2)}{k_1^2} \right]^2}}, \tag{7}$$

Nel corso di questa dissertazione viene dapprima notato che Eq. (6) rappresenta solo una delle possibili soluzioni per $\xi_1 \in \left[0, \frac{\pi}{2}\right]$, essendo invece l'insieme completo costituito da:

$$\xi_{c1} = \frac{1}{2}\gamma \tag{8}$$

$$\xi_{c2} = \frac{\pi}{2} - \frac{1}{2}\gamma \tag{9}$$

dove $\gamma = \arcsin\left[\mathrm{Im}(k_2^2)/(\beta_1\alpha_1)\right]$. Viene mostrato inoltre che anche il caso $\xi_2 = 0$ è una valida soluzione per entrambe le equazioni (8)-(9), che pertanto risultano soluzione di due problemi ben diversi: quella di attenuazione, caratterizzata da $\zeta_2 = 0$ e quella di fase, in cui $\xi_2 = 0$.

Il primo risultato teorico di questa tesi consiste nell'individuazione e differenziazione delle due soluzioni. Viene dimostrato che le soluzioni dipendono dalla quantità Ψ definita come segue:

$$\Psi = \frac{k_1^2}{\beta_1^2 + \alpha_1^2}\left(2\frac{\varepsilon_2'}{\varepsilon_1} - 1\right). \tag{10}$$

La soluzione ξ_{c1} risulta di fase quando $\cos\gamma \leq -\Psi$, altrimenti è di attenuazione. La soluzione ξ_{c2} è di fase se $\cos\gamma \geq \Psi$, altrimeti è di attenuazione, ovvero, essendo $\gamma \in [0; \pi/2]$:

$$\Psi < -1 \Rightarrow \begin{cases} \xi_{c1} \text{ di fase} \\ \xi_{c2} \text{ di fase} \end{cases} \tag{11}$$

$$-1 \leq \Psi < 0 \Rightarrow \begin{cases} \xi_{c1} \text{ variabile, dipendente da } \gamma \\ \xi_{c2} \text{ di fase} \end{cases} \tag{12}$$

$$\Psi = 0 \Rightarrow \begin{cases} \xi_{c1} \text{ di attenuazione} \\ \xi_{c2} \text{ di fase} \end{cases} \tag{13}$$

$$0 < \Psi \leq 1 \Rightarrow \begin{cases} \xi_{c1} \text{ di attenuazione} \\ \xi_{c2} \text{ variabile, dipendente da } \gamma \end{cases} \tag{14}$$

$$\Psi > 1 \Rightarrow \begin{cases} \xi_{c1} \text{ di attenuazione} \\ \xi_{c2} \text{ di attenuazione} \end{cases} \tag{15}$$

Si nota quindi, che per applicazioni pratiche, in cui il mezzo 1 è solitamente l'aria (assimilabile al vuoto) lo scenario più comune è quello rappresentato da $\psi \geq 0$ che si ottiene quando $\varepsilon_1 \leq 2\varepsilon_2'$, per cui esiste sempre una soluzione di attenuazione (penetrazione profonda è in teoria sempre possibile).

Due casi di interesse vengono illustrati rispettivamente per $\Psi = 0$ e $\Psi > 1$. Gli andamenti di ψ_2 and ζ_2 per questi due casi sono riportati in figure 2 e 3.

In particolare, in entrambe le figure 2 e 3 si può verificare l'esistenza di soluzioni tali che $\zeta_2 > 90^o$. Attraverso una dimostrazione basata sulla continuità della soluzione analitica viene dimostrato che questi valori sono accettabili, queste soluzioni danno origine ad un'onda piana la cui ampiezza cresce al crescere della distanza coperta dall'onda trasmessa all'interno del mezzo con perdite, dando origine ad un'onda che non rispetta la condizione di radiazione all'infinito, nota come condizione di Sommerfeld [8], qui accettabile perchè si trattano onde piane (che sono non fisiche).

L'ultimo aspetto su cui lo studio analitico di questa tesi si concentra è l'unicità della soluzione di penetrazione profonda. Per l'onda non omogenea nel mezzo 1 due soluzioni sono possibili, ovvero, detto θ l'angolo formato da $\underline{\beta}_1$ e $\underline{\alpha}_1$, $\theta = \pm 90^o$. Si studia il caso di interesse pratico in cui l'apertura che genera l'onda è parallela al mezzo con perdite: in questo caso è solo la soluzione impropria, caratterizzata da $\theta = -90^o$, [9]-[10] che permette penetrazione profonda, l'altra soluzione causa un'onda trasmessa attenuata.

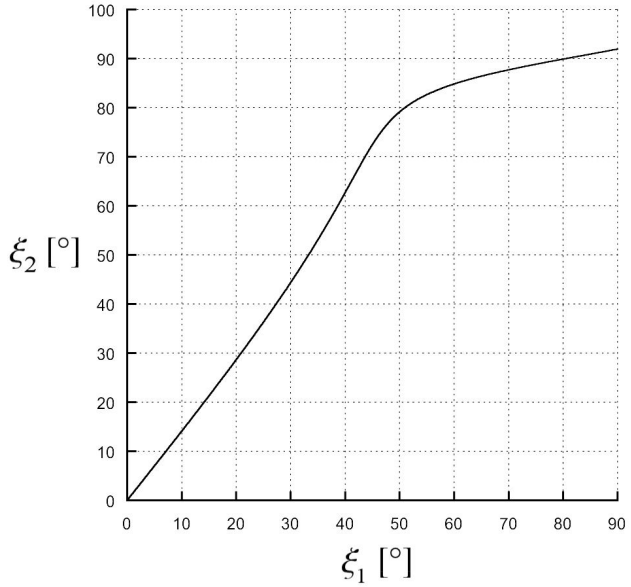

(a) Andamento di ξ_2 in funzione di ξ_1: la soluzione di fase richiede $\xi_1 > 45^o$, e si verifica quando $\xi_1 = 80^o$

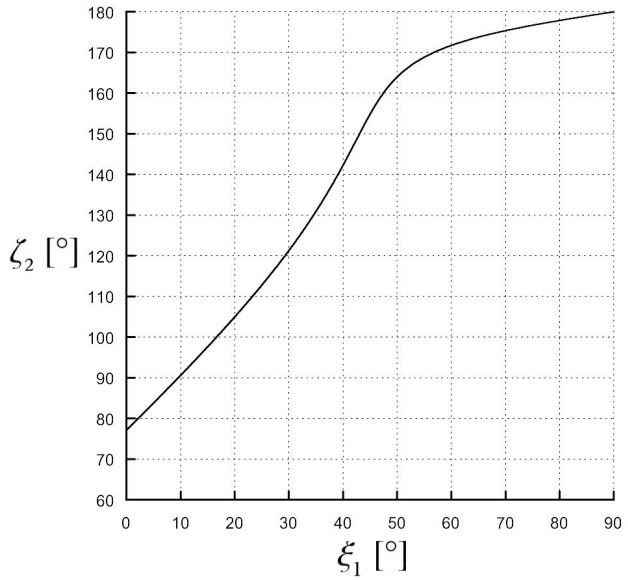

(b) Soluzione di attenuazione, che richiede $\xi_1 < 45^o$, e in particolare $\xi_1 \approx 15^o$. Questo grafico mostra la possibilità di ottenere un'onda la cui ampiezza cresce mentre si propaga nel mezzo con perdite, i.e. $\zeta_2 > 90^o$.

Figura 2. Valori di ζ_2 e ξ_2 nel caso in cui $\varepsilon_1 = 2$, $\varepsilon_2' = 1$, $\varepsilon_2'' = 0.1$ $\beta_1 = 1.01 \cdot \beta_c$: sono presenti soluzioni sia di attenuazione che di fase.

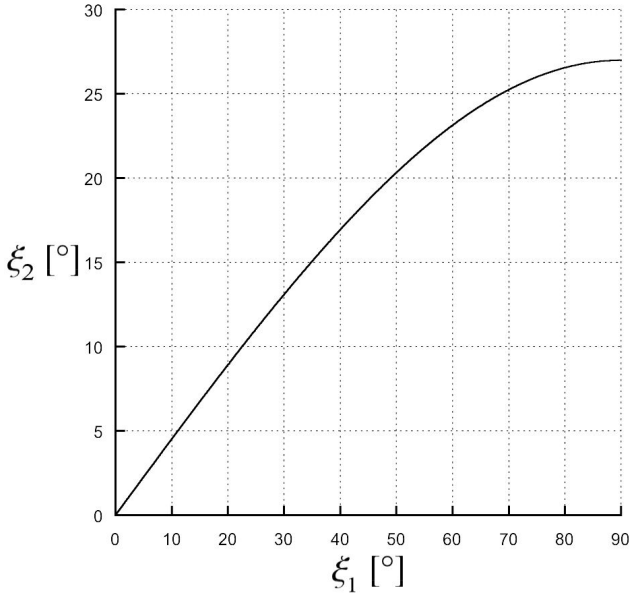

(a) ξ_2 in funzione di ξ_1. La soluzione di fase non è mai raggiungibile, l'angolo ξ_2 è acuto per qualsiasi scelta di ξ_1 all'interno del mezzo con perdite.

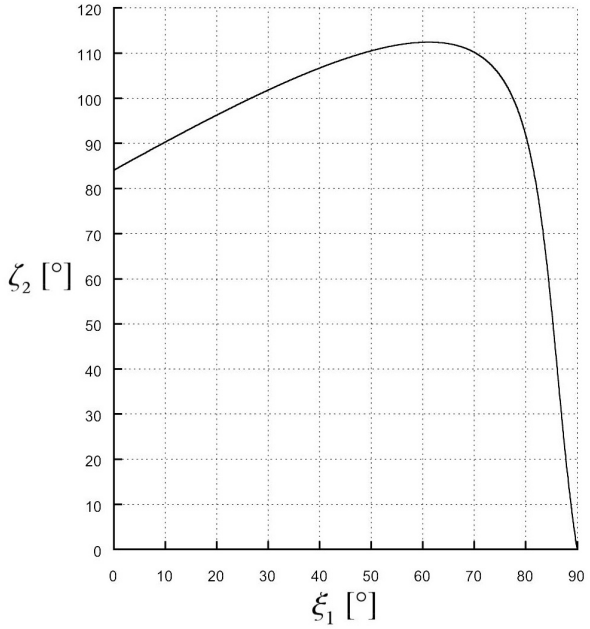

(b) ζ_2 in funzione di ξ_1. Ben due soluzioni di attenuazione sono disponibili: la prima per $\xi_1 \approx 18^o$ e la seconda per $\xi_1 \approx 72^o$, quindi una soluzione richiede $\xi_1 < 45^o$ e l'altra $\xi_1 > 45^o$.

Figura 3. Valori di ζ_2 e ξ_2 nel caso in cui $\varepsilon_1 = 2$, $\varepsilon_2' = 5$, $\varepsilon_2'' = 0.1$ $\beta_1 = 1.01 \cdot \beta_c$, si nota che esistono due soluzioni di attenuazione in questo caso, inoltre la soluzione $\zeta_2 > 90^o$, che rappresenta una soluzione di amplificazione nel mezzo con perdite, è anche presente.

Verifica numerica: penetrazione profonda attraverso antenne ad onda leaky

In questa parte della monografia si abbandona il caso di onda piana e si studiano onde che possono essere generate da sorgenti finite. Per verificare la penetrazione profonda è necessario innanzitutto generare un'onda non omogenea fisica. Possibili soluzioni per l'onda non omogenea sono l'onda laterale, l'onda superficiale e l'onda leaky [11]; l'unica soluzione tra le presentate che irradia nello spazio e non resta confinata in prossimità della superficie di separazione, è l'onda leaky, che può essere generata attraverso un'antenna detta anche essa leaky [9]-[10]. In particolare, posta l'apertura dell'antenna parallela alla superficie di separazione, un'antenna in grado di generare un'onda leaky impropria è necessaria. La sfida più grande nel progetto dell'antenna è dato dalla necessità di soddisfare l'equazione (7) che richiede un valore per β_1 alto rispetto ai valori comunemente imposti nel progetto di antenne leaky. Dopo una lunga fase di studio, la migliore candidata alla penetrazione profonda è stata trovata nell'antenna di Menzel [12], che è costituita semplicemente da una microstrip che irradia attraverso i modi di ordine superiore: la natura leaky di tali modi fu spiegata per la prima volta da Oliner e Lee in [13]-[14]. In questa dissertazione si considera un mezzo ipotetico tale che $\sigma_2 = 0.05$ Siemens/metro, $\mu_2 = \mu_0$ e $\varepsilon_2 = \varepsilon_0$: in particolare gli ultimi due parametri coincidono con gli stessi per il mezzo 1, questa scelta viene effettuata per ridurre gli effetti, non voluti e non pertinenti, legati alla riflessione.

Viene utilizzato un approccio numerico full-wave per la prima volta presentato in [15], per disegnare l'antenna scelta imponendo $\beta = \beta_{1c}$ per $\xi_1 = 45^o$ alla frequenza operativa di 12 GHz. La scelta fatta è sicuramente la più conveniente in termini di penetrazione profonda in quanto $\xi_1 = 45^o$ minimizza il β_{1c} per cui $\zeta_2 = 90^o$.

Il metodo utilizzato per il disegno è ottimizzato per antenne leaky monodimensionali periodiche. Questa antenna è invece uniforme, ma può es-

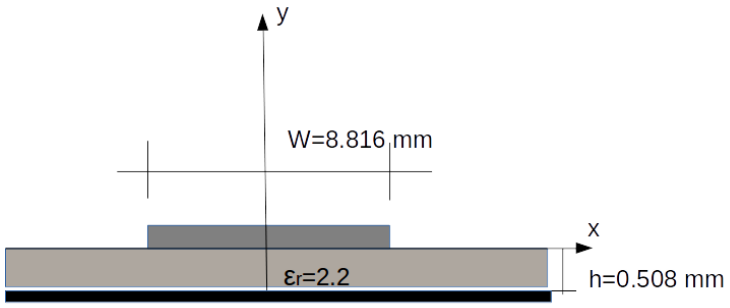

Figura 4. Dimensioni dell'antenna di Menzel ottimizzata per penetrazione profonda in un mezzo tale che $\epsilon_r = 1$, $\mu_r = 1$, $\sigma = 0.05$ Siemens/metro: sia la microstrip che il piano di massa sono assunte PEC e le perdite nel substrato sono assunte trascurabili.

sere studiata come struttura periodica il cui periodo è preso lungo l'asse longitudinale.

Bisogna notare che il progetto di antenne leaky viene solitamente effettuato in funzione delle ampiezze delle componenti tangenziali dei vettori di attenuazione e propagazione e non delle loro ampiezze in assoluto. Ipotizzando la direzione longitudinale coincidente con l'asse z, e supponendo il mezzo 1 come il vuoto, dall'equazione (7) segue, nel caso di radiazione a 45^o:

$$\frac{\beta_z}{k_1} =\approx 1.0027879\frac{\sqrt{2}}{2} \approx 0.711 \tag{16}$$

$$\frac{\alpha_{1z}}{k_1} \approx 0.0747234\frac{\sqrt{2}}{2} \approx 0.0528 \tag{17}$$

I valori trovati per il modo leaky prodotto dall'antenna di Menzel, di seguito mostrati, approssimano molto bene quelli richiesti:

$$\begin{cases} \frac{\beta_z}{k_0} = 0.7088 \\ \frac{\alpha_z}{k_0} = 0.05234 \end{cases} \tag{18}$$

L'equazione di dispersione per il modo richiesto, dispari rispetto all'asse di simmetria longitudinale, è mostrato in Fig. 5, mentre le dimensioni dell'antenna sono mostrate in Fig. 4.

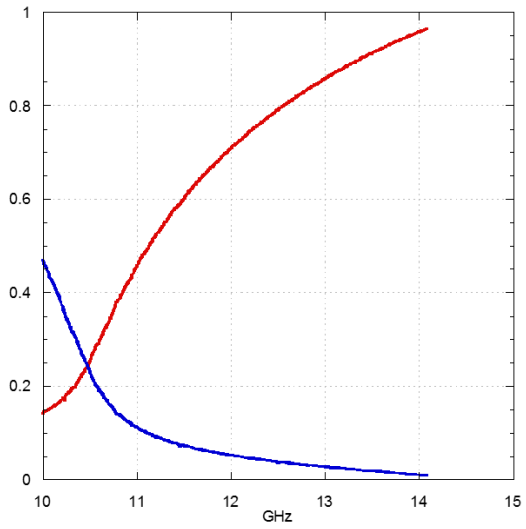

Figura 5. Diagramma di dispersione calcolato nella fase di disegno dell'antenna, sono rappresentati β_z/k_0 (in rosso) e α_z/k_0 (in blu).

L'antenna, le cui dimensioni sono state trovate attraverso un codice Fortran legacy, è quindi riprodotta attraverso il tool commerciale CST Microwave Studio [16] e il mezzo con perdite è inserito parallelamente all'apertura dell'antenna ad una distanza 1.5λ.

Il valore del campo elettrico all'interno del mezzo con perdite, calcolato nel piano passante per l'asse di simmetria della parete più larga dell'antenna horn è mostrato in figura 6, mentre il campo elettrico passante per l'asse di simmetria longitudinale dell'antenna leaky a microstrip è mostrato in figura 7. In entrambi i casi il campo elettrico è normalizzato rispetto al valore massimo dello stesso calcolato all'interfaccia del mezzo con perdite (i.e. a $y = 1.5\lambda = 37.5$ mm).

Risulta evidente come l'antenna leaky produca una penetrazione maggiore dell'antenna horn, almeno per il mezzo con perdite scelto.

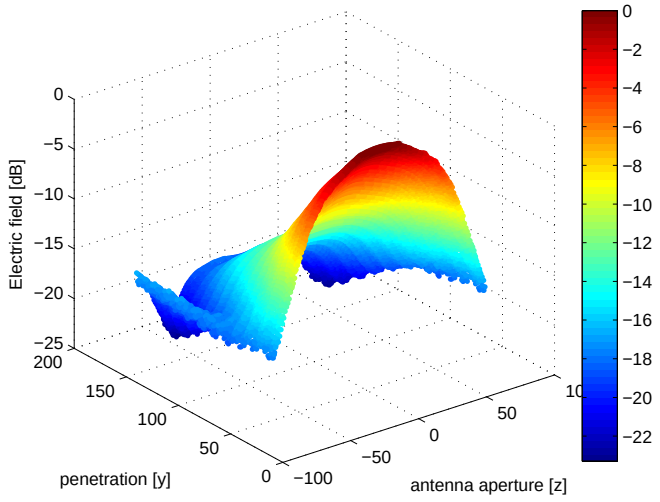

(a) Vista tridimensionale dell'ampiezza del campo elettrico prodotto dall'antenna horn all'interno del mezzo con perdite posto parallelamente all'apertura dell'antenna.

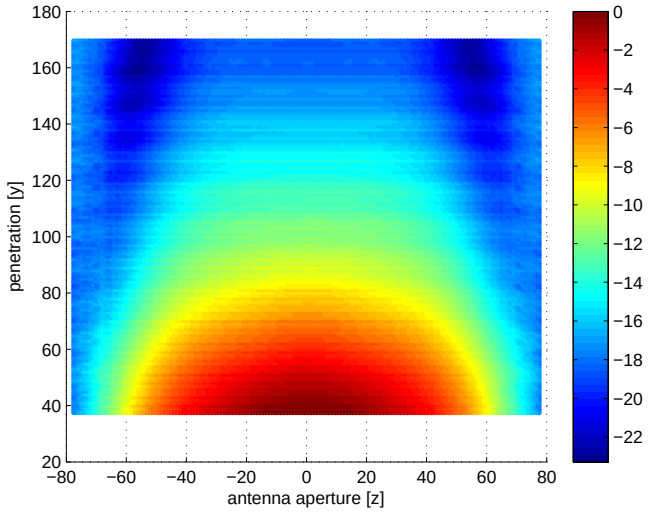

(b) Vista bidimensionale dell'ampiezza del campo elettrico prodotto dall'antenna horn all'interno del mezzo con perdite: in ascissa viene presentata la direzione longitudinale dell'apertura dell'antenna e in ordinata è posta la profondità del mezzo con perdite.

Figura 6. Campo elettrico valutato su uno dei piani di simmetria dell'antenna horn ($x = 0$) all'interno di un mezzo con perdite e rappresentante l'onda trasmessa generata da un'onda incidente prodotta nel vuoto da un'antenna horn. il mezzo con perdite è posto ad una distanza $y = 37.5\ mm$ dall'apertura dell'antenna.

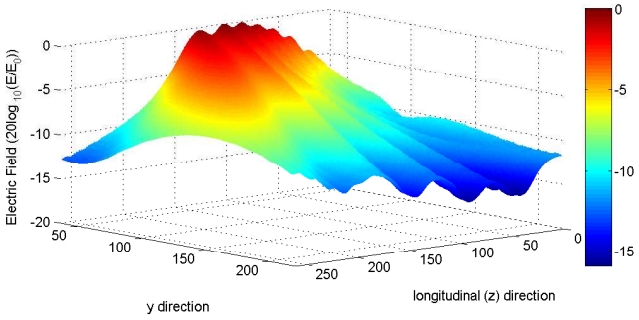

(a) Vista tridimensionale del campo elettrico prodotto dall'antennal leaky all'interno del mezzo con perdite posto parallelamente all'apertura dell'antenna.

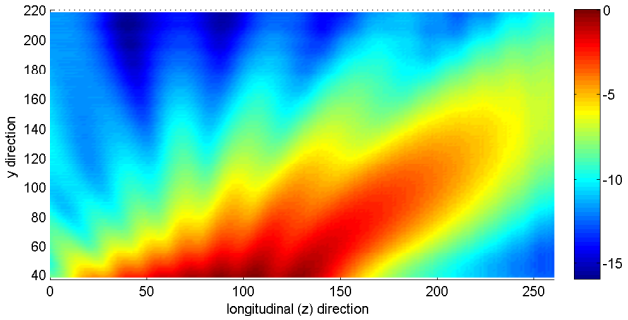

(b) Vista bidimensionale del campo elettrico prodotto dall'antennal leaky all'interno del mezzo con perdite posto parallelamente all'apertura dell'antenna: in ascissa viene presentata la direzione longitudinale dell'apertura dell'antenna, e in ordinata è posta la profondità del mezzo con perdite.

Figura 7. Campo elettrico valutato sul piano longitudinale di simmetria dell'antenna leaky ($x = 0$) all'interno di un mezzo con perdite e rappresentante l'onda trasmessa generata da un'onda incidente prodotta nel vuoto da un'antenna leaky. il mezzo con perdite è posto ad una distanza $y = 37.5\ mm$ dall'apertura dell'antenna.

Oltre che un andamento del valore puntuale del campo in funzione del valore massimo, risulta interessante anche un andamento mediato che può essere ottenuto dopo aver omogeneizzato in qualche modo i campi prodotti dai due diversi tipi di antenna. L'omogeneizzazione deve in qualche modo tenere conto del fatto che l'antenna leaky irradia a 45^o mentre quella horn irradia a 90^o. La soluzione non può essere rappresentata da una semplice rotazione del solido con perdite per omogeneizzare i due casi, in quanto, vista la minima distanza tra mezzo con perdite e antenna, una rotazione comporterebbe il rischio di inserire il mezzo con perdite in una zona di campo non radiativa ma reattiva [17], oppure potrebbe portare a una collisione tra mezzo con perdite ed antenna. Un algoritmo è stato sviluppato per tale scopo: in primo luogo si calcola la potenza irradiata dall'antenna leaky controllando la potenza disponibile al carico e si considera una quota di potenza all'apertura dell'antenna horn analoga. Dopo di che si applica, sull'apertura, che è disposta sull'asse z per entrambe le antenne, un campionamento, che nel caso particolare è preso di 1 mm. Fatto questo si hanno $N^{(h)}$ campioni per l'antenna horn e $N^{(l)}$ campioni per l' antenna leaky: in generale è $N^{(h)} \neq N^{(l)}$. Lo stesso passo di campionamento si applica sulla verticale (che si trova sull'asse y per entrambe le antenne) e per ogni quota y_i si considerano un numero n di campioni minimo tra:

- tali che il rapporto di campo tra massimo e minimo non sia superiore allo stesso rapporto calcolato alla quota y_{i-1}
- Il numero di campioni sia $N^{(h)}$ per l'antenna horn o N^l per l'antenna leaky.

Il campo medio per ogni y_i è quindi valutato secondo la formula che segue:

$$\overline{E}(y_i) = \frac{\sum_{k=n^{(i)}}^{k=N+n^{(i)}} |\underline{E}(0, y_i, z_k)|}{\sum_{j=m}^{j=m+N} |\underline{E}(0, y_{if}, z_j)|} \; \forall y_i \geq y_{if} \tag{19}$$

La penetrazione raggiunta dall'onda prodotta dall' antenna leaky rispetto a quella prodotta dall'antenna horn è visibile in Fig. 8

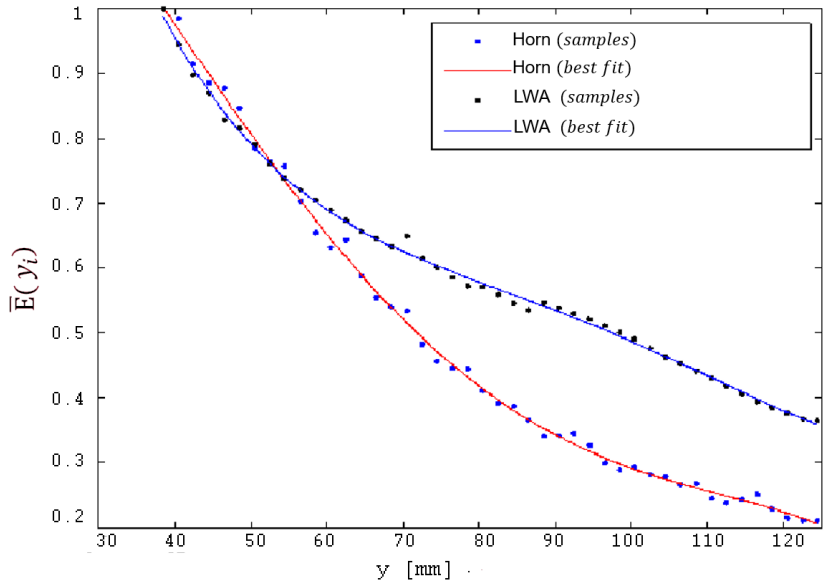

Figura 8. Confronto della penetratione media prodotta dal campo generato da un'antenna horn e una microstrip leaky in un mezzo con perdite: il valor medio del campo è calcolato attraverso l'algoritmo presentato in equazione (19). Le caratteristiche del mezzo con perdite scelto sono: $\sigma = 0.05\ S/m$, $\mu_r = 1$ e $\varepsilon_r = 1$.

Si nota in figura 8 un'interessante risultato: dapprima la curva che corrisponde alla penetrazione prodotta dall'onda leaky si trova al di sotto di quella prodotta dall'onda horn, per poi sorpassare quest'ultima per valori alti della variabile z. Un'attenta osservazione delle figure 6 e7 mostra lo stesso risultato. Questo andamento del campo è dovuto al fatto che le onde leaky sono dovute ad una somma continua contributi di campo provenienti dalle precedenti sezioni dell'antenna sull'asse z, e solo quando la distanza è sufficiente, allora il fenomeno leaky diventa apprezzabile.

Nel paragrafo corrente si è visto come sia possibile raggiungere una penetrazione profonda (non infinita come nel caso del paragrafo precedente che trattava onde piane) attraverso l'uso di onde leaky prodotte da antenne leaky. Il risultato è sicuramente confortante, tuttavia l'entità della penetrazione è modesta in quanto si è utilizzato un mezzo la cui conducibilità è appena $\sigma = 0.05$ Siemens/metro. Questo ridotto valore di conducibilità è stato scelto

per permettere la realizzabilità dell'antenna: un valore più alto richiederebbe un valore della componente longitudinale del vettore di attenuazione più alta, con necessaria riduzione della dimensione longitudinale, questo anticiperebbe la decadenza del campo che non sarebbe leaky per un numero di lunghezze d'onda adeguato. Per ottenere penetrazione in mezzi con un valore di σ interessante occorre studiare strutture di tipo diverso, tipo quella illustrata nel seguente paragrafo.

Il prisma con perdite

In questo capitolo vengono presentati risultati e ricerca di un più ampio argomento ancora in corso di discussione, in cui si sta studiando l'applicazione di un prisma con perdite al problema della penetrazione profonda in mezzi con perdite. Il prisma con perdite è stato presentato per la prima volta come una figura piana indefinita avente i due lati opposti non paralleli in [18], chiaramente equivalente ad una figura tridimensionale indefinita lungo un terzo asse, su cui tutte le sezioni ortogonali rappresentino superfici congruenti. Il principio di funzionamento del prisma con perdite è piuttosto semplice e si basa sulla conservazione della componente tangenziale del campo elettromagnetico. Immaginiamo questo prisma immerso in un mezzo privo di perdite e irradiato ad uno dei due lati da un'onda limitata (per evitare gli effetti di bordo) ma trattabile in approssimazione di onda piana omogenea. Alla prima interfaccia del prisma, è presente il solo vettore di propagazione $\underline{\beta}_1$, pertanto, all'interno del mezzo con perdite, sono presenti un vettore $\underline{\beta}_2$ la cui direzione è descritta dalla legge di Snell, e un vettore $\underline{\alpha}_2$ che è necessariamente ortogonale alla superficie di separazione. Quando l'onda raggiunge l'altro lato della struttura, essendo questo non parallelo al primo, allora esiste una componente tangenziale di $\underline{\alpha}_2$ che deve conservarsi necessariamente, pertanto, nel mezzo privo di perdite al di la del prisma l'onda deve essere non omogenea e in particolare il vettore di attenuazione $\underline{\alpha}_3$ deve esistere.

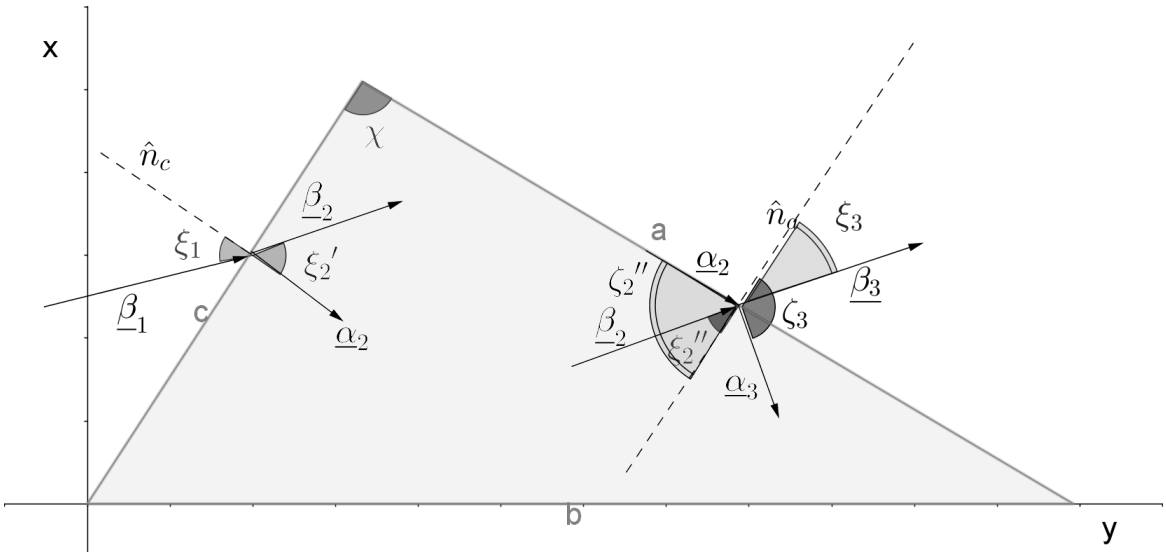

Figura 9. Geometria di un prisma con perdite caratterizzato da un generico angolo χ. La struttura mostrata deve essere in considerata illimitata, i.e. tale che la lunghezza dei lati a e c tenda ad infinito.

Un'importante osservazione che va riportata è che, nell'antenna leaky le perdite sono prevalentemente di radiazione [9]-[10], tanto che la LWA non ha necessita di un dielettrico con perdite per irradiare l'onda non omogenea, solo una piccola parte dell'energia di solito viene dissipata su un carico posto ad una estremità dell'antenna. Nel prisma sono invece necessarie delle vere perdite per dissipazione nel dielettrico: la dissipazione di parte dell'energia fornita all'antenna causa un abbassamento dell'efficienza totale della struttura.

Anche se l'energia fornita non viene tutta irradiata, ma una parte è dissipata sotto forma di calore, il concetto di prisma con perdite riveste comunque un' interessante applicazione in tutti quei casi in cui il limite di potenza è imposto dalla massima potenza che si può irradiare o per regolamentazioni o per sensibilità degli strati superficiali esposti a tale radiazione (e.g. hypertermia).

Il modello più generico di prisma con perdite analizzato nel corso di questo dottorato è riportato in Fig. 9

Con riferimento alla Fig. 9, è possibile dimoostrare che l'ampiezza dell'angolo ξ_3 formato dal vettore di propagazione $\underline{\beta}_3$ nel mezzo privo di perdite all'interfaccia **a** e l'ampiezza di β_3 dello stesso vettore possono essere espresse

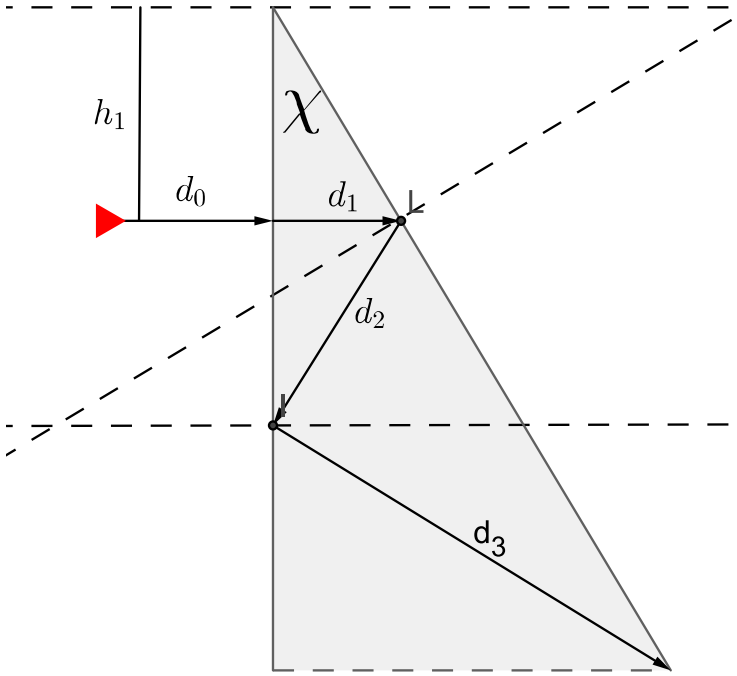

Figura 10. Prisma con perdite: configurazione in cui $\chi < 90^o$, analisi dei cammini riflessi.

come:

$$\begin{cases} \beta_3 = f(\chi, \xi_1, \varepsilon_1, \varepsilon_2, \sigma_2) \\ \xi_3 = g(\chi, \xi_1, \varepsilon_1, \varepsilon_2, \sigma_2) \end{cases}, \tag{20}$$

in cui ξ_1 è l'angolo di incidenza del vettore di fase $\underline{\beta}_1$ all'interfaccia **c**, ε_1 è la costante dielettrica del mezzo privo di perdite, e ε_2 e σ_2 sono rispettivamente costante dielettrica e conduttività nel mezzo con perdite. I due mezzi sono qui assunti non magnetici, oltre che omogenei, isotropi, e non dispersivi.

Un primo studio sul prisma con perdite ha riguardato la struttura riportata in Fig. 10, dove un raggio in approssimazione ottica viene considerato e in cui è $\chi < 90^o$. In questo tipo di figura l'onda radiata nello spazio 3 può certamente risentire della presenza di riflessioni multiple all'interno del prisma. Il cammino della prima riflessione può essere caratterizzato da semplici considerazioni geometriche, derivanti dalla legge di riflessione ottica ottenendo:

$$d_1 = h_1 \tan \chi \tag{21}$$

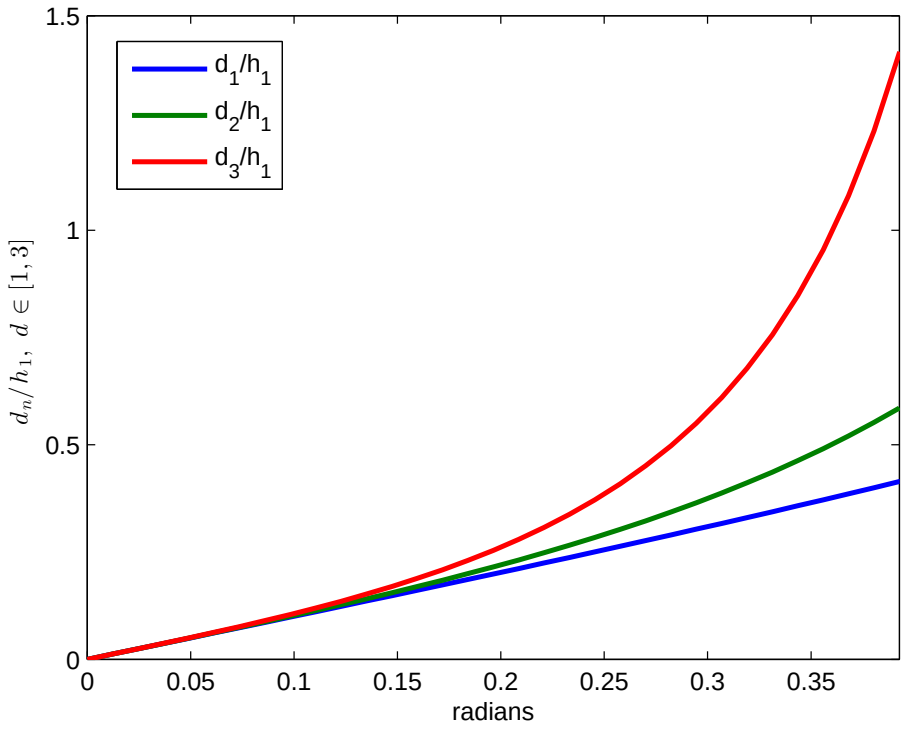

Figura 11. Prisma con perdite: lunghezza dell'onda diretta d_1/h_1, della prima riflessione d_2/h_1, e del terzo cammino di riflessione d_3/h_1 al variare di $\chi \in [0,\ \pi/8]$.

Per $\chi \geq \pi/4$, il cammino d_2 non interseca mai l'interfaccia illuminata, mentre per $\chi < \pi/4$ la raggiunge, e la sua espressione è la seguente:

$$d_2 = \frac{d_1}{\cos 2\chi} \tag{22}$$

Quando si verifica la condizione $\chi < \pi/6$, anche il cammino d_3 raggiunge l'interfaccia e la sua ampiezza è la seguente:

$$d_3 = \frac{[h_1 + d_1 \tan(2\chi)] \sin \chi}{\cos 3\chi} \tag{23}$$

In Fig. 11 si riportano d_1/h_1, d_2/h_1 e d_3/h_1 per $\chi \in]0, \pi/8]$ radianti.

Una simulazione del prisma con perdite avente angolo $\chi = 5^o$ è stata effettuata in [19] attraverso l'uso del software commerciale CST, e utilizzando FR4 (lossy) come materiale per il prisma: questa simulazione ha confermato sia la possibilità di generare onde inomogenee, ma anche la presenza degli effetti

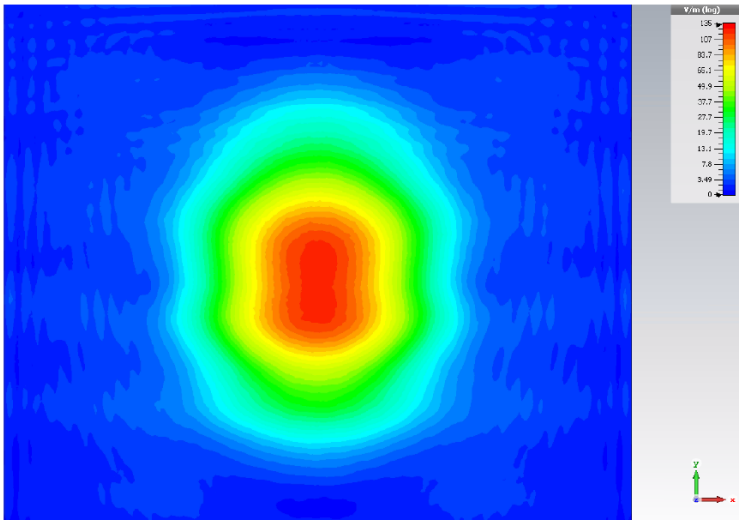

Figura 12. Simulazione di incidenza normale su prisma con perdite di angolo $\chi = 5^o$ e materiale FR4: Campo all'interfaccia verticale.

di cammini multipli tra le due facce del prisma; in Fig. 12 e 13 si mostrano l'effetto della prima riflessione (cammino d_2) e quello della seconda riflessione (cammino d_3) in questo scenario.

La ricerca si è infine spostata su una diversa configurazione del prisma con perdite in cui $\xi = 90^o$. Il motivo di questa configurazione è abbastanza semplice. Se $\xi = 90^o$ allora il vettore di attenuazione $\underline{\alpha}_2$, ortogonale alla prima interfaccia, risulta parallelo alla seconda interfaccia, pertanto viene conservato per la sua intera ampiezza. Inoltre questa configurazione impedisce che la riflessione torni all'interfaccia illuminata. In questo caso, se il mezzo omogeneo è il vuoto si dimostra che:

$$\frac{\beta_3}{k_0} = \frac{1}{\sqrt{2}}\sqrt{1+\sqrt{1+\left[\frac{2\sigma_2}{\omega\varepsilon_0\sin(2\xi_3)}\right]^2}} \tag{24}$$

$$\frac{\alpha_3}{k_0} = \frac{1}{\sqrt{2}}\sqrt{1+\sqrt{\left[\frac{2\sigma_2}{\omega\varepsilon_0\sin(2\xi_3)}\right]^2}-1} \tag{25}$$

$$\xi_1 = \arcsin\left[\sqrt{\varepsilon_{r2}+\beta_{3n}^2\cos\left(2\xi_3\right)-\cos^2\xi_3}\right], \tag{26}$$

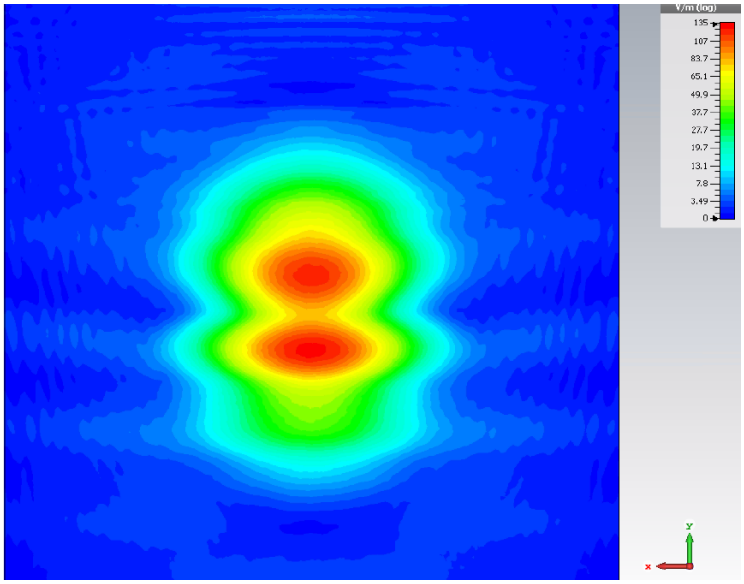

Figura 13. Simulazione di incidenza normale su prisma con perdite di angolo $\chi = 5^o$ e materiale FR4: Campo all'interfaccia obliqua.

Si dimostra che, attraverso un mezzo tale che $\varepsilon = \varepsilon_0$, $\sigma \geq 0.008$ Siemens/metro e $\xi_3 = \pi/4$, si ottiene una onda non omogenea avente un vettore di fase la cui ampiezza β_3 è maggiore di quella ottenibile attraverso la LWA mostrata al paragrafo precedente.

In Fig. 14 si dimostra la dipendenza dell'angolo ξ_3 da ξ_1 per $\beta_3/k_0 \in [1.1, 1.8]$ quando $\varepsilon_{r2} = 1$: l'angolo ξ_3 diventa sempre meno dipendente da ξ_1 quanto più è forte β_3/k_0 (che si aumenta aumentando la conducibilità σ_2.

In Fig. 15, invece si mostra la dipendenza di ξ_3 da ξ_1 quando la costante dielettrica $\varepsilon_2 \in [0.2,\ 2]$: per $\varepsilon < 1$, ξ_3 tende a 0 mentre per $\varepsilon > 1$, ξ_3 tende to 90^o, in particolare più è scelto piccolo ε_{r2}, più ξ_3 tende a broadside, che però non può mai essere raggiunto.

La configurazione attuale del prisma con perdite presenta alcune importanti caratteristiche che lo rendono il miglior candidato per esplorare la penetrazione profonda, tuttavia una opportuna antenna deve essere disegnata tale da permettere la radiazione attraverso questa struttura. L'impegno della ricerca è attualment e concentrata sullo studio di fattibilità di suddetta antenna.

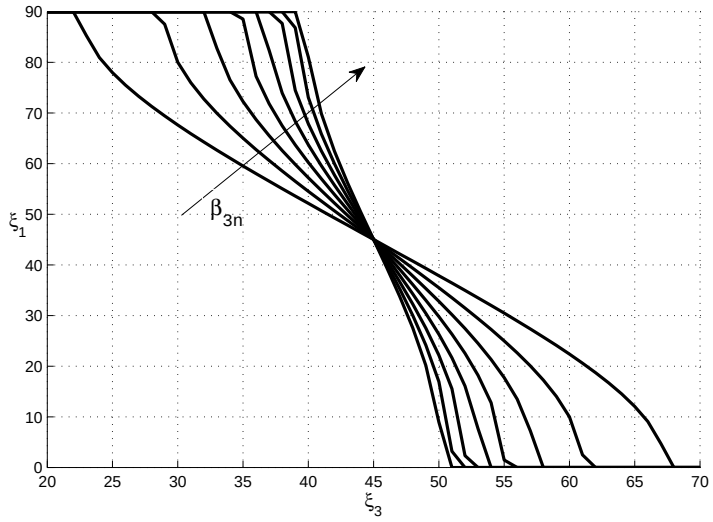

Figura 14. Prisma con perdite: andamento dell'angolo ξ_3 del vettore di fase dell'onda trasmessa dal prisma quando l'angolo di incidenza sul prisma ξ_1 varia nell'intervallo $]0^o, 90^o[$ e nel caso in cui $\beta_{3n} \in [1.1; 1.8]$, avendo scelto un prisma con perdite tale che $\varepsilon_{r2} = 1$.

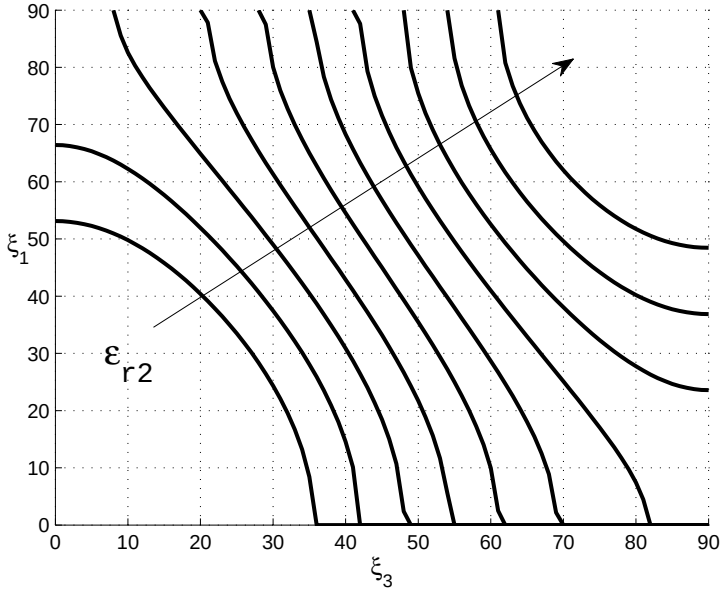

Figura 15. Prisma con perdite: andamento dell'angolo ξ_3 del vettore di fase dell'onda trasmessa dal prisma quando l'angolo di incidenza sul prisma ξ_1 varia nell'intervallo $]0^o, 90^o[$ e nel caso in cui il prisma sia caratterizzato da $\varepsilon_{r2} \in [0.2,\ 2]$, e nel caso in cui $\beta_{r2} = 1.2$.

Elenco delle figure

Bibliografia

[1] F. Frezza, *A Primer on Electromagnetic Fields*. Springer, 2015.

[2] J. Holmes and C. Balanis, "Refraction of a uniform plane wave incident on a plane boundary between two lossy media," *IEEE Transactions on Antennas and Propagation*, vol. 26, pp. 738–741, sep 1978.

[3] R. D. Radcliff and C. A. Balanis, "Modified propagation constants for nonuniform plane wave transmission through conducting media," *IEEE Trans. Geosci. Remote Sensing*, vol. vol. GE-20, pp. 1206–1215, July 1982.

[4] R. B. Adler, L. J. Chu, and R. M. Fano, *Electromagnetic Energy Transmission and Radiation*. MIT Press, nov 1968.

[5] J. Roy, "New results for the effective propagation constants of nonuniform plane waves at the planar interface of two lossy media," *Transaction on Antennas and Propagation*, vol. 51, pp. 1206–1215, 2003.

[6] F. Frezza and N. Tedeschi, "Deeply penetrating waves in lossy media.," *Optics letters*, vol. 37, no. 13, pp. 2616–8, 2012.

[7] F. Frezza and N. Tedeschi, "Deeply penetrating waves in lossy media," *Optics letters*, vol. 37, no. 13, pp. 2616–8, 2012.

[8] A. Sommerfeld, *Partial Differential Equations in Physics (Pure and Applied Mathematics: A Series of Monographs and Textbooks, Vol. 1)*. Academic Press, 1949.

[9] D. R. Jackson and A. A. Oliner, "Leaky-wave antennas," in *Modern Antenna Handbook* (C. Balanis, ed.), pp. 325–367, New York: Wiley, 2008.

[10] A. A. Oliner and D. R. Jackson., *John Volakis,Antenna Engineering Handbook*. McGraw Hill Professional, 4th ed., 2015.

[11] F. Frezza and N. Tedeschi, "Electromagnetic inhomogeneous waves at planar boundaries," *Journal of the Optical Society of America A*, vol. 32, no. 8, pp. 1485–1501, 2015.

[12] W. Menzel, "A new travelling wave antenna in microstrip," in *8th European Microwave Conference, 1978*, no. 2, pp. 302–306, 1978.

[13] A. Oliner and K. Lee, "Microstrip leaky wave strip antennas," in *Antennas and Propagation Society International Symposium, 1986*, vol. 24, pp. 443–446, IEEE, 1986.

[14] A. A. Oliner, "Leakage from higher modes on microstrip line with application to antennas," *Radio Science*, vol. 22, no. 6, pp. 907–912, 1987.

[15] P. Baccarell, C. D. Nallo, S. Paulotto, and D. R. Jackson, "A full-wave numerical approach for modal analysis of 1-D periodic microstrip structures," *IEEE Transactions on Microwave Theory and Techniques*, vol. 54, no. 4, pp. 1350–1362, 2006.

[16] C. M. Studio, "3d em simulation software," *Computer Simulation Technology*, 2014.

[17] C. A. Balanis, *Antenna Theory: Analysis and Design*. Wiley, iv ed., 2016.

[18] N. Tedeschi and F. Frezza, "An analysis of the inhomogeneous wave interaction with plane interfaces," in *General Assembly and Scientific Symposium (URSI GASS), 2014 XXXI URSI*, pp. 109–112, IEEE, 2014.

[19] N. Tedeschi, V. Pascale, F. Pelorossi, and F. Frezza, "Generation of inhomogeneous electromagnetic waves by a lossy prism," in *Electromagnetic*

Theory (EMTS), 2016 URSI International Symposium on, pp. 838–841, IEEE, 2016.

Acknowledgements

I wish to thank Prof Frezza for having provided me the opportunity to join his wonderful research team, and for having been not only a great tutor but also a good example, a friend and a great aid in many of the activities directly or indirectly related to this dissertation. I am also deeply indebted to Dr Tedeschi and Dr Baccarelli for all their highly skilled professional help provided during the whole project, from the theoretical study up to the antenna design and the publications. I am also indebted to the TU1208 COST Action, dedicated to the civil engineering applications of Ground Penetrating Radar (GPR), which, thanks to its network activities, aided the successful development of the challenging topic presented in this research. I finally wish to spend few words to thank my wife Eida, who supported the choice to start this ph.D study and who was always at my side, even in the difficult moments in which this activity took my presence away from my family, and expecially from her and my daughter Mya. Without her support, presence and, above all, patience, this objective could not be achieved.

Contents

Chapter 1

Introduction to topic and structure of the dissertation

1.1 Introduction to the topic of the dissertation

The topic of this dissertation is the study of deep penetration of Electromagnetic field in lossy media achieved by means of inhomogeneous waves. A so-called lossy medium opposes to electromagnetic-wave propagation because of its non-null conductivity value: a high value of this coefficient is fundamental for conducting electric current, anyway the conductivity also represents an obstacle in many practical applications in which a high penetration of electromagnetic field represents an important requirement. The achievement of electromagnetic deep penetration is of extreme importance in many applications, e.g., detection of buried or immersed objects, information transmission in lossy media, material analysis and microscopy, interaction with biological tissues. Different techniques were employed in literature to reduce the issue represented by a non-null conductivity, for instance, optimisations of antenna design were employed in [1]. In typical geophysical applicationss such as the *Ground Penetrating Radar* (GPR), whose maximum penetration is established by the radar equation [2], the operating frequency is instead commonly reduced to improve penetration, see for example [3]: this reduction of the frequency brings to an obvious reduction

of resolution [4], therefore a compromise between resolution and penetration needs to be achieved. Lowering the frequency also causes an increase of the antenna dimensions, so that in literature, design of miniaturised antennas had to be proposed, for instance in [5]. A different and innovative approach is considered here by exploiting properties which are typical of inhomogeneous waves: such waves are characterised by an attenuation vector present even in lossless media. It is demonstrated here that employing inohomogeneous waves leads to an increase of penetration without a frequency reduction, and therefore, without losses in the resolution. This method, which is relatively new, sees its preliminary theoretical aspects illustrated in [6], where a sufficient condition for deep penetration was demonstrated; anyway in [6], a full analysis was not performed, leading to some uncertainty on the practical implications. The theoretical aspects introduced in [6] are therefore expanded and completed as a part of the present dissertation.

The analytical approach followed, which constitutes the necessary background for practical applications and simulations, is developed to demonstrate the properties, conditions and constraints that allow deep-penetration. Such a theory employs inhomogeneous plane waves, which are non physical. The theory is then proved abandoning the plane-wave hypothesis and designing, instead, an opportune and realistic structure, and in particular a Leaky-Wave Antenna (LWA) [7]-[8], that can generate inhomogeneous waves in lossless media having the characteristics required by the theoretical approach. The performance of the designed structure is analysed by means of numerical simulations with the objective of demonstrating limits, advantages and feasibility of the proposed strategy, this is achieved comparing the penetration achieved by the LWA with the penetration obtained through conventional high-directive antennas such as the horn antenna. Finally, results and limits of the present methodology are shown and some ongoing and near-future study development, concerning new non-conventional antenna concepts will be proposed to improve the obtained, already positive, results.

1.2 Structure of the dissertation

From a structural point of view, the dissertation can be divided into three main blocks: the first block is fully dedicated to a presentation of the theoretical and practical aspects that constitute the background needed to properly understand and follow the topic, starting from the essential principles of Electromagnetism: all the exposed preliminary concepts are commented with the final result in mind and they are meant to be an aid for readers who are not familiar with inhomogeneous plane-waves or with leaky-wave antennas to approach this thesis. Moreover, those sections provide an opportune context for the choices overtaken in the course of the research; note that the exhaustive deployment of the introductory arguments is beyond the scope of this dissertation, therefore all the necessary references are provided so that the reader can expand, if needed, the concepts exposed here.

The second part of the dissertation is dedicated to the theoretical analytic study of inhomogeneous plane-waves penetration in lossy media: at first, the previous results obtained in literature are presented and then the new findings, that aim to complete previous studies, and that were part of this research, are described.

The last part of the dissertation regards numerical simulation that was performed with the objective of demonstrating limits and applicability of the theoretical results found in the previous section, but taking in consideration more realistic leaky-wave structures, both conventional (i.e. metal-patch bidimensional and microstrip leaky-wave antennas) and innovative (i.e. “lossy prism”), and to the analysis of the obtained results,

To facilitate the reading, every chapter of this dissertation starts with a tiny abstract that briefly resumes the specific contents of the presented topic to give the reader a quick overview of the contents that follow.

Part I

Inhomogeneous waves and leaky-wave antennas.

Chapter 2

Homogeneous and inhomogenous plane waves

2.1 Abstract

The present chapter introduces the general concepts of Electromagnetism that constitute the necessary theoretical background to understand the sections which follow. This chapter starts presenting the Maxwell equations, which are introduced with the objective of familiarizing with the notations and the formalism adopted in this dissertation and to introduce both homogeneous and inhommogeneous plane waves as solutions of the Helmotz equation. In the first part of this chapter both inhomogeneous and homogeneous waves are illustrated purely from a mathematical point of view, while in the second part a brief description of the physical acceptable inhomogeneous-wave solutions is given and different kind of inhomogeneous waves are briefly described to show which solutions can be exploited for deep-penetration purposes.

2.2 Introduction to Plane Waves and their characteristics

The well-known Maxwell equations are a system of four differential equations, which link electric and magnetic fields providing a description of the Electromagnetic phenomenon as function of the point. In the time domain, such equations are usually written as follows:

$$\begin{cases} \nabla \times \underline{E} = -\frac{\partial \underline{B}}{\partial t} \\ \nabla \times \underline{H} = \underline{J} + \frac{\partial \underline{D}}{\partial t}, \\ \nabla \cdot \underline{D} = \rho \\ \nabla \cdot \underline{B} = 0 \end{cases} \tag{2.1}$$

where"$\times$" indicates the vector product, while "$\cdot$" is used for the scalar product (also said dot or internal product), this convention will be adopted broadly in the dissertation. In Eq. (2.1) $\underline{E}$ represents the electric field, $\underline{D}$ the electric induction, $\underline{H}$ the magnetic field, $\underline{B}$ the magnetic induction, $\underline{J}$ the density of electric current and finally ρ the density of free charges. The above system of equations is not symmetric in respect to the Electric and Magnetic magnitudes, but it can be manipulated in order to assume a symmetric shape, so that the duality principle can be applied. The concept of duality is a handy tool: if we know the solution of one of the two dual problems, we obtain the solution of the other by simply interchanging symbols (see [9], [10] and [11]). The duality principle requires the definition of the extra fictitious quantities $\underline{J}_m$ and ρ_m representing the duals of $\underline{J}$ and ρ for the magnetic field [11]: $\underline{J}_m$ is the density of magnetic current and ρ_m the density of free magnetic charges. Having a symmetric system will allow us to concentrate exclusively on the Electric field $\underline{E}$ in most of the theoretical formulas and numerical simulations presented.

The system of equations illustrated above contains both fields and inductions, but the inductions can be eliminated exploiting the constitutive relations, that associate $\underline{D}$ to $\underline{E}$ and $\underline{B}$ to $\underline{H}$. The media considered in this dissertation

are homogeneous, isotropic and non-dispersive both in space and in time; in this scenario the constitutive relations become simply linear:

$$\begin{aligned} \underline{D} &= \varepsilon \underline{E} = \varepsilon_r \varepsilon_0 \underline{E} \\ \underline{B} &= \mu \underline{H} = \mu_r \mu_0 \underline{H} \\ \underline{J_c} &= \sigma \underline{E} \end{aligned} \tag{2.2}$$

The quantity J_c defined in Eq. (2.2) is the component of the density of current induced by the field in the conductor; the impressed current J_i represents, instead, a known term and therefore is not part of the constitutive relation. In general all the currents and the density of charges introduced can be defined as the sum of an impressed quantity and an induced one:

$$\begin{aligned} \rho &= \rho_i + \rho_c \\ \rho_m &= \rho_{mi} + \rho_{mc} \\ \underline{J} &= \underline{J}_i + \underline{J}_c \\ \underline{J}_m &= \underline{J}_{mi} + \underline{J}_{mc} \end{aligned} \tag{2.3}$$

The quantities $\underline{J}_{mc}$ and ρ_{mc} in the above equations must always be assumed equal to zero [11]. The three quantities ε, μ and σ are absolute permittivity (measured in Farad/meter), absolute permeability (measured in Henry/meter) and conductivity (measured in Siemens/meter), while ε_r and μ_r are relative permettivity and permeability (in respect to the vacuum) and ε_0, μ_0 are permittivity and permeability of a vacuum. We will usually deal with "non-magnetic" media in this dissertation, therefore $\mu_r = 1$ will be often assumed. The value of the conductivity quantifies the losses in a medium, the conductivity parameter is therefore fundamental in the study of penetration explored in this work.

Under all the hypotheses considered and moving to the frequency domain[1]:

$$\begin{cases} \nabla \times \underline{E} = -\underline{J}_{mi} - j\omega\mu \underline{H} \\ \nabla \times \underline{H} = \underline{J}_i + (\sigma + j\omega\varepsilon)\, \underline{E} \end{cases} \tag{2.4}$$

[1] Remember that $(d[\,]/dt \Rightarrow j\omega)$ when the Fourier transform is applied

In (2.4), only the equations with the rotors were written because the other two (the ones with the divergence) are dependent on these ones in the dynamic case[2] [11]. A complex permittivity, with takes in account for the losses is usually defined, this permettivity can be defined in different ways:

$$\varepsilon_c = \varepsilon - j\sigma/\omega \tag{2.5}$$

$$\varepsilon = \varepsilon' - j\varepsilon'' \tag{2.6}$$

$$\varepsilon = \left|\frac{D}{E}\right| (\cos\delta + i\sin\delta) \tag{2.7}$$

where the quantity δ is known as loss angle, such a value is rarely used while its tangent is more frequently encountered, in particular the $\tan\delta$, called "loss tangent" is expressed by the following:

$$\tan\delta = \frac{|J|}{|J_d|} \tag{2.8}$$

where J is the magnitude of the conduction current and J_d represents the magnitude of the displacement current density. In a homogeneous, isotropic medium it is $J = \sigma E$ and $J_d = j\omega\epsilon E$, it follows that $\tan\delta$ can be written as:

$$\tan\delta = \frac{\sigma}{\omega\varepsilon} = \frac{\varepsilon''}{\varepsilon'} \tag{2.9}$$

The quantity $\tan\delta$ determines how lossy is a medium, i.e. $\tan\delta$ tends to zero when the losses tend to 0.

The expressions in Eqs. (2.5), (2.6) and (2.9) will be all largely employed in this dissertation, while the loss angle defined through (2.7) won't be used.

The Eqs. (2.4) are differential in the first order, with both Electric field $\underline{E}$ and Magnetic field $\underline{H}$ present as variables, those equations, when boundary and initial conditions are known, permit to describe the behaviour of the

[2] In the static case, which is not of interest here, the four MAxwell equations are evidently all independnent

Electromagnetic field in the medium of interest; anyway, treating a system of two coupled differential equations of the first order may be particularly uncomfortable for an analytical study of the electromagnetic problem, while in numerical simulations, when the full-wave approach is taken (e.g *Finite-Difference Time Domain* (FDTD) method [12]-[13]), Maxwell Equations are directly employed.

One of the achievements of this dissertation is the analytical demonstration of the penetration properties of inhomogeneous radiation: in this case a solution of the second-order differential equation in a single vector variable (i.e. $\underline{E}$ or $\underline{H}$), said Helmotz equation [14] is preferred. The Helmotz equation can be obtained by opportunely re-arranging the Maxwell equations[3] The Helmotz equation, in general non homogeneous, is reported below:

$$\nabla^2\underline{E} + k^2\underline{E} = \nabla \times \underline{J}_{mi} + j\omega\mu\underline{J}_i - \frac{\nabla\nabla\cdot\underline{J}_i}{j\omega\mu} \tag{2.10}$$

Eq. (2.10) becomes homogeneous when no electromagnetic sources are considered, in other words, when all sources are outside the domain of interest, i.e. $\underline{J}_{mi} = \underline{J}_i = 0$. The plane wave, which is studied in theoretical part of this dissertation, is a solution of the homogeneous Helmotz equation and it is defined as follows:

$$\underline{E} = \underline{E}_0 e^{-j\underline{k}\cdot\underline{r}} \tag{2.11}$$

The former equation is solution of the Maxwell equations only if $\nabla\cdot\underline{E} = 0$ is verified, i.e.:

$$\underline{E}_0 \cdot \underline{k} = 0, \tag{2.12}$$

From the second of Eq. (2.4) it follows:

[3]The Helmotz equation is obtained by applying a derivative to Maxwell equation therefore its solutions are broader of the ones admitted by Maxwell equation, therefore the third Maxwell equation $\nabla\cdot\underline{E} = 0 \rightarrow \underline{k}\cdot\underline{E} = 0$ for the homogeneous case has to be enforced to restrict properly the solution set of the Helmotz equation.

$$\underline{H} = \frac{\underline{k} \times \underline{E}}{\omega\mu} \tag{2.13}$$

From Eqs. 2.12-2.13 follows that the plane-wave is wave transverse in respect to direction of propagation for both electric and magnetic components, moreover 2.13 demonstrates that we can just concentrate on the electric field, because the behavior of the magnetic fields follows easily.

In Eq. (2.11), $\underline{k}$ is called wave vector, is it in general complex and can be therefore expressed as a linear combination of two real vectors as follows:

$$\underline{k} = \underline{\beta} - j\underline{\alpha} \tag{2.14}$$

$\underline{\beta}$ is called *phase vector* as its direction is orthogonal to all equi-phase surfaces and $\underline{\alpha}$ is said *attenuation vector* as its direction is orthogonal to all equi-amplitude surfaces: in practice $\underline{\beta}$ determines the propagation direction and $\underline{\alpha}$ the attenuation direction. It has to be noted that, for a lossy medium, the energy does not generally propagate in the direction of $\underline{\beta}$, while this is true for a lossless medium, as can be verified looking at the Poyinting vector [15].

The amplitude of the wave vector $\underline{k}$ is called *wave number*, indicated here with k, and it is given by:

$$k = \omega\sqrt{\mu\varepsilon_c} \tag{2.15}$$

In a lossless medium $\varepsilon_c = \varepsilon$, therefore the wave number is real.

A plane wave is said *uniform* or *homogeneous* when there is no attenuation component (i.e. $\underline{\alpha} = 0$) or when the wave attenuates in the same direction in which it propagates ($\underline{\alpha} // \underline{\beta}$). The medium in which a plane wave propagates influences the value of the amplitude of both $\underline{\alpha}$ and $\underline{\beta}$, moreover it restricts the value that the θ angle, formed by those two vectors, can assume; combining (2.15) and (2.14), we obtain $(\underline{\beta} - j\underline{\alpha}) \cdot (\underline{\beta} - j\underline{\alpha}) = \omega\mu(\varepsilon - j\sigma/\omega)$, and so:

$$\begin{cases} \beta^2 - \alpha^2 = k^2 \\ \alpha\beta\cos\theta = \frac{\omega\mu\sigma}{2} \end{cases} \tag{2.16}$$

where β and α are the amplitudes of phase and attenuation vectors, respectively: note that $\sigma \geq 0$ implies $\theta \leq \pi/2$ always [11]. Assuming $\sigma > 0$ in Eq. (2.16), it is possible to obtain an equation in a single variable, either α or β, with a simple substitution; such a substitution in Eq. (2.16) is not allowed for $\sigma = 0$, therefore such an equation can not be obtained in the lossless scenario. In order to obtain an equation in which only the amplitude β is present, it is sufficient to eliminate α from Eq. (2.16): this can be achieved by rewriting the first of Eq. (2.16) as $\alpha^2 = \beta^2 - k^2$, squaring the second equation, and substituting α^2 with the expression just mentioned, obtaining the following:

$$\beta^4 - \left(\omega^2 \varepsilon \mu\right) \beta^2 - \left(\frac{\omega \mu \sigma}{2 \cos\theta}\right)^2 = 0,$$

We have to choose the positive solution for this bi-quadratic equation, because β must be both real and positive, it follows that the only solution allowable is [15]:

$$\beta = \frac{\omega\sqrt{\varepsilon\mu}}{\sqrt{2}} \sqrt{\sqrt{1 + \left(\frac{\sigma}{\omega \varepsilon \cos\theta}\right)^2} + 1} \tag{2.17}$$

because μ and ε are, for common, non artificial, materials at least at microwave frequencies, which are the frequencies of our interest, positive.

The quantity $\omega\sqrt{\varepsilon\mu}$ can be found in literature indicated as k_0 because it represents the wave vector that would be present for the same medium in absence of losses, this notation may be confusing because in literature k_0 also usually indicates the wave number of a vacuum. The equation for α follows from the first of Eq. (2.16)

$$\alpha = \frac{\omega\sqrt{\varepsilon\mu}}{\sqrt{2}} \sqrt{\sqrt{1 + \left(\frac{\sigma}{\omega \varepsilon \cos\theta}\right)^2} - 1} < \beta \tag{2.18}$$

A different expression for α may be obtained using, instead, the second of Eq. (2.16):

$$\alpha = \frac{\frac{\sigma}{2}\sqrt{\frac{\mu}{\varepsilon}}}{\sqrt{\sqrt{1+\left(\frac{\sigma}{\omega\varepsilon\cos\theta}\right)^2}+1}} \tag{2.19}$$

The values of α and β depend on the medium, on the frequency and on the angle formed by phase and attenuation vectors; anyway, in this, lossy case, it is always $\alpha < \beta$ and $\beta > k$. In a lossness scenario, instead, it is $\beta \geq k$, and, in particular $\beta = k$ when $\alpha = 0$, the other possible solution, for which $\theta = \pi/2$, requires, again, $\beta > k$. It is worth nothing that α and β are fully known in a lossy medium when the parameters of the medium ($\varepsilon,\ \mu,\ \sigma$), the frequency ($f = \omega/2\pi$) and the angle θ are known, while this is not true for a lossless medium: in this case α and β values are not determined and infinite pairs α, β satisfying the Eq. (2.16) are all valid solutions of the electromagnetic problem. This consideration is fundamental for the dissertation presented, because such an ambiguity allows a degree of freedom that can be exploited to produce an incident wave in a lossless medium whose β value is chosen "large enough" to allow deep-penetration in a lossy medium posed beyond a separation interface: this "large enough" value is always achievable with plane waves. Plane waves are non physical, and they cannot be generated, as a consequence, in practical scenarios, it could be challenging to generate a wave whose characteristics satisfy the deep-penetration conditions, as it will be demonstrated in the next chapters.

A material has large losses when $\sigma >> \omega\varepsilon\cos\theta$, and it has small losses when $\sigma << \omega\varepsilon\cos\theta$, it is possible to apply some approximations in those two cases: in the first scenario the real part of the wave vector is negligible compared to the imaginary part, therefore we can write:

$$k \approx -\sqrt{j\omega\mu\sigma} \approx (1-j)\sqrt{\frac{\omega\mu\sigma}{2}} \tag{2.20}$$

so, it is evidentely [15]:

$$\alpha \approx \beta \approx \sqrt{\frac{\omega\mu\sigma}{2\cos\theta}} \tag{2.21}$$

while in the second scenario it is:

$$\begin{cases} \beta \approx \omega\sqrt{\varepsilon\mu} \approx k_0 \\ \alpha \approx \frac{1}{2}\frac{\sigma}{\cos\theta}\sqrt{\frac{\mu}{\varepsilon}} \end{cases} \tag{2.22}$$

Note again that the Eq. (2.22) is not valid when $\theta \to \frac{\pi}{2}$, in this case, which happens when the medium is lossless, i.e. $\sigma = 0$, we have to go back to (2.16), that permit us to find two solutions $\alpha \perp \beta$ (inhomogeneous) and $\alpha = 0$ (homogeneous).

The inverse of the quantity under the square root in Eq. (2.20) is known as skin depth and is usually indicated with the δ symbol [16]:

$$\delta \approx \sqrt{\frac{2}{\omega\mu\sigma}} \ \ [m] \tag{2.23}$$

The skin depth is used to calculate the penetration depth, anyway Eq. (2.23) does not represent the general expression for the penetration, which is more generally defined, instead, as the inverse of α:

$$\delta = \frac{1}{\alpha} \ , \tag{2.24}$$

i.e. the penetration is defined as the depth to which a field amplitude reduces of a factor $1/e$. The definition in Eq. (2.24) must be assumed when high-losses approximation cannot be applied, which is the case that will be usually considered in this dissertation where we will not deal with high-loss materials, like conductors for which, instead Eq. (2.23) is usually assumed in literature.

The impedances inside the conductor, usually approximated as surface impedance, are usually written as a function of δ [16] through the following:

$$\zeta = \frac{i + j}{\sigma\delta} \tag{2.25}$$

Note that the Eqs. (2.23)-(2.25) are defined considering plane waves, and a lossy medium whose thickness is infinite, moreover the separation interface is

always considered a planar surface. Anyway, the validity of those equations is more general: the conductor does not need to be have infinite dimension and the separation interface does not need to be planar, for instance, the formulas are still valid as soon as the thickness of the lossy medium is at least twice the value of δ [17] and the curvature is very large compared to the wavelength [16].

Up to now we only touched on the propagation characteristics of plane waves, which are depending on $\underline{k}$; the term $\underline{E}_0$ in the wave equation 2.11 is, instead, responsible for the polarization of the plane wave, which is elliptic in general but can assume circular shape or it can degenerate into a linear form; the elliptic polarization can be always expressed as superposition of linearly polarised plane waves (see [11],[18] and [19]).

This study concentrates on the propagation characteristics of electromagnetic waves, therefore the polarization properties won't be generally investigated or considered, a mention to the polarization will be reported in relation to the pseudo-Brewster angle [20], when an opportune lossy medium will be designed to exploit deep-penetration properties.

2.3 Inhomogeneous waves classification

In the previous paragraph characteristics in terms of attenuation and propagation of inhomogeneous and homogeneous plane waves were introduced from a mathematical point of view, without considering the physics around inhomogeneous waves. In this sections the physical characteristics of inhomogeneous waves will be analysed. We are interested in the penetration of an inhomogeneous wave through a planar interface, therefore, after having briefly introduced this category of waves, we will concentrate on the study of inhomogeneous wave at planar boundaries (see [21]). Inhomogeneous waves that can be physically found at the interface between two media can be classified as lateral waves [22], surface waves [23], and leaky waves; the latter are the most interesting for the present project and they will therefore monopolize this first part of the dissertation. The study of inhomogeneous waves is not a new in

literature, but, at best of our knowledge, started with Zennek and Sommerfled at the beginning of the 20^{th} century. In particular, the former studied bounded inhomogeneous plane waves at the interface between two media [24] in 1907, and the latter analysed the radiation produced by an electrical vertical dipole located above the planar interface between two homogeneous media [25] in 1909.

While the study of inhomogeneous waves started very early in the last century, the first example of a leaky-wave antenna was prototyped only in 1940, thanks to Hansen, who requested a patent for an open waveguide that could be used as a radiating structure. Such an antenna was realised by simply opening a longitudinal slit in the side of a rectangular waveguide [26]: the patent for the mentioned antenna, shown in Fig. 2.1, was finally granted in 1946; even though the first leaky-wave antenna was prototyped, its working principle remained obscure and unexplained, it took other 20 years to have an understanding of the radiation mechanisms, mainly because the leaky radiation can lead to a violation of the Sommerfeld condtion at infinity, and was therefore rejected; in fact, as we will see, leaky waves may increase the amplitude of their field while propagating. It is only through the work of Marcuvitz in [27], and to the joint work of Glodstone and Oliner, on the radiation produced by the leak of power in opened rectangular [28] and circular [29] waveguides, in the late fifties, that we started having an understanding of this form of radiation.

In the remaining sections of this chapter we will illustrate the basic principles around the three mentioned inhomogeneous waves, the reader is redirected to [21] and its references for a deeper insight into the subjects.

2.3.1 Lateral wave

This kind of wave, whose name is due to the characteristic of propagating sideways parallel to the interface, can be found in many different application: for example, it was first discovered in acoustics. In Electromagnetism [30], which is the application relevant to us, such a wave is historically described as

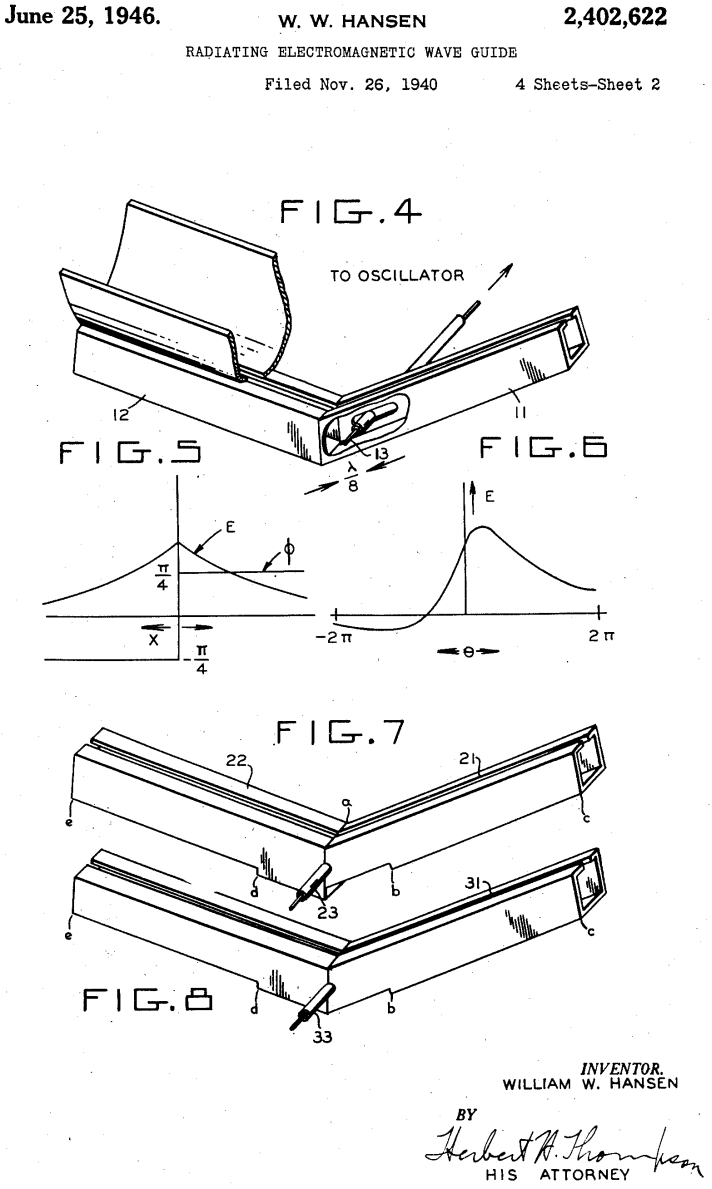

Figure 2.1. The very first leaky-wave antenna, after patent concession $US8264410\ B1$ to Hansen in 1946.

a particular type of surface wave [31] "that occurs when a finite source, for instance a vertical or horizontal dipole is on or near the boundary between materials which have large difference in their wavenumbers" [32], i.e. with quite different characteristic wave velocities. Air to earth interface is a typical example of media interface to which this kind of wave is applicable, where earth intended either as soil, or lake water, or sea water. Another relevant example is constituted by the interface between the sea floor and sea water. In practice, posed a dipole parallel to the separation surface between two media, this wave is propagating on a planar interface on the side of the bottom medium, and it radiates in the top medium [33]. For example, in [31] it is reported the example a horizontal dipole on the surface of a lake that sends out spherical radio waves[4] which radiate both into the air (called region 1) and in the lake (called region 2). The waves traveling in the air have a velocity that well approximate the velocity of the light in a vacuum ($\nu_1 = c$) while the waves in the lake move in water with a speed which approximately nine times slower, i.e. $\nu_2 \approx c/9 = \nu_1/9$. Both the wave front in the air and the one in the water can be observed by receivers: one posed in medium 1 and the other in medium 2. The spherical wave travelling in air along the surface of the water continuously generates lateral waves that propagate into the water with a critical angle determined by the ratio of velocities between the two media [36]: in King's example $\nu_1/\nu_2 = 9$ which is sufficiently large to assume an angle of refraction in the water of $\pi/2$ radians. The receiver, posed in the water, detects the lateral wave before the direct wave since the lateral wave travels in air for most of the path and then only a short distance is covered in water while the direct wave travels entirely in water at one ninth of the speed of the lateral wave.

The described example is reported in Fig. 2.2 and it illustrates the importance of the lateral wave for soil and water subsurface communications.

[4] A point source always generate spherical waves[11], and, independently from the complexity of the radiation, the Huygens-Fresnel principle explains wave propagation itself as the superposition of spherical waves generated at each point along a wavefront [34]-[35].

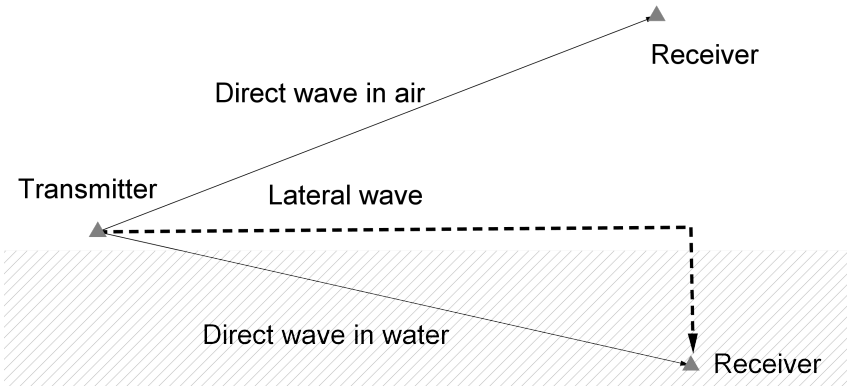

Figure 2.2. Spherical direct wave and lateral wave generated by a horizontal dipole on the air-water surface, after King [31]

Typical applications of the lateral wave are for instance, submarine communications (using both horizontal and vertical dipoles) [31], measurement of the conductivity of the oceanic crust, for exampled carried with a vertical electric dipole [37], or detection of buried bodies [38].

The lateral wave, which as mentioned is useful for detecting objects, sometimes acts as a disturb. A typical example of disturbing lateral wave is found in some radar techniques such as Ground Penetrating Radar (GPR): in this case the forementioned wave can cause anomalous effects of subsurface electromagnetic wave propagation and scattering [39].

From a theoretical point of view, the lateral wave has been accurately and extensively studied in relation to total reflection phenomena not only in electromagnetiscs, but in other environments such as sismics, acoustics and optics; in particular this approach to lateral wave is followed by both Brekhovskikh [30], and Tamir [33], [40]. The works just cited contain extensive and complete lists of references, therefore the reader is referred to those to retrieve a deeper insight on this kind of propagating-wave. As pointed out by Tamir in the chapter 13 of [40] and reported by King in [31], a lateral wave is generated *"by a bundle of rays or a beam of bounded extent at an angle θ close to θ_c ,"* where θ_c is the critical angle of internal reflection. *"A lateral wave is absent if the incident field is an infinite plane wave, so that the realistic finite*

width of the incident field is instrumental in producing the lateral wave. In this context, the lateral wave manifests itself by (a) producing a lateral shift of the bounded reflected field, and (b) exciting a weak field that accompanies the reflected field. Neither of these two effects is accounted for by geometrical optics".

The lateral wave needs therefore high numbers of frequencies and it is necessarily produced by a near-field radiation produced in a medium 1 and in proximity to the interface with a medium 2, having higher permittivity. The lateral wave, finally, is also present in literature with the name of "head wave", even though this term is more commonly used in seismology [31], and "refraction arrival wave". Those different definitions also highlights different important characteristics of the wave. In particular, the name "head wave" indicates that this wave is the refracted wave that provides the first response in certain regions of the medium containing the source, very similarly to the illustration given in Fig 2.2. The "refraction arrival wave" denomination highlights the refraction as a fundamental mechanism in the establishment of this waveform [41].

2.3.2 Surface waves

Even though, as we have seen in the previous paragraph, the lateral wave is sometimes defined as a particular kind of surface wave in literature [31], a surface wave is more strictly defined as a field propagating along a planar surface, but without radiation. This characteristic makes such an inhomogeneous waves strongly different from both the lateral wave, explained in the previous paragraph and the leaky wave, that will be illustrated in the next paragraph, because those two clearly present radiation phenomena. The way in which the surface wave propagates can be recognised as a guiding behavior. The guiding behaviour allowed scientists and engineers to exploit the surface wave in many applications, starting from the half of the last century (see [42]). The surface wave was in particular applied not only to transmission lines [43], which

represent the most logic application, but also, interestingly, for communications [44]. Nowadays, the surface wave still represents a fundamental tool for a set of applications: for instance, they are fundamental in the analysis of guided propagation in open stratified structures [45] and metasurfaces [46]. Moreover, surface waves are of great importance in the development of nanophotonics, where they are applied because such waveforms have the ability of exceeding the diffraction limit [47]. In antenna design, expecially in planar antennas such as microstrip antennas, the surface wave is, instead, a problematic and unwanted mode that needs to be usually reduced or, better, suppressed: many techniques have been involved in years for dealing with this unwanted radiation: photonic band-gap structures (PBG) [48], electromagnetic bandgap (EBG) geometries, and more innovative kind of compact soft-surface [49] or through the introduction of defected ground structures (DGS) [50].

The surface waves presence is an issue in the design of leaky-wave antennas, that can be minimized either implying one of the mentioned techniques or designing the antenna such that it radiates in a region in which the surface wave does not propagate: this approach is followed, for instance, in [51], where the proposed LWA is designed to operate on the fundamental TM_0 mode, instead of the conventional TE_1 mode [52] so that, in the frequency range chosen, a single mode propagates and there is no interference of unwanted surface waves.

2.3.3 Leaky waves

While both the inhomogeneous-wave types presented in the previous paragraphs of this chapter are confined to a region in the proximity of the separation interface between two media, and therefore they cannot achieve large penetration, leaky waves [7] radiate away from the aperture at configurable angles, and this characteristic makes them perfect candidates for exploiting the inhomogeneous wave deep-penetration properties in lossy media.

The leaky-wave properties, as already mentioned, were mainly discovered

through the early work of Oliner [28] and Tamir [53, 54] starting from the late 50s up to the early 70s. The first relevant structures were based on tridimensional rectangular or circular waveguides modified in order to radiate energy leaked either from a continuous fenditure or from periodic slots [28]; later also planar structures were introduced, at first uniform, and then quasi-periodic and periodic: those structures could be either mono-dimensional or two-dimensional, as it is the case of the antenna presented in [55] and [56]. The leaky wave is an electromagnetic field generated by radiation losses that are present in a guiding structure not fully bounded inside a conductor. Note that, when a mode loses energy for radiation, its propagation constant k must contain an attenuation component, therefore the mode must be complex and can describe a leaky mode ([53]-[54]), which represents a continuum spectrum that exist alongside with the typical discrete spectrum of the guided modes.

Leaky waves are called "improper" when they do not satisfy the Sommerfeld condition [57], that, for Electromagnetic fields in a homogeneous, isotropic and non-conducting medium, is described by the so-called Silver-Müller equations [58]:

$$\begin{matrix} \lim\limits_{r\to\infty} r\left(\underline{E} - \eta \underline{H} \times \hat{r}\right) \\ \lim\limits_{r\to\infty} r\left(\underline{H} - \dfrac{\underline{E} \times \hat{r}}{\eta}\right) \end{matrix} \tag{2.26}$$

The Eqs. (2.26) must be verified by any field generated by a finite source. Leaky waves do not satisfy the Eqs. (2.26), despite of this, such waves can be radiated in a limited region of space, by the leaky-wave antennas introduced above [7].

The leaky-wave antennas are structures that can create a narrow beam with high gain and with the property that the beam angle scans varying the frequency. The frequency scan of LWAs, represents both a problem for some applications (e.g. telecommunication), and a fundamental feature for others (radar communications).

We will study in this paper the advantages in terms of penetration in lossy

media that these antennas can guarantee when compared with traditional antenna structures.

2.3.4 Non homogeneous wave generated by planar structures

This dissertation will consider planar leaky-wave antennas, it is therefore necessary to briefly introduce what kind of waveforms planar structures may generate: above all, any radiation generated by planar structures can be simply described in the spectral domain through TE (Transverse Electric) and TM (Transverse Magnetic) [59]-[60], or hybrid (EH,HE) modes.

Let us assume an open and two-dimensional planar guiding structure, in the space (x, y, z), which extends to infinity on the z and x directions. The infinite and planar separation interface with the surrounding medium, e.g. air, appears, instead, on the y direction. The problem is further simplified assuming that all sources are aligned onto the straight line described by $x = 0$ on the (x, z) plane, so that, due to the symmetry of the problem, the components along the x axis can be ignored. The propagation vector, in general complex, can be expressed, according to the separability condition of the structure considered, as:

$$k_0^2 = k_{0y}^2 + k_z^2 = \omega^2 \mu_0 \varepsilon_0 \tag{2.27}$$

where μ_0 and ε_0 are permeability and permittivity of a vacuum, assumed as surrounding medium. In this case, k_0 must be real, therefore, when a complex solution for $\underline{k}$ must be assumed, it follows that only $k_{0y} = \beta_y - j\alpha_y$ and $k_z = \beta_z - j\alpha_z$ are allowed to be complex.

Now, let us graphically show what kind of waves can be achieved from Eq. (2.16) having added the constraints represented by Eq. (2.27). The uniform solution is guaranteed when there are no losses, in this case $\underline{\alpha} = 0$ and the wave simply enters or exit from the separation surface. If (radiation) losses are present, then $\underline{\alpha} \neq 0$ and we may have three categories of wave: either *surface waves*, or waves propagating inside the dielectric ($y < 0$) or, finally, *leaky waves*. All those different set of waves are shown in Fig. 2.3

In particular, the waves illustrated in Figs. 2.3c and 2.3d may be caused by a lossy dielectric in the antenna structure: note that, while this kind of wave requires losses in the structure, the leakage associated to the leaky wave, instead, (Fig. 2.3e and Fig. 2.3f) can exist also when the dielectric is lossless.

All waves shown in Fig. 2.3 may be either proper and improper: in particular all the solutions of Figs. 2.3a, 2.3c and 2.3e are known as improper because the relative direction of $\underline{\alpha}$ in respect to $\underline{\beta}$ produces a field whose amplitude increases moving away from the source of radiation (aperture), resulting in an infinite power at infinite, thus does not respect the boundary conditions at infinite established by Eqs. (2.26).

Among the waveforms presented in Fig. 2.3, only two solutions propagate away from the antenna aperture and therefore they can be investigated to achieve deep penetration: those two solutions are the proper and improper leaky waves; and it will be demonstrated in the following chapters that only the second kind of leaky radiation can produce deep-penetration on a lossy medium when the planar separation interface is chosen parallel to the antenna aperture.

It is worth recalling, finally, that in typical planar structures more than one kind of mode can be present in a given frequency range, therefore, when surface waves are present in the region of the wished leaky wave, it is usually essential to eliminate, or at least reduce, the surface-wave solutions.

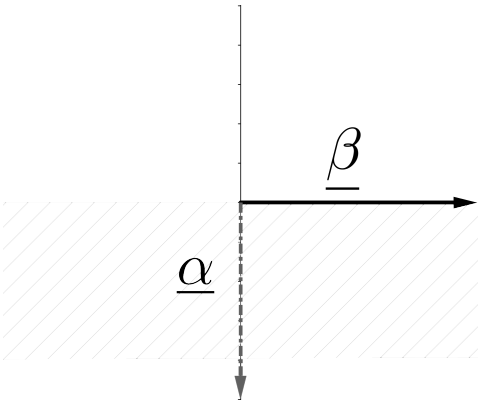

(a) Improper surface wave

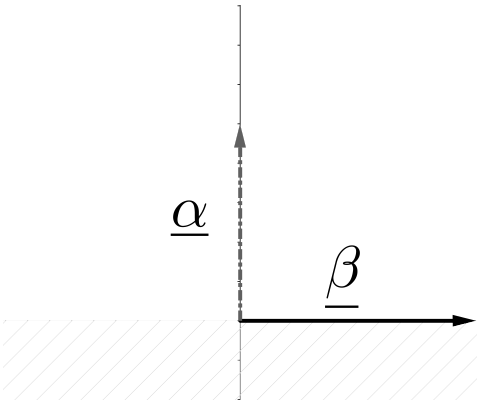

(b) Proper surface wave

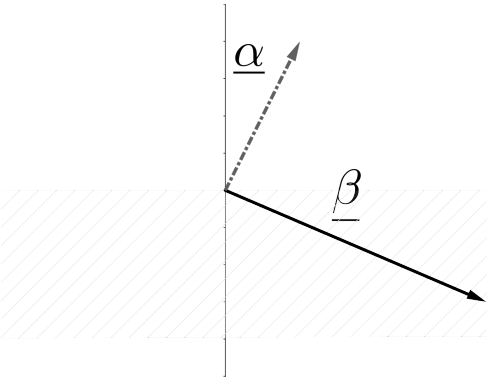

(c) improper wave penetrating in the the radiating structure

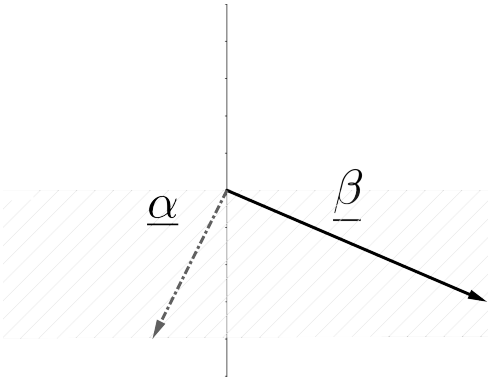

(d) proper wave penetrating in the the radiating structure

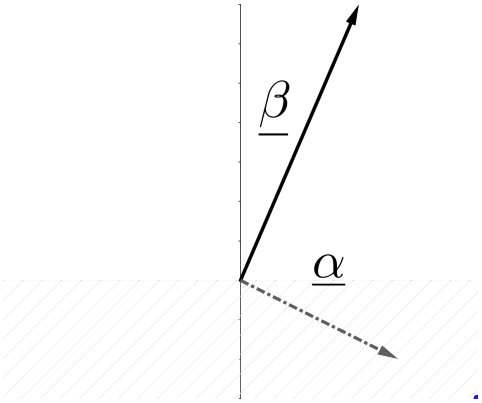

(e) Improper wave radiating away from the radiating structure (leaky wave)

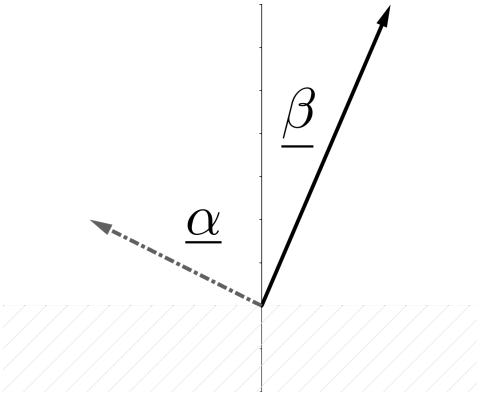

(f) Proper wave radiating away from the radiating structure (leaky wave)

Figure 2.3. Possible inhomogeneous-wave solutions generated by planar and opened waveguides.

Chapter 3

Microstrip leaky-wave antennas

3.1 Abstract

In the previous chapter, leaky waves were defined, in this chapter a brief description of Leaky-Wave Antennas (LWAs) and their properties is presented. After this short and necessary introduction, the properties and layout of the microstrip LWA derived from the Menzel antenna will be fully described because this LWA structure resulted the most suitable for deep penetration, and therefore it was designed, optimised, and simulated to numerically verify the deep-penetration properties of inhomogeneous waves.

3.1.1 Introduction to leaky-wave antennas

All leaky-wave antennas are representable as guiding structures whose power leakage creates radiation. We have seen that the very first example of such an antenna was designed by Hansen in 1940 and it was constituted by a rectangular wave guide with a longitudinal slit cut [26]. The antenna prototype was shown in Fig. 2.1 and a sketch that shows the working principle of the structure is reported in Fig. 3.1.

The antenna aperture of such a homogeneous LWA can be shorter or equal to physical slit cut, depending on the intensity of the power leaked. If the leakage is strong enough, all the power is radiated before the end of of the slit,

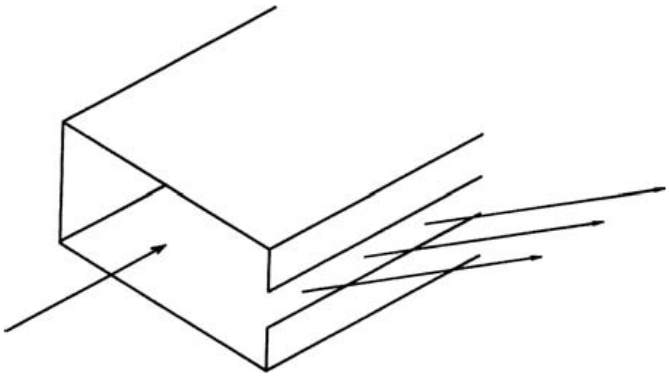

Figure 3.1. Hansen leaky-wave antenna: design principle (after Volakis Ch. 11)

this causes the antenna aperture to be shorter than the slit length, otherwise the two apertures coincide.

In particular, a larger cut cross-section implies larger losses, consequently a larger beam and a shorter electrical antenna aperture. The antenna just described is defined mono-dimensional (or 1-D) and uniform. Several different types of LWAs were developed after the very first prototype mentioned, and we won't list them all here, anyway an appropriate overview may be found in [7].

It is worth mentioning that the LWAs are divided into categories depending on their geometrical layout into mono-dimensional, or 1-D, and two-dimensional, or 2-D. A further division is done depending on the periodicity of the structure geometry, i.e. LWAs can be uniform, quasi-uniform or periodic.

A mono-dimensional LWA is an antenna in which the guiding structure is mono-dimensional: such a structure permits to generate a wave travelling in a single direction (forward direction, $z > 0$); for such a structure it is arduous to obtain a radiation at broadside using a single feeder, this happens because the frequency of the broadside radiation coincides with the cut-off frequency of the leaky-wave antenna. The radiation at broadside, if needed, can be achieved through a workaround obtained for instance by radiating just above the cut-off frequency and feeding the structure from both terminations.

3.1.2 LWA attenuation and phase vectors

The leaky wave is characterised by a complex propagation vector, i.e. by a phase vector $\underline{\beta}$ and a non-null attenuation vector $\underline{\alpha}$.

The radiation in a leaky-wave antenna occurs through a fast wave, i.e. $\beta_z < k_0$, assuming the longitudinal direction of the guiding structure directed towards the z direction, and assuming to radiate in a vacuum, whose wave-number is defined as $k_0 = \omega\sqrt{\varepsilon_0\mu_0}$. LWAs are usually designed to radiate from 90% to 95% of the power, while the remaining power is absorbed by a load that terminates the antenna.

The attenuation (longitudinal) number α_z, in general, affects the beamwidth, but, when the antenna aperture is chosen such that α_z is small enough, then the dimension of the aperture characterises the beamwidth but α_z impacts mainly on the efficiency of the radiation and its effects on the beamwidth are only secondary [8].

The phase (longitudinal) number β_z controls, instead, the scanning angle. To understand how the scanning angle depends on β_z, let us assume a uniform guiding structure having longitudinal direction on the z axis, which corresponds to the guided wave propagation direction; let us put the cross section on the x axis and let us assume that the power is leaked along the y axis. Let us impose, without loss of generality, that the electric field distribution produced is linearly polarised: $\underline{E} = E_x(y,z)\,\underline{y}_0$.

In particular, let us pose, again without loss of generality, the antenna aperture on the $y = 0$ plane, then the field at the aperture must be described by:

$$E_x(0,z) = Ce^{-j\underline{k}\cdot\underline{r}}$$

being $\underline{k}$ the phase vector and $\underline{r}$ a vector laying on the $y = 0$ plane. For the symmetry imposed by the chosen structure, which does not depend on the x direction, it needs to be:

$$E_x(0,z) = Ce^{-jk_z z}$$

Now let us assume the presence of radiation losses. We have seen in the previous chapter that a loss always requires a complex wave number; therefore (longitudinal) wave number k_z must be composed of a phase constant β_z and a leakeage constant α_z, i.e. $k_z = \beta_z - j\alpha_z$. Above the radiating structure ($y > 0$), it must be:

$$E_x(y,z) = Ce^{-jk_z z}e^{-jk_y y}$$

Assuming to radiate in a vacuum, it is $k_y^2 + k_z^2 = k_0^2$, i.e.:

$$\beta_y^2 - \alpha_y^2 - 2j\alpha_y\beta_y + \beta_z^2 - \alpha_z^2 - 2j\alpha_z\beta_z = k_0^2$$

which, separating real and imaginary parts gives:

$$\begin{cases} \beta_z^2 + \beta_y^2 - (\alpha_z^2 + \alpha_y^2) = k_0^2 \\ \alpha_y\beta_y = -\alpha_z\beta_z \end{cases} \tag{3.1}$$

If the wave leaks in the positive y direction ($\beta_y > 0$) and $\alpha_z > 0$, then $\beta_z > 0$ implies $\alpha_y < 0$, i.e. the field increases at infinity violating the Sommerfeld condition, the wave produced in this way is said *improper*. If instead $\beta_z < 0$, then it is $\alpha_y > 0$, and the wave is said *proper*. Both proper and improper leaky-wave solutions can be generated through LWAs, even though not all LWAs can generate both: while periodic structures can generate both proper and improper leaky waves, uniform structures can only generate improper solutions. For both proper and improper solutions α_z must be assumed positive[1], therefore the direction of β_z varies generating the two different waveforms. The leaky wave obtained by means of a LWA is also defined in literature as "forward" when $\beta_z > 0$ and as "backward" when $\beta_z < 0$.

We adopt in this chapter the convention for which θ_0 is defined as the angle of maximum radiation that the phase vector $\underline{\beta}$ ($\underline{\beta} = \beta_y \underline{y}_0 + \beta_z \underline{z}_0$) forms with

[1] it is an obvious assumption, because α_z exists because of the presence of radiation losses

the end-fire direction, i.e. the z axis [7]. This is not the only convention used in the literature, often, the complementary angle is instead considered, in this case θ_0 is defined as the angle of maximum radiation that the phase vector $\underline{\beta}$ forms with the broadside direction [8].

The convention chosen maps directly into the conventional spherical coordinate system represented in Fig. 3.3. From the definition given for the θ_0 angle, it follows:

$$\theta_0 = \arctan\left(\frac{\beta_z}{\beta_y}\right)$$

Assuming a small value for the amplitude α of the attenuation vector $\underline{\alpha}$, then $k_0 \approx \beta$, and it follows:

$$\beta_z = \beta\cos\theta_0 \approx k_0\cos\theta_0$$

, so:

$$\theta_0 \approx \arccos\left(\frac{\beta_z}{k_0}\right) \tag{3.2}$$

Usually β_z is simply indicated as β in the LWA literature (see for instance[7] and [8]), anyway we will not adopt such a notation here to avoid confusion between the tangential component of $\underline{\beta}$ and the amplitude of $\underline{\beta}$ which we already indicated with β. It is crucial to distinguish the two components using different notations because both amplitude and tangential component of the phase vector are extensively used in this dissertation.

The frequency-scanning ability, which is fundamental in radar applications (see for instance [61], [62], [63], [64], and [65]), where LWAs are successfully employed, it is not, instead, an important feature here, therefore the LWA will be designed to radiate at a specific beam angle opportunely chosen.

3.2 Uniform LWA having finite longitudinal length

Let us now consider an uniform LWA having finite dimension on the z longitudinal direction, and whose electromagnetic source is placed at one extreme of the longitudinal length, that for simplicity we set at the origin of the axes, in particular the source is at $z = 0$ on the longitudinal direction: this configuration will be exploited for the final antenna design presented in the next chapters, where a waveguide port will be used as field source.

The working principle for this uniform leaky-wave antenna can be derived looking at Fig. 3.2 where the presence of a shadow cone, in which the field is negligible, needs to appear, as it is easy to guess. The shadow cone is centered on the the origin of the axes, where the field source is present, and has an angular amplitude of $\phi = \pi/2 - \theta_0$, being θ_0 the angle for which the field is maximum.

Such a shadow cone is never present, instead, in the case in which the antenna has infinite source distributed along the antenna and infinite amplitude along its longitudinal direction, because, in such a structure, the field projected in free space from previous sections of the leaky-wave antenna is always present.

Let us study now the effects of the shadow cone on the leaky-wave radiation: let us take a vertical segment on the y axis posed at a longitudinal quota $z_i > 0$ on the z axis. The field increases on the y direction from $y = 0$ to $y = y_{MAX}$. The line passing for the origin of the axis and (z_i, y_{MAX}) forms an angle $\theta = \theta_0$ with the z axis; in (z_i, y_{MAX}) the shadow cone is met and the radiation start decreasing rapidly for $y > y_{MAX}$, i.e. the electromagnetic field decays.

The shadow cone describes the region in which the finite uniform structure behaves as a LWA, and it ensure that the Sommerfeld condition is satisfied: for the study of this dissertation, such a cone describes how long the deep-penetration can be sustained by an uniform LWA.

Let us now study the radiation characteristics of the antenna considered. To simplify the problem let us assume the LWA geometry as a half line on the z axis having origin in $z = 0$; the source is, instead, finite and concentrated

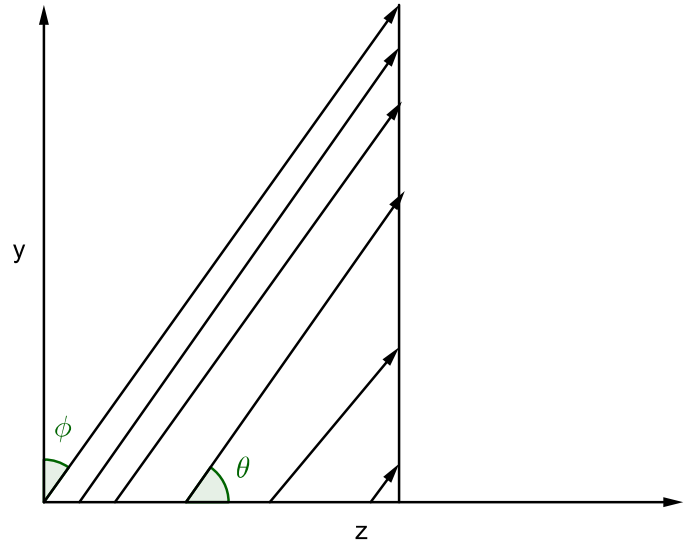

Figure 3.2. Uniform LWA structure radiating from the origin of the z axis. The density of the rays drawn is higher toward the origin of the aperture to show that there is more power leaked near the source. Note the shadow cone described by the angle ϕ and the radiation angle θ.

at $z = 0$. The semi-line design approximates the scenario in which a finite LWA length is assumed but the power is almost fully radiated by the LWA before arriving to its termination. The field along the aperture is given by the following expression:

$$E_x(0, z) = Ae^{-jk_z z}, \ z > 0 \tag{3.3}$$

therefore it decreases exponentially, with attenuation constant α_z. The exact distribution of the electrical field at a given point in the (y, z) plane can be evaluated using the Fourier transform commonly used for the *aperture antennas* [66]:

$$E_x(y, z) = \frac{1}{2\pi} \int_{-\infty}^{+\infty} \widetilde{E}(0, K'_z) e^{-jk'_z z} e^{-jk'_y y} dk'_z \tag{3.4}$$

where $\widetilde{E}(0, K'_z)$ is:

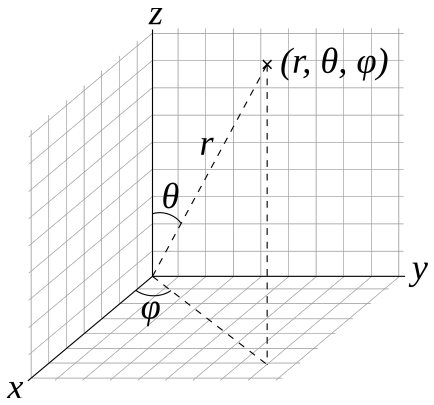

Figure 3.3. Adopted spherical coordinate system. Note that the definition of θ is congruent with the formalism adopted for the beam angle of the wave generated by a leaky-wave antenna (see Fig. 3.2).

$$\widetilde{E}(0, K_z') = A\left[\frac{2jk_z}{k_z'^2 - K_z^2}\right] \tag{3.5}$$

It is also possible an alternative approach that requires the use of image theory and equivalence principle ([18] and [9]): through such an approach it can be concluded that the radiation of the leaky field in $y > 0$ is approximately due to a z-direction magnetic current flowing along the z axis of the form $J(z) = Ae^{-jk_z z}$ [7], the magnitude of the far field produced by such a distribution on the $0 < z < +\infty,\ y > 0$ quarter of space, is [7]:

$$|E_\phi(r,\theta)| = |A|\left|\frac{e^{-jk_0 r}}{4\pi r}\right|\sqrt{\frac{\sin^2\theta}{(cos\theta - \beta_z/k_0)^2 + (\alpha_z/k_0)^2}}\ ,\ ^{2} \tag{3.6}$$

where θ, ϕ and r are the spherical coordinate system reference described in Fig. 3.3.

The radiation pattern shape in far-field is independent on the radius r [18], therefore, removing the A constant and the factor depending on r (which is therefore assumed constant, as usual) which do not contribute to the radiation pattern shape, it is [8][3] :

[2]Refer to [7] for further details

[3]Note, again, that θ in Eq. (3.7) is the complementary of θ presented in [8], therefore $\cos\theta$ is present here while in [8] the equation is function of $\sin\theta$.

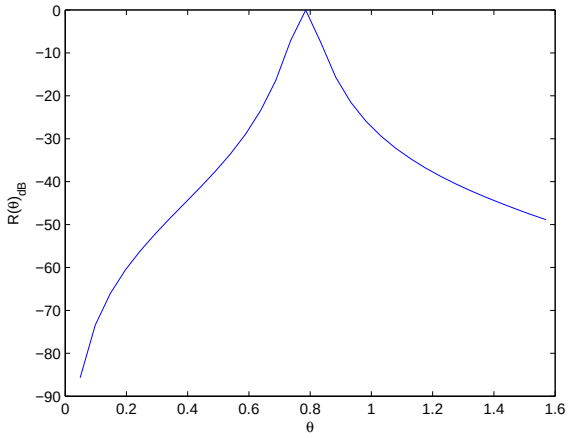

Figure 3.4. Radiation pattern $R(\theta)$ generated by a uniform mono-dimensional LWA, of infinite length on the longitudianl direction ($z > 0$), expressed in dB and evaluated for every value of $\theta \in [0, \pi/2]$, $\beta_z/k_0 = 0.71$ and $\alpha_z/k_0 = 0.03$.

$$R(\theta) = \frac{\sin^2\theta}{(cos\theta - \beta_z/k_0)^2 + (\alpha_z/k_0)^2} \tag{3.7}$$

For every value of β_z/k_0 this function describes a curve that starts from its minimum (at $\theta = 0$, increases up to its maximum at $\theta = arcos(\beta_z/k_0)$ (in the hypothesis that $\alpha_z << k_0$) and then it decreases again quickly encountering the shadow cone, a typical example of radiation pattern is given in Fig. 3.4, where $R(\theta)$ is plotted in dB for $\theta \in [0; \pi/2]$, $\beta_z/k_0 = 0.71$ and $\alpha_z/k_0 = 0.03$. The total absence of grating lobes is due to the infinite dimension on the longitudinal direction of the LWA described by Eq (3.7); we will see, in the next chapter, that grating lobes do appear when a finite dimension is imposed.

To see how the maximum radiation angle relates to the $\beta_{zn} = \beta_z/k_0$ ratio, it is simpler to consider R as a function of $\chi = \cos\theta$:

$$R(\chi) = \frac{1 - \chi^2}{(\chi - \beta_{zn})^2 + (\alpha_{zn})^2} \tag{3.8}$$

Fig. 3.5 shows $R(\chi) \forall \chi \in [-1,\ 1]$ normalised by its maximum value when $\beta_{zn} \in [0; 1]$ and $\alpha_{zn} = 0.01$. Finally, the maximum of $\chi = \cos\theta$ as a function of β_{zn} is shown in Fig. 3.6 for the same β_{zn} and α_{zn} values: it is easy to verify

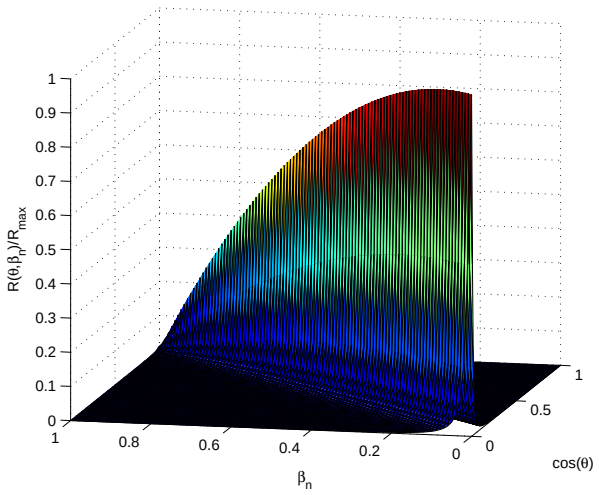

Figure 3.5. Radiation pattern $R(\chi = cos\theta)$ normalised by its maximum amplitude and generated by an uniform mono-dimensional LWA of infinite length on the longitudianl direction ($z > 0$). $R(\chi = cos\theta)$ is evaluated for every value $\chi \in [0, 1]$, for $\beta_{zn} = \beta_z/k_0 \in [0; 1]$ and for $\alpha_{zn} = \alpha_z/k_0 = 0.01$.

that $\theta \approx \theta_0$ where θ_0 is the one previously given in (3.2). The radiation pattern is shown in Fig. 3.5, where the resulting beamwidth of the is very narrow.

In general, for 1-D LWA of finite longitudinal length L, the beam width depends primarily on the leaky-wave longitudinal dimension L through the following [8]:

$$\Delta\theta \approx \frac{C}{(L/\lambda_0)\sin\theta_0} \tag{3.9}$$

Follows from Eq. (3.9) that the beamwidth mainly increases reducing the length L, being θ_0, again, the angle of the maximum of the beam defined as in (3.2). The parameter C assumes instead different constant values depending on the geometrical aperture: for a constant, non-tapered, aperture distribution it is usually assumed $C \approx 0.88$ while for tapered apertures $C \geq 1.25$. The value $C = 1$, which is an average of the two may be assumed when there is no indication on the specific aperture distribution [8]. In our project we won't taper the antenna distribution (to have a higher α value), therefore $C \approx 0.88$ should be taken.

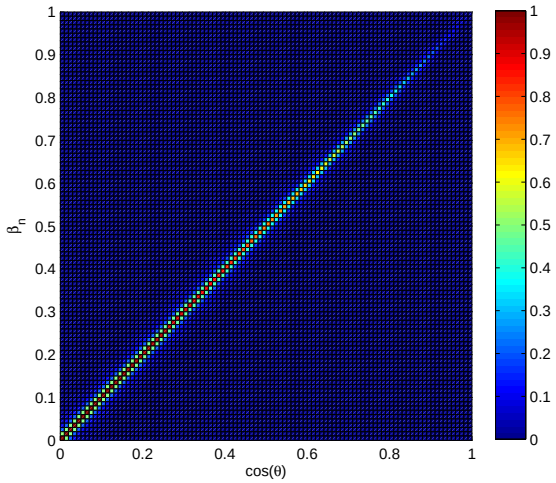

Figure 3.6. χ values for which the radiation pattern $R(\chi = cos\theta)$ generated by an uniform mono-dimensional LWA, of infinite length on the longitudianl direction ($z > 0$), is maximum assuming $\beta_{zn} = \beta_z/k_0 \in [0; 1]$ and $\alpha_{zn} = \alpha_z/k_0 = 0.01$.

Finally, it is possible to decide the correct antenna length to be applied for a given radiated power percentage, because the power at the load must necessarily be $P(L) = e^{-2\alpha_z L}P(0)$, therefore:

$$\frac{L}{\lambda} = -\frac{1}{2\alpha_z\lambda}\ln\frac{P(L)}{P(0)} = -\frac{1}{4\pi}\frac{k_0}{\alpha_z}\ln\frac{P(L)}{P(0)} \tag{3.10}$$

3.3 Microstrip

The Microstrip is one of the simplest planar structures and one of the most succesful, too. It is employed in a vast range of frequencies, from microwave to millimeter wavelenghts. The microstrip was firstly prototyped in 1952 [67] as a guiding structure and in 1953 [68] as an antenna structure. The Microstrip simply consists of a conducting strip and a ground plane separated by a dielectric slab called “substrate”, whose relative permittivity ε_r is usually greater than the one of the air. This structure, shown in Fig. 3.7 resembles very closely a parallel-plate guide in which one of the plates is smaller, on the cross-section, than the other. The success of the Microstrip is mainly

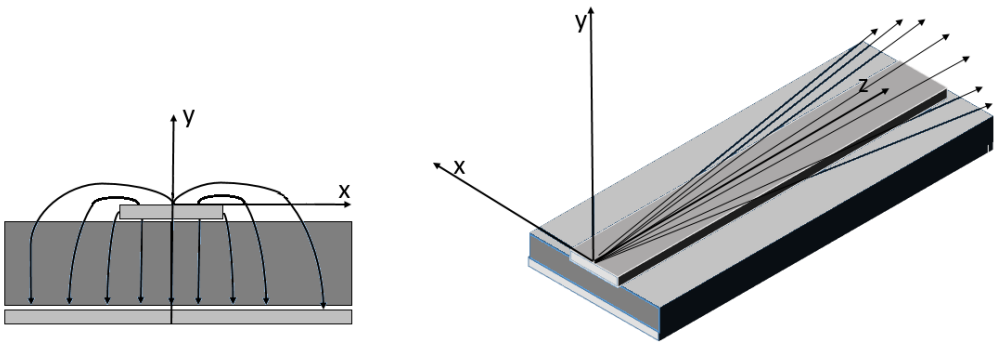

Figure 3.7. Microstrip LWA: sketch of the electric field of the Q-TEM bounded mode (left) and of the leaky-wave radiating mode (right).

related to its low profile, low cost, light weight, easy of fabrication and easy accommodation of curve lines. The Microstrip shows, anyway, limits when compared to waveguides in terms of both maximum power handling and losses: in particular losses are also larger than the ones present in the Stripline[4]. The asimmetry of the Microstrip causes the electromagnetic field of its bounded fundamental mode to propagate partially in air and partially in the Microstrip substrate, i.e. the propagation happens in an inhomogeneous medium, for this reason the Microstrip does not support a TEM mode, which is instead supported by both the parallel plate guide and the Stripline.

In general, the modes in the Microstrip are instead hybrid (both electric and magnetic fields possess longitudinal components). However, the dielectric substrate is usually electrically very thin, yielding longitudinal components much smaller than transverse components: this allows for a quasi-TEM approximation (QTEM) of the fundamental mode [67]. Most of the electric field lines of the QTEM fundamental mode reside in the substrate and only small parts of some lines are in the air, as illustrated in Fig 3.7.

Instead of studying the Microstrip in an inhomogeneous environment, the microstrip line, in its whole, can be studied considering it as a guiding line

[4]The Stripline was invented by Robert M. Barrett of the Air Force Cambridge Research Centre in 1950, preceding the inventionof the Microstrip that was then presented as a possible alternative to such a structure.

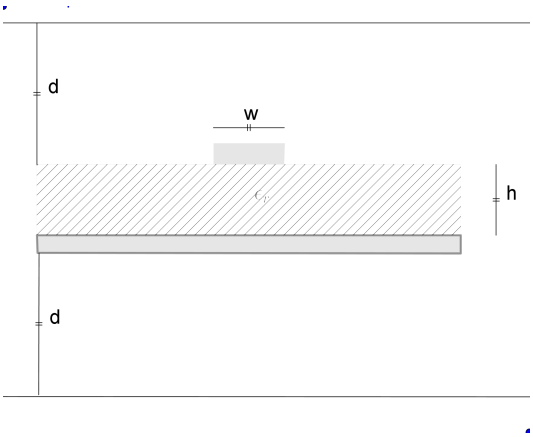

Figure 3.8. Microstrip structure studied by Ermert to derive the higher order radiation modes in the LWA. In [72] the following values were chosen: $d = 5h$, $h = 0.635\ mm$, $w = 3\ mm$, $\varepsilon_r = 9.8$.

composed by a homogeneous dielectric whose dielectric constant is greater than the one of the air, but smaller than the one of the substrate: this average permittivity is denominated in literature *effective permittivity*, and, for the QTEM mode, is closer to the one of the substrate, because, as said, most of the field lines reside in the substrate (see Fig. 3.7) [69]. This strategy of considering an effective averaged quantities is not limited to the Microstrip, but it is also popular in periodical 2-D LWAs, where the top plane is assumed as a PRS (Partial Reflective Screen) whose equivalent impedance is close to the one of the chosen metal so that the Transverse Resonance Method can be used [70].

Even though the fundamental mode in a Microstrip is always bounded and does not radiate, higher order modes may be able to radiate away from the antenna. In 1975 Ermert [71]-[72] first reported the propagation constant of the higher order modes on a microstrip line, but he discarded the leaky-wave improper solutions as non physical. The study was carried on a covered microstrip (several times the dielectric layer thickness) where the cover was both above the microstrip line and below the groundplane, the structure studied by Ermert is shown in Fig. 3.8.

Menzel first presented a microstrip LWA back in 1979, but he did not

realize the leaky nature of the radiation, even though he supposed that such a radiation was due to propagation of high order modes in the Microstrip, as it would be reasonable to expect considering the bounded nature of the fundamental QTEM mode. However, the result achieved by Menzel was quite puzzling at the time because, as mentioned, in 1976 Ermert [71] showed that such a mode could not exist in the given frequency range. Then, Oliner and Lee in [73] and then Oliner in [74], completed and corrected the study of the propagation of high order modes on a Microstrip operated by Ermert, and recognised that Ermert's "radiation" region associated to the Menzel antenna was characterized in *"a highly convergent manner by essentially a single leaky mode"*, this study was performed through the Transverse Resonance Method (TRM), in which the Microstrip structure was represented as a section of parallel plate transmission line having two complex impedances at the two ends, derived using the Wiener-Hopf approach [75]: such complex impedances described the discontinuity that appears between the parallel plate and the grounded electric slab. The TRM resulted in a dispersion relation that leaded to a Sommerfeld integral [76] which was then analysed through the Steepest-Descent method [77]-[78] around the two poles. It was demonstrated that the two poles were related to different form of leakeage: the first pole corresponded to a space-type leakage and the second pole is related to a surface-type leakage and it was due to power lost from the microstrip into the TM_0 mode of the dielectric substrate.

In total three different propagation regime modes where therefore found:

- A bounded-mode regime (the fundamental EH_0 mode is always part of this regime), characterised by a real longitudinal propagation constant in the approximation of low losses.

- A surface-wave regime, whose longitudinal propagation constant is complex but with tiny imaginary part ($\alpha_s \to 0$) so that the radiation is confined to the surface of the conductor. This kind of radiation is excited in the film layer of the integrated circuit background structure. Surface

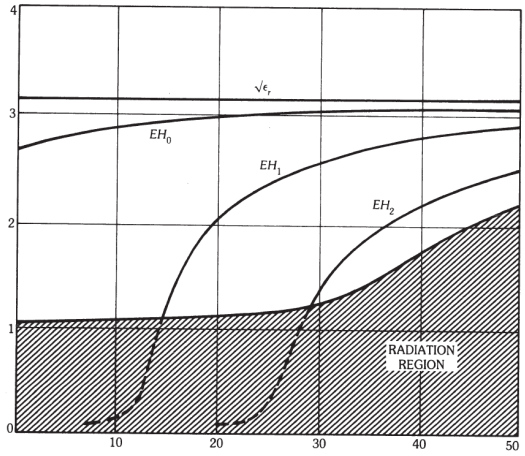

Figure 3.9. Dispersion diagram obtained for the Microstrip, with a top cover, shown in Fig. 3.8, in abscisse the Frequency expressed in GHz and in ordinate the normalised β_z/k_0 magnitude are shown. The dashed lines represent the improper leaky modes added by Lee and Oliner ([73] and [74]). (*After Oliner and Lee* © 1986 IEEE [73])

.

waves travel away from the axis of the transmission line, and energy from the transmission line mode is transferred to these unguided modes.

- A propagation regime. This is a radiation regime, characterized from relatively large amplitude of the longitudinal attenuation constant $\underline{\alpha_l}$ (i.e. $\alpha_l >> \alpha_s$). This kind of radiation is generated from both excitation of surface waves in the film layer and the radiation into the cover medium surrounding the microstrip line.

The third regime is usually strictly named "leaky-wave regime", but in literature every kind of non-bounded regime may be defined as leaky, therefore both the second and the third kind of propagation regime may be defined sometimes as leaky, like it happens in [79]. We will only refer the third regime as leaky.

In Fig. 3.9 the modes, both originally evaluated by Ermert and after the correction of Oliner in [74] are shown, in particular the area corrected by Oliner and Lee is shown as *dashed*.

Let us look at Fig. 3.9. As mentioned, two kind of radiation are possible,

leaky waves and surface waves: the surface wave has a wave number k_s containing component in both z and y direction, the component on z direction is the same as the one of the leaky wave, since all the constituents are part of the same leaky modal field, it is therefore $k_z = \beta_z$. The dispersion relation is $k_y = k_s^2 - \beta_z^2$; the leakeage requires $k_y \in Re \Rightarrow k_y^2 > 0$, it follows that the leakeage is only possible if $\beta_z < k_s$, this region is the radiation region, and it is dashed in Fig. 3.9. So, when β_z decreases below k_s the power leaks away in the form of a surface wave and, if the power is further decrease a space wave appears.

After this first approach to the microstrip LWA due to Oliner and Lee, several researchers dedicated their time to the microstrip LWA, for instance, in [79] an approach based on the spectral-domain integral equation was proposed, then the Method of Moments was applied to the integral equation to obtain the numerical results. A similar approach will be adopted in this dissertation to obtain a microstrip LWA capable of deep penetration.

Part II

Analytic considerations on deep-penetration conditions for plane waves

Chapter 4

Previous results concerning penetration of inhomogeneous waves

This chapter analyses former theoretical studies which illustrate, either explicitly or implicitly, deep-penetration characteristics of inhomogeneous waves in lossy media. Such studies constitute theoretical background on top of which the analytical study deployed in this dissertation was built. This dissertation deals specifically with the case of an inhomogeneous wave incoming from a a lossless medium and impinging on a lossy medium through a planar interface, where both media are assumed homogeneus, isotropic and non magnetic. Comments and analysis present in the current chapter are mostly oriented to such a context.

4.1 Penetration properties of inhomogeneous and homogeneous waves

The idea behind the deep-penetration achievement by means of inhomogeneous waves is, in principle, immediate and it is a direct consequence of the conservation of the tangential component of electric and magnetic fields at

the planar interface between two media [11], which is applicable to all media apart from PEC (Perfect Electric Conductors), characterised by $\sigma \to \infty$, and PMC (Perfect Magnetic Conductor), characterised by $\sigma_m \to \infty$[1] When PEC and PMC are considered, surface electric current J_s and the magnetic surface current J_{ms}, respectively, need to be introduced, i.e.:

$$PEC : \hat{n} \times \underline{E} = 0;\ \hat{n} \times \underline{H} = \underline{J}_s.$$

$$PMC : \hat{n} \times \underline{H} = 0;\ \hat{n} \times \underline{E} = -\underline{J}_{ms}.$$

In the above equations $\hat{n}$ represents the unit-vector normal to the planar infinite separation surface between two media. Conservation of tangential component of the magnetic field does not yield for PEC media and the one for electric field does not apply to PMC media [80]. Anyway, both PEC and PMC are purely mathematical abstractions and therefore they can be neglected: doing so, we can assume that the tangential component is always conserved at the planar boundaries between two media.

In general, when a homogeneous wave incoming from a lossless medium impinges on a separation surface with a lossy medium, than a transmitted wave is produced; for such a wave the attenuation vector $\underline{\alpha}_2$ must always exist and its amplitude needs comply with the expression given in Eq. (2.18). Anyway, under the reasonable assumption that the tangential components of electromagnetic field are always conserved, we have to distinguish two different scenarios. If the incoming wave is homogeneous (i.e. attenuation vector $\underline{\alpha}_1 = 0$), then the direction of $\underline{\alpha}_2$ is forced to be orthogonal to the separation surface, minimizing the penetration, as it can be seen in Fig. 4.1: this is due to the fact that, independently from the incident angle, no attenuation vector exists for the incident wave, therefore a null tangential component must be conserved for such a vector.

If the incident wave is, instead, inhomogeneous, then, a tangential compo-

[1] The σ_m is just an abstration to allow simmetry of the Maxwell equations, and to allow the applicability of the equivalence principle[80].

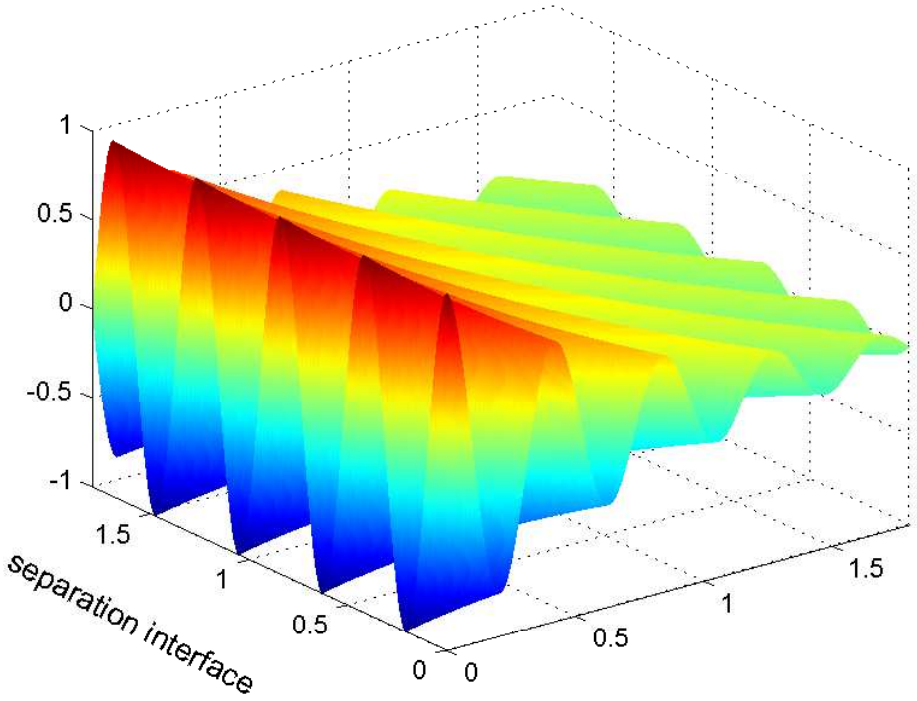

Figure 4.1. 1 GHz nplane wave of 1 Volt amplitude propagating in a lossy medium ($\sigma = 0.005\ S/m$) with a propagation angle $\xi_2 = \pi/4$ and having attenuation vector normal to the separation interface

nent of $\underline{\alpha}_2$ must exist[2]: the existence of this component may have beneficial effect on the penetration depth as, for instance, it is shown in Fig. 4.2, where $\underline{\alpha}_2$ is tangent to the separation interface, this means that there is no attenuation in the direction of penetration, which is different from the direction of propagation that is, instead, 45^o in Fig. 4.2.

The waves produced in a lossy medium illustrated in Figs 4.1-4.2, and produced by varying the direction of the $\underline{\alpha}_2$ vector, are also reported in Fig. 4.3 using a planar view to allow an easier comparison between the two proposed scenarios.

[2]Remember that in the lossless medium is $\underline{\beta}_1 \perp \underline{\alpha}_1$ therefore, if the wave penetrate, which means that the incident angle is not 90^o, then the direction of $\underline{\alpha}_1$ cannot be orthogonal to the interface between the two media.

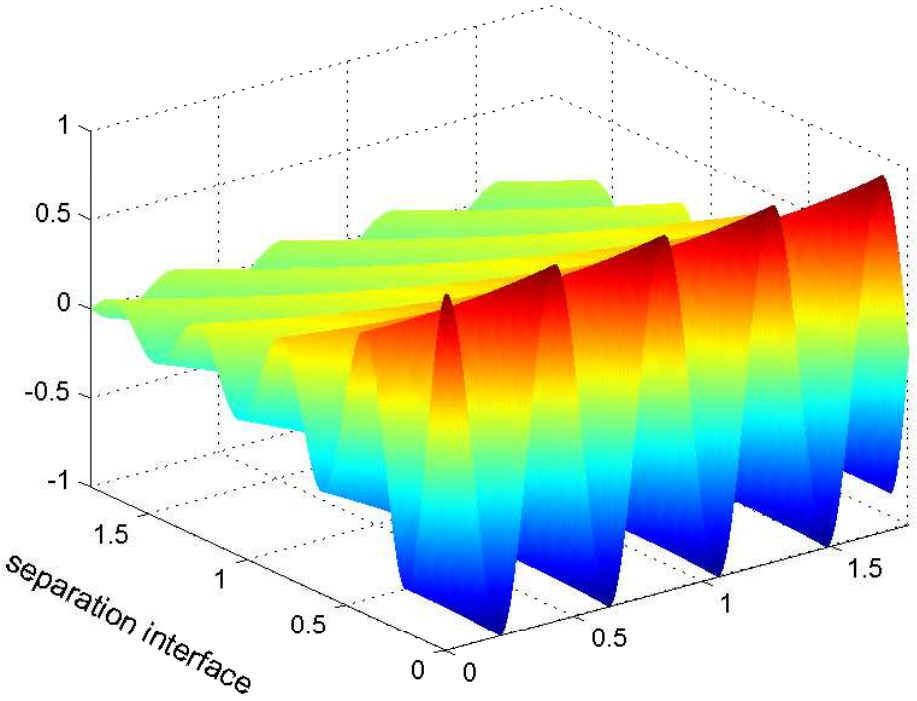

Figure 4.2. 1 GHz plane wave of 1 Volt amplitude propagating in a lossy medium ($\sigma = 0.005\ S/m$) with a propagation angle $\xi_2 = \pi/4$ and having attenuation vector parallel to the separation interface

Eqs. (2.17) and (2.18) show that, in a lossy medium[3], the only degree of freedom for both the amplitudes of phase vector $\underline{\beta}$ and attenuation vector $\underline{\alpha}$, once both the medium and the operating frequency are known, is given by the amplitude of the angle θ that $\underline{\beta}$ forms with $\underline{\alpha}$. A degree of freedom is also given to the direction of the transmitted wave, that depend on the incident angle through the Snell law.

We are going to demonstrate that, in the case in which the plane wave in the lossy medium is produced by means of a plane wave impinging on the separation surface, the amplitude of θ and the direction of both $\underline{\alpha}_2$ and $\underline{\beta}_2$ directly depends on the incident wave, and on the lossy medium characteristics.

[3]The formulations shown are only valid in a lossy medium.

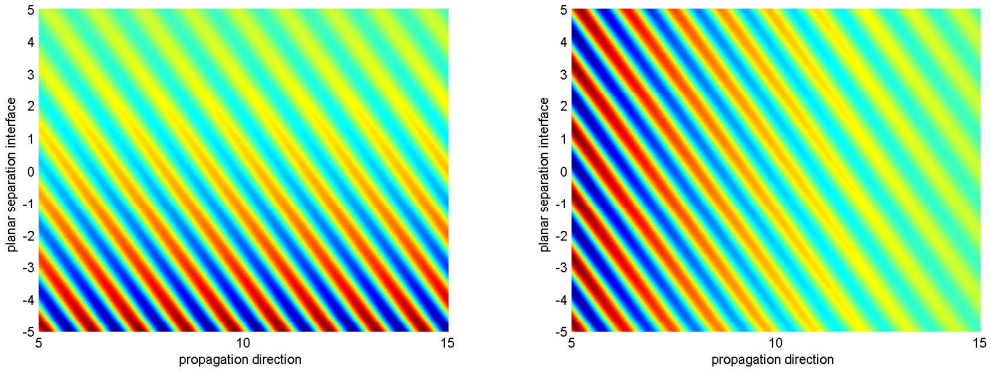

(a) Transmitted wave produced by an inhomogeneous incident wave, 2D view

(b) Transmitted wave produced by a homogeneous incident wave

Figure 4.3. Comparison, on a two-dimensional plane, between the plane wave illustrated in Fig. 4.1 and the one illustrated in Fig. 4.2.

4.2 Problem description

Let us now introduce some symbols and formalism that will allow to simplify the description that follows. We are going to consider a plane wave incoming from a homogeneous, isotropic and, in general, lossy medium, but that may be also lossless. In particular we will consider the lossless medium explicitly in the second part of this chapter. Such a medium is defined, for sake of brevity, as medium 1 (white in Fig. 4.4). The plane-wave, incoming from medium 1, impinges on an infinite planar interface with a homogeneous and isotropic medium 2 (gray in Fig. 4.4) which, instead, is assumed lossy always. Both media are assumed non-magnetic. The geometry of the problem is illustrated in Fig. 4.4.

The phase vector of the incident wave is $\underline{k}_1 = \underline{\beta}_1 - j\underline{\alpha}_1$, where, as usual, $\underline{\beta}_1$ represents the phase vector and $\underline{\alpha}_1$ the attenuation vector, ξ_1 and η_1 are the angles that $\underline{\beta}_1$ and $\underline{\alpha}_1$ form with the normal to the separation surface, respectively, while θ_1 is the angle that $\underline{\beta}_1$ forms with $\underline{\alpha}_1$. Analogously, for the transmitted wave, the wave vector is $\underline{k}_2 = \underline{\beta}_2 - j\underline{\alpha}_2$, where $\underline{\beta}_2$ is the phase vector and $\underline{\alpha}_2$ the attenuation vector, ξ_2 and η_2 are the angles that $\underline{\beta}_2$ and $\underline{\alpha}_2$

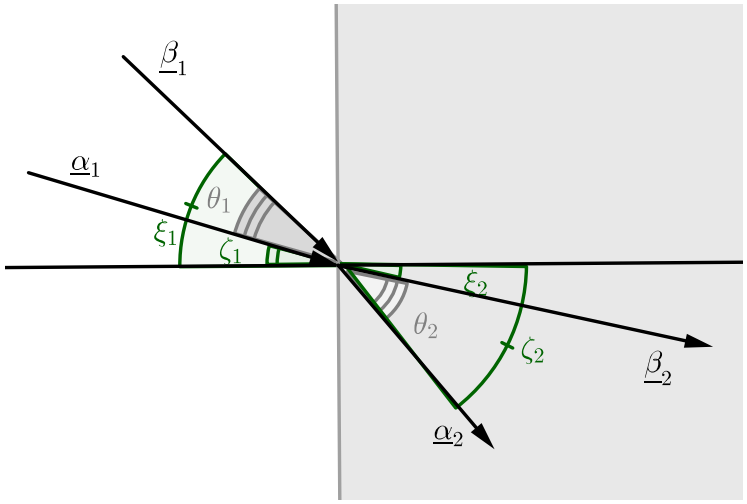

Figure 4.4. Angles and vectors of the considered problem, in the generic case in which both media are lossy. When the first media is assumed lossless then the angle θ_1 formed by β_1 and α_1 is 90^o.

respectively form with the normal to the separation surface and θ_2 is the angle formed by $\underline{\beta}_2$ and $\underline{\alpha}_2$. The incident and transmitted plane waves are:

$$\begin{cases} \underline{E}^i = \underline{E}^i_0 \; e^{-j\underline{\beta}_1 \cdot \underline{r}} \; e^{-\underline{\alpha}_1 \cdot \underline{r}} \\ \underline{E}^t = \underline{E}^t_0 \; e^{-j\underline{\beta}_2 \cdot \underline{r}} \; e^{-\underline{\alpha}_2 \cdot \underline{r}} \end{cases} \tag{4.1}$$

where $\underline{E}^i_0$ and $\underline{E}^t_0$ represent the polarization components of the plane-waves considered; those component won't be further considered in this dissertation because we concentrate on direction of propagation, which does not depend on the polarization. The impinging, more accurately said incident wave, causes a transmitted wave in medium 2 and a reflected wave in medium 1 that we ignored both in Eq. (4.1) and in Fig. 4.4, as reflected wave effects are not relevant in the presented studies.

The permittivity of medium 2, lossy by hypothesis, is complex: it follows that, because of the Snell law, the transmission angle must be complex too. Anyway, a different, and more physically consistent approach is shown by the Adler-Chu-Fano formulations [15], illustrated in the first chapter of this dissertation where the refracted angle remains real, but the wave vector assumes

complex value, and can be described, as we have already shown, in terms of two real vectors: a phase vector $\underline{\beta}$ and an attenuation vector $\underline{\alpha}$. In particular, the so called generalized Snell law can be applied to the described scenario gives the following:

$$\beta_1 \sin \xi_1 = \beta_2 \sin \xi_2 \tag{4.2}$$

$$\alpha_1 \sin \eta_1 = \alpha_2 \sin \eta_2 \tag{4.3}$$

where it is worth noting that $\underline{\alpha}_2 \neq 0$, while $\underline{\alpha}_1$ may or may not be equal to 0, as observed in the first chapter of this dissertation.

The Adler-Chu-Fano formalism is a fundamental tool for all the works preliminary to the one proposed in this dissertation, and therefore it also covers a central role in this dissertation. The demonstration of the equivalence between the complex angle and the complex vector (with real angles), approach is first introduced in [15], and then generalised by Roy in the Appendix of [81]. The second approach was followed in both studies presented in this chapter and in the one illustrated in the following one.

We are going to study here the properties of the transmitted wave assuming that $\underline{\beta}_1$, $\underline{\alpha}_1$ and $\hat{n}$ are coplanar, where $\hat{n}$ indicates the normal to the separation surface between medium 1 and medium 2; but, before achieving this task, we need to consider here a different notation for the Adler-Chu-Fano formulas, which will be helpful in the illustration of the different contributes introduced by researchers on the inhomogeneous waves study: the demonstration of those formulas won't be reported here but it employes a very similar approach to the one followed in the first chapter for Eqs. (2.17)-(2.19), anyway all the steps are carefully described in [15]. For non-magnetic media it is:

$$\alpha_0 = \frac{\omega\sqrt{\mu_0\varepsilon_r\varepsilon_0}}{\sqrt{2}}\sqrt{\sqrt{1+\left(\frac{\sigma}{\omega\varepsilon_r\varepsilon_0}\right)^2}-1} \tag{4.4}$$

$$\beta_0 = \frac{\omega\sqrt{\mu_0\varepsilon_r\varepsilon_0}}{\sqrt{2}}\sqrt{\sqrt{1+\left(\frac{\sigma}{\omega\varepsilon_r\varepsilon_0}\right)^2}+1} \tag{4.5}$$

where the notation

$$\varepsilon_c = \varepsilon_r \varepsilon_0 - j\frac{\sigma}{\omega}$$

was adopted. β_0 and α_0 are known as intrinsic phase and attenuation constants, respectively. and they are defined through the phase number k_{0m} of the medium considered: $k_{0m} = \beta_0 - j\alpha_0 = \omega\sqrt{\mu_0\varepsilon_c} = \sqrt{\varepsilon_c}k_0$, being k_0 the wave number of free space, as usual. Note that the amplitudes β and α of $\underline{\beta}$ and $\underline{\alpha}$, respectively, introduced in Ch.2 and always used ever since, do not coincide with β_0 and α_0 defined here unless the case of normal incidence is considered; in the generic case, is, in facts:

$$\alpha^2 - \beta^2 = \alpha_0^2 - \beta_0^2, \tag{4.6}$$

and it is also:

$$\alpha\beta\cos\theta = \alpha_0\beta_0 \ , \tag{4.7}$$

having noticed that that the simple product between two scalars (α_0 and β_0) is here compared to a scalar product of two vectors ($\underline{\alpha}$ and $\underline{\beta}$), and therefore the cosine of the angle (θ) between the two vectors has to be considered.

Imposing Eq. (4.6) and Eq. (4.7) in Eqs. (4.4)-(4.4) α and β can be re-written as a function of the intrinsec quantities α_0 and β_0, repsectively [15], [81]:

$$\alpha = \frac{\beta_0^2 - \alpha_0^2}{\sqrt{2}}\sqrt{\sqrt{1 + \left[\frac{2\alpha_0\beta_0}{(\beta_0^2 - \alpha_0^2)\cos\theta}\right]^2} - 1} \tag{4.8}$$

$$\beta = \frac{\beta_0^2 - \alpha_0^2}{\sqrt{2}}\sqrt{\sqrt{1 + \left[\frac{2\alpha_0\beta_0}{(\beta_0^2 - \alpha_0^2)\cos\theta}\right]^2} + 1} \tag{4.9}$$

Eqs. (4.8)-(4.9) are equivalent to the Eqs. (2.18) and (2.17) and, therefore they are only valid in the lossy scenario, while Eqs. (4.4) and (4.5) have general applicability.

4.3 Theoretical background: former studies on inhomogeneous waves

The earlier studies concerning inhomogeneous waves at the planar boundary between two media assumed the validity of Eqs. (4.8)-(4.9), implying that both medium 1 and medium 2 needed to be considered lossy.

The first notable work was due to Holmes [82] that limited the study to a homogeneous incident wave. In this particular case the following expressions for β_2 and α_2 were found:

$$\beta_2 = \sqrt{\frac{|k_\parallel|^2 + \mathrm{Re}(k_{02}^2) + |k_\parallel^2 - k_{02}^2|}{2}} \tag{4.10}$$

$$\alpha_2 = \sqrt{\frac{|k_\parallel|^2 - \mathrm{Re}(k_{02}^2) + |k_\parallel^2 - k_{02}^2|}{2}} \tag{4.11}$$

where $k_\parallel$ is given by the following expression:

$$k_\parallel = \beta_{01} \sin\xi_1 - j\alpha_{01} \sin(\zeta_1) \tag{4.12}$$

Eq. (4.12) is correct in the case of an incident homogeneous wave, but for a general solution the actual phase and attenuation vectors must replace the intrinsic quantities, therefore the following expression must be assumed:

$$k_\parallel = \beta_1 \sin\xi_1 - j\alpha_1 \sin(\zeta_1) \tag{4.13}$$

Radcliff [83] generalised the study of Holmes studying the case of an inhomogeneous incident wave. Anyway Radcliff used the expression in Eq. (4.12) instead of the Eq. (4.13). Consequentely, also in the following Snell equations:

$$\alpha_1 \sin\zeta_1 = \alpha_2 \sin\zeta_2 \tag{4.14}$$

$$\beta_1 \sin\xi_1 = \beta_2 \sin\xi_2 \tag{4.15}$$

Radcliff considered α_{01} instead of α_1 and β_{01} instead of β_1: this solution resulted therefore formally correct only when $\theta_1 = 0$, as it can be verified by comparing, again, Eqs. (2.17)-(2.18) with Eqs. (4.5)-(4.4). The results found by Radcliff can only represent a good approximation of the correct solution when the θ_1 angle is small, so in the quasi-homogeneous scenario.

Roy, in [81], corrected the formula given by Radcliff considering, as it should be, $\underline{\beta}_1$ and $\underline{\alpha}_1$ in Eq. (4.12). Roy considered inhomogeneous plane waves of arbitrary incident angles and with polarization either parallel or normal to the interface, finding a complete solution: it is well known that the solution for a generic polarisation can be always given by a combination of vertical and parallel polarisations [84], [11]. From the Snell law and from Eqs. (4.10)-(4.11) Roy found expressions for both the angle ξ_2 (15) and for the angle $\theta_2 = \zeta_2 - \xi_2$ (16). The equations determined by Roy are reported here:

$$\xi_2 = \begin{cases} \arcsin\left(\frac{W}{\beta_2}\right) \\ \pi - \arcsin\left(\frac{W}{\beta_2}\right) \end{cases} \tag{4.16}$$

$$\theta = \begin{cases} \arcsin\left(\frac{V}{\alpha_2}\right) - \arcsin\left(\frac{W}{\beta_2}\right) \\ \pi - \arcsin\left(\frac{V}{\alpha_2}\right) - \arcsin\left(\frac{W}{\beta_2}\right) \\ \arcsin\left(\frac{W}{\beta_2}\right) + \arcsin\left(\frac{V}{\alpha_2}\right) - \pi \\ \arcsin\left(\frac{W}{\beta_2}\right) - \arcsin\left(\frac{V}{\alpha_2}\right) \end{cases} \tag{4.17}$$

where:

$$\begin{cases} W = \beta_1 \sin\xi_1 \\ V = \alpha_1 \sin\zeta_1 \end{cases} \tag{4.18}$$

While obtaining the above systems of equations looks quite straightforward, distinguishing when those equations are relevant, i.e. which conditions on $\underline{\beta}_1$,$\underline{\alpha}_1$ is suitable for a particular solution of the systems of equations shown above, is quite challenging.

A searching roots routine had to be applied by Roy to find the solutions pertinent to different cases. Note that Roy was the first, at best of our

knowledge, that recognised the possibility of obtaining solutions having either $\eta_2 \geq \pi/2$ or $\xi_2 \geq \pi/2$ suggesting a total reflection of the attenuation or phase vector respectively. Roy did not highlight, or notice, the impacts in term of penetration that those solutions could imply. The observation of the existence of such critical angles was done exclusively for the coplanar case.

Finally, it is worth mentioning that Roy also treated the expressions for the case in which $\underline{\alpha_1}$, $\underline{\beta_1}$ and $\hat{n}$ are not coplanar, the results of this analysis are not reported here but may be found in [81].

A different, analytical, approach was taken in [6]. In this paper the particular case represented by $\zeta_2 = \pi/2$ was studied. The authors initially analysed the case, again, of a lossy medium 1 (we remind that the medium 2 is always assumed lossy). Starting from the generalised Snell law and the dispersion equations, the following equation was obtained:

$$(\chi - 1)\tan^2\xi_1 - \tan\zeta_1 \tan\xi_1 + \chi = 0 \tag{4.19}$$

being as usual ξ_1 the incident angle of the phase vector and ζ_1 the incident angle of the attenuation vector, and being χ defined as follow:

$$\chi = \frac{\mathrm{Im}\,(k_2^2)}{\mathrm{Im}\,(k_1^2)} \tag{4.20}$$

Resolving the Eq. (4.19) it was found the following:

$$\tan\xi_{\pm} = \frac{\tan\eta_1 \pm \sqrt{\tan^2\eta_1 - 4\chi\,(\chi - 1)}}{2\,(\chi - 1)} \tag{4.21}$$

Two conditions were then found, one which allows $\xi_2 = \pi/2$ and the other, more interesting, which permits $\zeta_2 = \pi/2$, i.e. deep-penetration, and in case of TE polarization, the power flow is found to be real. more details may be found in [6]. More interesting for this dissertation, also the interface between a lossless medium and a lossy medium was analysed in [6] by combining the generalised Snell law and the separability condition for a lossless medium (for which $\zeta_1 = \theta_1 - \pi/2$), then $\zeta_2 = \pi/2$, it followed:

$$\begin{aligned} \beta_1\alpha_1 \sin(2\xi_1) &= \mathrm{Im}\left(k_2^2\right) \Rightarrow \\ \Rightarrow \xi_c &= \frac{1}{2}\arcsin\left[\frac{\mathrm{Im}\left(k_2^2\right)}{\beta_1\alpha_1}\right] \end{aligned} \tag{4.22}$$

This critical angle can be reached for a value of β greater or equal to a critical value β_c defined as follow:

$$\beta_c = \frac{k_1}{\sqrt{2}}\sqrt{1+\sqrt{1+\left[\frac{2\mathrm{Im}\left(k_2^2\right)}{k_1^2}\right]^2}} \tag{4.23}$$

This result proved analytically, and explicitly, that $\zeta_2 = \pi/2$ can be obtained and it showed, moreover, that $\zeta_2 = \pi/2$ is never possible for normal incidence. It was further shown here that the studied deep-penetration condition requires at least a value of β greater of equal to a certain quantity (indicated as β_c in Eq. (4.23)), demonstrating that not only the incident angle, but also the amplitude of the incident wave, matters. Moreover, increasing the value of β, the angle ξ_c for which $\zeta_2 = \pi/2$ reduces and it tends to 0 when $\beta \to +\infty$.

In the next chapter it will be shown that, even though the Eq. (4.22) is a valid solution, it results only in a partial solution, moreover the case represented by $\zeta_2 = \frac{\pi}{2}$ represents only a limit case for deep penetration, that may be possible even beyond this value.

Chapter 5

Theoretical demonstration of deep-penetration.

5.1 Abstract

This chapter illustrates the study that we performed in order to complete the theoretical and analytical approach to deep-penetration phenomenon by means of inhomogeneous plane waves at the planar boundary between a lossless medium and a lossy one, whose preliminary studies were reported in the previous chapter. Particular attention is given here to the determination of the requisites that media have to possess in order to allow deep-penetration solutions, combined with the properties that the incident wave has to exhibit in terms of both amplitudes of attenuation and phase vectors to produce an opportune deep-penetrating wave in the lossy media, remembering that the behavior of the transmitted wave, which is in the lossy medium, is defined by Eqs. (4.4)-(4.9)*, and, as already highlighted, for a given frequency and material permits only degree of freedom on the direction of phase and attenuation vectors; moreover, this study uniquely identifies the non-homogeneous wave solutions which exhibit deep penetration, distinguishing them from the ones that can only experience attenuation in lossy media, such a dinstinction is not recognized in [6], and it is fundamental for the choice of antenna design usable to exploit deep-penetration.*

The final objective of this chapter is to provide the theoretical support needed to drive the experimental verification of this important phenomenon and, possibly, design practical antennas, for instance leaky-wave antennas [7], capable to generate the suitable field distributions. The experimental verification is then carried out in the next chapter.

5.2 Minimal condition for deep penetration

Here, the incidence of an inhomogeneous plane wave on a plane separation surface between two media is, again, considered; the incident wave is incoming from medium 1 and impinges on the separation surface producing, in general, a reflected wave in medium 1 and a transmitted wave in medium 2. We suppose such media non magnetic, homogeneous and isotropic; the medium 1 is strictly considered lossless, with a real relative permittivity ε_1, while the medium 2 dissipative, with a complex relative permittivity $\varepsilon_2 = \varepsilon_2' - j\varepsilon_2'' = \varepsilon_2' - j\sigma_2/(\varepsilon_0\omega)$. Let us define the incident electric field as $\underline{E}_1 = \underline{E}_{01}e^{-j\underline{k}_1\cdot\underline{r}}$, where $\underline{k}_1$ is the wave vector. The complex wave vector $\underline{k}_1$ is, as usual, $\underline{k}_1 = \underline{\beta}_1 - j\underline{\alpha}_1$, where $\underline{\beta}_1$ is the phase vector and $\underline{\alpha}_1$ is the attenuation vector; $\underline{\beta}_1 \perp \underline{\alpha}_1$ being the medium 1 lossless and assuming to deal strictly with inhomogeneous plane waves. Analogously, the transmitted electric field is $\underline{E}_2 = \underline{E}_{02}e^{-j\underline{k}_2\cdot\underline{r}}$, where $\underline{k}_2 = \underline{\beta}_2 - j\underline{\alpha}_2$, being $\underline{\beta}_2$ and $\underline{\alpha}_2$ phase and attenuation vectors; the angle θ_2 between these two vectors is always acute, being the medium 2 lossy by hypothesis. The reflected wave is not relevant to the present study, as it happened for the preliminary studies presented in the previous chapter, therefore we can ignore such a wave also here. Let us now define with ξ_1 and ζ_1 the angles that the vectors of the incident wave in the medium 1, $\underline{\beta}_1$ and $\underline{\alpha}_1$, respectively, form with the normal to the separation surface, and with ξ_2 and ζ_2 the relevant angles for the transmitted wave as reported in Fig. 5.1. Let us note that this figure is a particular case of Fig. 4.4 in which the angle θ_1 formed by $\underline{\beta}_1$ and $\underline{\alpha}_1$ assumes a value of $\pi/2$ radians.

The condition $\zeta_2 = \frac{\pi}{2}$ can be obtained when the incident wave is inhomo-

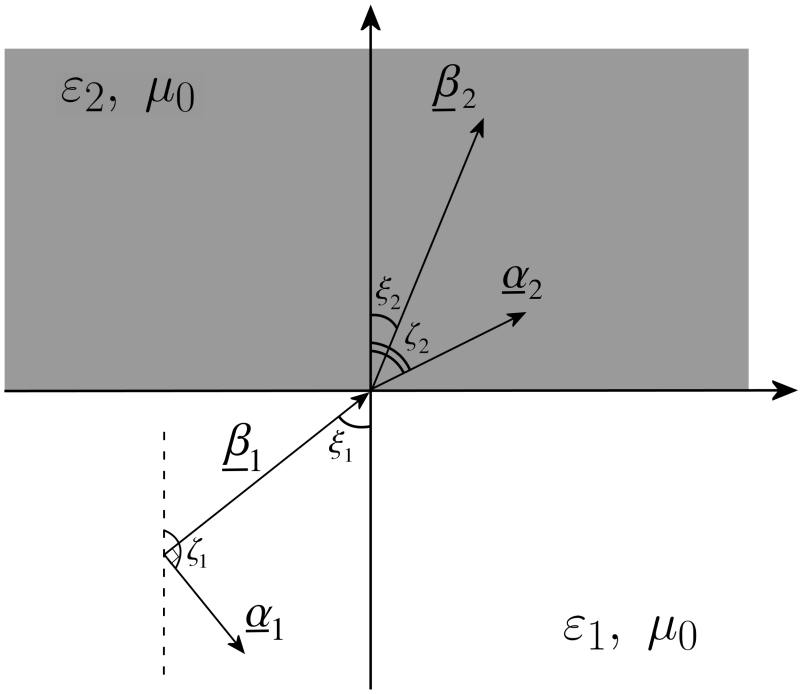

Figure 5.1. Incident and transmitted inhomogeneous waves at infinite planar boundaries between lossless and lossy media: angles and vectors definition.

geneous, as it was illustrated in the previous chapter, under the condition demonstrateed in [6]; such a condition guarantees deep penetration as there is no component of the attenuation vector directed along the direction normal to the separation surface and opposing to penetration. We have seen that, in the case in which the medium 1 is lossless, the condition $\zeta_2 = \frac{\pi}{2}$ is met if the amplitude of the incident phase vector $\underline{\beta}_1$ is at least equal to the critical value reported in Eq. (4.23), i.e:

$$\beta_1 \geq \beta_{1c} = \frac{k_1}{\sqrt{2}} \sqrt{1 + \sqrt{1 + \left[\frac{2\ \mathrm{Im}\,(k_2^2)}{k_1^2}\right]^2}}, \tag{5.1}$$

where $k_1 = k_0\sqrt{\varepsilon_1}$ and $k_2 = k_0\sqrt{\varepsilon_2}$ are the wavenumbers of the incident and transmitted wave, respectively, with k_0 the free-space wavenumber.

According to [6], the incident angle for which Eq. (5.1) is verified is given by Eq. (4.22) that we can rewrite as:

$$\xi_1 = \xi_c = \frac{1}{2}\gamma, \qquad \text{where} \quad 0 < \xi_c \leq \frac{\pi}{4} \tag{5.2}$$

where we introduced the quantity $\gamma = \arcsin\left[\mathrm{Im}(k_2^2)/(\beta_1\alpha_1)\right]$, and where, as usual, α_1 is the amplitude of $\underline{\alpha}_1$, and β_1 is the amplitude of $\underline{\beta}_1$. As we already observed in the previous chapter, the larger is the β_1, the smaller is the critical angle ξ_c for which $\zeta_2 = \frac{\pi}{2}$.

We are going to demonstrate here that Eq. (5.2) only represent one of the possible solutions that allows Eq. (5.1), and that, in fact, there are two valid solutions that yield $\zeta_2 = \frac{\pi}{2}$. Moreover, the two solutions may not always imply deep penetration, an accurate analysis of the two media involved will follow to determine when deep penetration is achievable. Furthermore, this study will resolve the ambiguity on the sign of α_1 demonstrating that only a specific direction for $\underline{\alpha}_1$ can guarantee deep-penetration effect. Finally conditions for deeper penetration, i.e., negative normal component of the transmitted field in the lossy medium, will be discussed.

The critical angle, ξ_c, is the solution of the following equation:

$$\beta_1\alpha_1 \sin(2\xi_1) = \mathrm{Im}(k_2^2) \tag{5.3}$$

The complete set of solutions of this equation in the interval $\xi_1 \in \left[0, \frac{\pi}{2}\right]$ is given by:

$$\xi_{c1} = \frac{1}{2}\gamma \tag{5.4}$$

$$\xi_{c2} = \frac{\pi}{2} - \frac{1}{2}\gamma \tag{5.5}$$

Both the expressions of ξ_c in Eq. (5.4) and Eq. (5.5) need to be physically interpreted.

The first medium is supposed lossless, therefore, if we consider an incident inhomogeneous wave and we apply the generalized Snell laws and the separability condition in the second lossy medium, we obtain the following

equations:

$$\beta_1 \sin \xi_1 = \beta_2 \sin \xi_2 \tag{5.6}$$

$$\alpha_1 \sin \zeta_1 = \alpha_2 \sin \zeta_2 \tag{5.7}$$

$$\beta_2^2 - \alpha_2^2 = \mathrm{Re}(k_2^2) \tag{5.8}$$

$$2\beta_2\alpha_2 \cos(\zeta_2 - \xi_2) = \mathrm{Im}(k_2^2) \tag{5.9}$$

The Eq. (5.7) can be rewritten exploiting the orthogonality of the phase and attenuation vectors in the first medium. From Fig. 5.1, it follows that:

$$\zeta_1' = \frac{\pi}{2} + \xi_1 \rightarrow \alpha_1 \sin \zeta_1' = \alpha_1 \sin\left(\frac{\pi}{2} + \xi_1\right) = \alpha_1 \cos \xi_1 \tag{5.10}$$

but, in medium 1, both the proper and the improper inhomogeneous wave solutions [7] need to be considered, as it is was first illustrated in Fig. 2.3 and reported, for the specific case, in Fig. 5.4, where is evident that a second determination of α_1 is also possible taking the other solution for the angle ζ_1, i.e.:

$$\zeta_1'' = -\frac{\pi}{2} + \xi_1 \rightarrow \alpha_1 \sin \zeta_1'' = -\alpha_1 \sin\left(\frac{\pi}{2} - \xi_1\right) = -\alpha_1 \cos \xi_1 \tag{5.11}$$

We choose to investigate the problem observing what happens using the Eq. (5.11), and, later in this paper we will analyse the ambiguity of the sign, taking in account the Eq. (5.10), i.e. we will only consider the positive α_1 value and we will include the study of the sign in the analysis of the direction of the vector $\underline{\alpha}_1$. Imposing the condition of Eq. (5.10), Eq. (5.7) becomes:

$$\alpha_1 \cos \xi_1 = \alpha_2 \sin \zeta_2 \tag{5.12}$$

Introducing Eqs. (5.6) and (5.12) into Eq. (5.9) we obtain:

$$2\beta_2\alpha_2 \cos \zeta_2 \cos \xi_2 + \alpha_1\beta_1 \sin(2\xi_1) = \mathrm{Im}(k_2^2) \tag{5.13}$$

If we look for the critical angle at which the transmitted attenuation vector $\underline{\alpha}_2$ is parallel to the interface, we must impose $\zeta_2 = \frac{\pi}{2}$ in Eq. (5.13), obtaining Eq. (5.3). However, if we look for the critical angle at which the transmitted

phase vector $\underline{\beta}_2$ is parallel to the interface, we must impose $\xi_2 = \frac{\pi}{2}$ obtaining, again, Eq. (5.3). The conditions found classify two very different physical problems, the former represents deep penetration, while the latter reminds very closely the so-called Zenneck wave at the interface between two lossy media [85], but that differs from the Zenneck wave for the absence of the total-transmission effect [86].

We need to distinguish the two solutions represented by Eq. (5.3), i.e., we must find a way to understand which solution is relevant to a transmitted phase or attenuation vector parallel to the interface, respectively. To obtain such a condition, we can consider the expressions of the magnitudes assumed by both the transmitted phase and attenuation vectors given in [81], first reported here in Eq. (4.10) and Eq. (4.11) and written down here again to facilitate the reading:

$$\beta_2 = \sqrt{\frac{|k_\parallel|^2 + \mathrm{Re}(k_2^2) + |k_\parallel^2 - k_2^2|}{2}} \tag{5.14}$$

$$\alpha_2 = \sqrt{\frac{|k_\parallel|^2 - \mathrm{Re}(k_2^2) + |k_\parallel^2 - k_2^2|}{2}} \tag{5.15}$$

where $k_\parallel$ is the component of the incident wave vector parallel to the interface. Let us consider the absolute value under square root: hence, by using Eq. (5.3), i.e., under the hypothesis that $\zeta_2 = \frac{\pi}{2}$ or $\xi_2 = \frac{\pi}{2}$, we can find the following expression:

$$\begin{aligned} |k_\parallel^2 - k_2^2| =& |\beta_1^2 \sin^2 \xi_1 - \alpha_1^2 \cos^2 \xi_1 - \mathrm{Re}(k_2^2)| = \\ =& |\mathrm{Re}(k_\parallel^2) - \mathrm{Re}(k_2^2)| \end{aligned} \tag{5.16}$$

Substituting (5.16) in (4.10) and (4.11), we found that the solution $\xi_2 = \frac{\pi}{2}$, corresponding to the transmitted phase vector parallel to the interface, is consistent with $\mathrm{Re}(k_\parallel^2) \geq \mathrm{Re}(k_2^2)$, while $\zeta_2 = \frac{\pi}{2}$, corresponding to the transmitted attenuation vector parallel to the interface, requires $\mathrm{Re}(k_\parallel^2) < \mathrm{Re}(k_2^2)$.

It is now important to understand when the two solutions of Eqs. (5.4) and (5.5) are relevant either to the case $\xi_2 = \frac{\pi}{2}$ or $\zeta_2 = \frac{\pi}{2}$. For the sake of brevity, we will call the solution of the "phase" type when it is relevant to the case $\xi_2 = \frac{\pi}{2}$ and of the "attenuation" type when it is relevant to the case $\zeta_2 = \frac{\pi}{2}$. Let us impose the phase type solution, $\mathrm{Re}(k_\parallel^2) - \mathrm{Re}(k_2^2) \geq 0$ in (5.16), it follows $\beta_1^2 \sin^2 \xi_1 - \alpha_1^2 \cos^2 \xi_1 - \mathrm{Re}(k_2^2) \geq 0$. By applying bisection-trigonometrical formulas, it is:

$$\cos(2\xi_1) \leq -\frac{2\mathrm{Re}(k_2^2) - k_1^2}{\beta_1^2 + \alpha_1^2} \tag{5.17}$$

Let us simplify the Eq. (5.17) defining a quantity Ψ as follows:

$$\Psi = \frac{k_1^2}{\beta_1^2 + \alpha_1^2}\left(2\frac{\varepsilon_2'}{\varepsilon_1} - 1\right) \tag{5.18}$$

So that Eq. (5.17) can be written as:

$$\cos(2\xi) \leq -\Psi \tag{5.19}$$

which represents the condition of deep penetration. This, using the two conditions Eq. (5.4) and Eq. (5.5) can be written in terms of γ obtaining, respectively:

$$\cos\gamma \leq -\psi \tag{5.20}$$

for ξ_{c1} and:

$$\begin{aligned} \cos(\pi - \gamma) \leq -\psi \Rightarrow \\ \Rightarrow \cos\gamma \geq \psi \end{aligned} \tag{5.21}$$

for ξ_{c2}.

So, ξ_{c1} is of the phase type when $\cos\gamma \leq -\Psi$, otherwise is of the attenuation type; ξ_{c2} is of the phase type if $\cos\gamma \geq \Psi$, otherwise is of the attenuation type. From such conditions it is possible to foresee the type of the solutions in many cases, in fact (recalling that $\gamma \in [0, \pi/2]$): if $\Psi < -1$, both ξ_{c1} and ξ_{c2} solutions are of the phase type; if $-1 \leq \Psi < 0$, the ξ_{c1} type is determined by the value of γ, while ξ_{c2} is of the phase type; if $\Psi = 0$, ξ_{c1} is of the attenuation type,

while ξ_{c2} is of the phase type; if $0 < \Psi \leq 1$, ξ_{c1} is of the attenuation type, while the ξ_{c2} type is determined by the value of γ; finally, if $\Psi > 1$, both the solutions are of the attenuation type.

Looking at the expression (5.18), we see that the sign of Ψ is determined by the ratio of the real parts of the permittivities (note, both medium 1 and medium 2 are assumed non magnetic). The case in which both the solutions are of phase type ($\Psi < -1$) requires either $\varepsilon_2' < 0$ or $\varepsilon_1' < 0$ [1]: the negative real permittivity, which is not uncommon at the optics frequencies (e.g., gold and silver exhibit $\varepsilon_2' < 0$ value at optical frequencies below the plasma frequency) or in artificial engineered metamaterials [87], it is quite exotic at microwave frequencies and for media occurring in nature, therefore we can say that, in case of microwave radiation, adopted in many applications such as the Ground Penetrating Radar (GPR), an attenuation type solution always exists in practical scenarios.

In particular, $\Psi \geq 0$ when $2\varepsilon_2' \geq \varepsilon_1$. In this scenario, that is typically met, e.g., the case of incidence from a vacuum, the solution ξ_{c1} is always of the attenuation type. The behavior of ξ_{c2} depends on the characteristics of the incident wave and in particular on the parameter β_1/k_1: in fact the quantity in brackets in Eq. (5.18) is multiplied by a function of such parameter that is a decreasing function bounded in the interval $(0, 1)$. As a consequence, the larger is β_1/k_1, the smaller is Ψ, making the determination of the type of ξ_{c2} depending on γ also for high ratio $\varepsilon_2'/\varepsilon_1$.

The cases for $\Psi = 0$ and $\Psi > 1$ are illustrated in Fig. 5.2 and Fig. 5.3, respectively. In Fig. 5.2, a medium 1 having $\varepsilon_1 = 2$ and a medium 2 with $\varepsilon_2 = \varepsilon_2' - j\varepsilon_2''$, where $\varepsilon_2' = 1$ and $\varepsilon_2'' = 0.1$ are considered, the phase vector of the incident wave is $\beta_1 = 1.01 \cdot \beta_c$. In particular, ξ_2 as a function of ξ_1, i.e. $< \xi_1 | \xi_2 >$ using the Dirac notation [88], is illustrated in Fig. 5.2a: the only solution of phase type appears when $\xi_1 \approx 80^o$. In Fig. 5.2b, ζ_2 as a function of ξ_1, i.e. $< \xi_1 | \zeta_2 >$, is shown: the only solution of attenuation type appears for

[1] $0 < \frac{k_1^2}{\beta_1^2 + \alpha_1^2} = \frac{\beta_1^2 - \alpha_1^2}{\beta_1^2 + \alpha_1^2} < 1$ always, it follows that, in this case, $2\varepsilon_2'/\varepsilon_1 - 1 < -1 \rightarrow \varepsilon_2' < 0$.

$\xi_1 \approx 15^o$, beyond this value ζ_2 keeps incrementing for higher ξ_1 values, giving rise to a wave that grows entering into the lossy medium (improper solution), in the next paragraph it will be demonstrated that the mentioned negative value for $\underline{\alpha}_2$ (i.e. a value of $\zeta_2 > 90^o$) is an acceptable solution for the given problem.

Finally, comparing Fig. 5.2a with Fig. 5.2b it can be seen that ξ_2 grows when ζ_2 also is increasing, this means that β_2 vector tends to be parallel to the separation surface when the penetration gets stronger, tending to a surface wave: the combined effects of the two vectors should be therefore considered in practical applications where the improper effect can only be guaranteed for a limited space region, because such a low $\underline{\beta}_2$ slope may imply modest penetration even though the direction $\underline{\alpha}_2$ would suggest a stronger deep-penetration effect then the one obtained for $\zeta_2 = 90^o$.

In Fig. 5.3 is shown instead the typical scenario in which both solution are of attenuation type, i.e. $\Psi > 1$: in this case it is $\varepsilon_1 = 2$, $\varepsilon_2' = 5$, $\varepsilon_2'' = 0.1$, and $\beta_1 = 1.01 \cdot \beta_c$. It can be noticed that the transmitted phase vector is never parallel to the interface (see Fig. 5.3a) while the transmitted attenuation vector is parallel to the separation interface for two values of the incident angle: $\xi_1 \approx 18^o$ and $\xi_1 \approx 72^o$ (see Fig. 5.3b. Also in this second scenario, similarly to what happend for $\Psi = 0$ (see Fig. 5.2), there is an angular region in which ζ_2 assumes values larger than 90^o, this happens while also the value ξ_2 is increasing, but, differently from what was seen in Fig. 5.2, in this case the growth of ξ_1 may never lead to a surface-wave behaviour when the wave improper behaviour gets stronger.

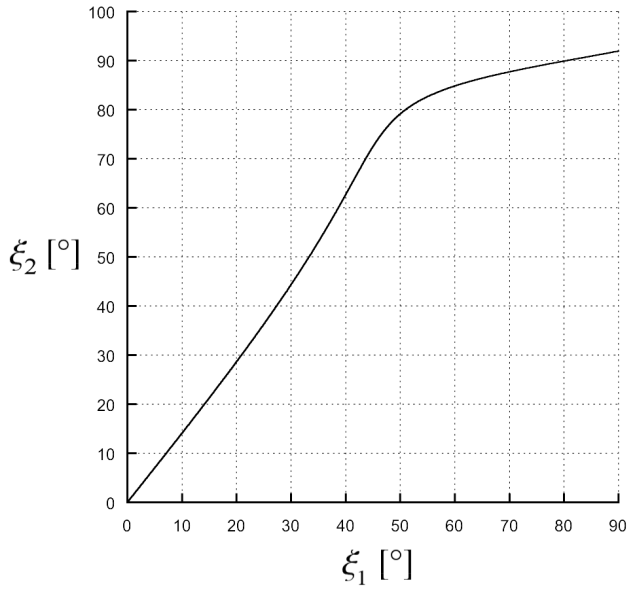

(a) Phase solution: this requires a ξ_1 incidence angle wider than $\pi/4$. In particular, the propagation vector of the transmitted wave ξ_2 is parallel to the separation surface when $\xi_1 = 80^o$

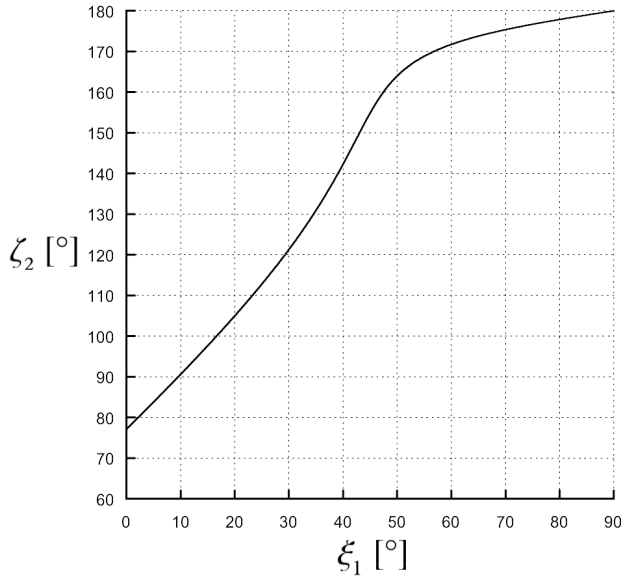

(b) Attenuation solution: the incident angle needs to be smaller than $\pi/4$, the attenuation vector of the transmitted wave is parallel to the separation surface for an angle of incidence $\xi_1 \approx 15^o$, note that increasing the value of the ξ_1 angle the value of ζ_1.

Figure 5.2. Values of ζ_2 and ξ_2 when $\varepsilon_1 = 2$, $\varepsilon_2' = 1$, $\varepsilon_2'' = 0.1$, and $\beta_1 = 1.01 \cdot \beta_c$: it must be observed the presence of both phase and attenuation solutions.

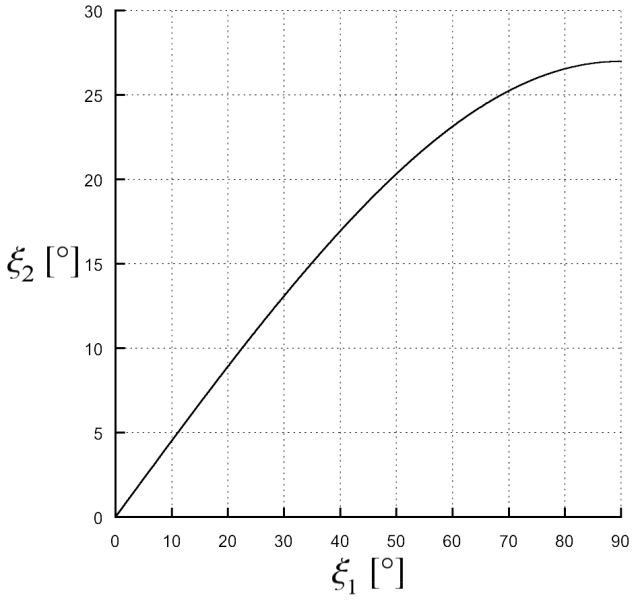

(a) ξ_2 as a function of ξ_1 is shown here. A phase solution is never possible, the ξ_2 angle is is acute for any ξ_1 value.

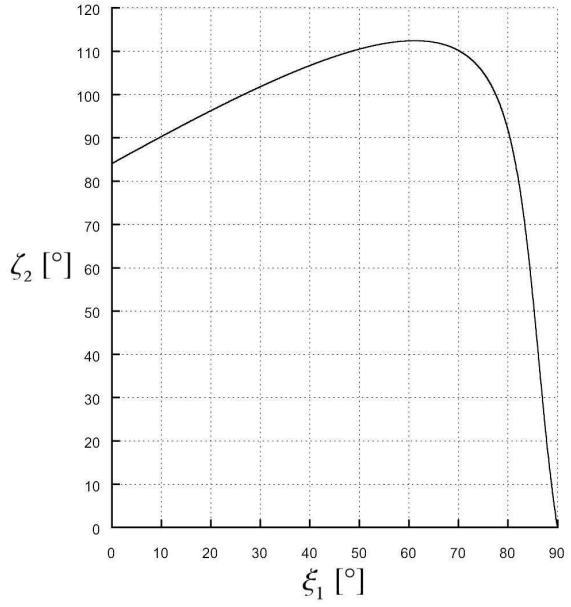

(b) ζ_2 as a function of ξ_1 is shown here. There are two attenuation solutions, one for $\xi_1 \approx 18^o$ and one for $\xi_1 \approx 72^o$, so one solution is found for $\xi_1 < 45^o$ and one for $\xi_1 > 45^o$

Figure 5.3. Values of ζ_2 and ξ_2 angles when $\varepsilon_1 = 2$, $\varepsilon_2' = 5$, $\varepsilon_2'' = 0.1$, and $\beta_1 = 1.01 \cdot \beta_c$: it must be observed that both solutions are of attenuation type.

5.3 Determination of the suitable deep-penetration solution for the direction of the attenuation vector

We anticipated the presence of two solutions, opposite in sign, for the quantity α_1 in Eqs. (5.10) and (5.11), those solution will be studied here discussing the impact of the direction of the attenuation vector $\underline{\alpha}_1$, this analysis will lead to the determination of crucial practical implications that will also be consequently illustrated.

When both the critical phase-vector amplitude β_1 and angle of incidence ξ_c are found from Eq. (5.1) and Eqs. (5.4)-(5.5), respectively, the amplitude α_1 of the incident attenuation vector is determined, being the medium 1 known, as $\alpha_{1c} = \sqrt{\beta_{1c}^2 - k_1^2}$, while the angle formed by $\underline{\beta}_1$ and $\underline{\alpha}_1$ is $\pm\pi/2$, being the medium 1 lossless. The ambiguity on the sign corresponds to an ambiguity in the direction of the attenuation vector, illustrated in Fig. 5.4. We are going to demonstrate that only one solution for the attenuation vector of the incident wave allows deep penetration, and specifically the one that causes a field increase while approaching the interface (see Fig. 5.4); the other solution produces, instead, an attenuated transmitted wave. Let us observe Fig. 5.4: the incident inhomogeneous wave admits $\underline{\alpha}_1 = \underline{\alpha}_1^{(1)}$, for which the field grows entering in medium 2 and $\underline{\alpha}_1 = \underline{\alpha}_1^{(2)} = -\underline{\alpha}_1^{(1)}$ for which the field decreases entering in medium 2. The condition for deep penetration $\zeta_2 = \pm\frac{\pi}{2}$ translates either into $\underline{\alpha}_2 = \underline{\alpha}_2^{(1)}$ or into $\underline{\alpha}_2 = \underline{\alpha}_2^{(2)}$ in Fig. 5.4. With reference to Fig. 5.4, the phase vector $\underline{\beta}_1$ is incoming from the III quadrant and impinges on the origin of axes: it follows that the vector $\underline{\beta}_2$, if the critical angle is of the attenuation type, can only be in the I quadrant due to the conservation of the tangential component of $\underline{\beta}_1$. In the illustrated case, the angle formed by $\underline{\alpha}_2$ and $\underline{\beta}_2$ must be always less than $\pi/2$, because:

$$\underline{\beta}_2 \cdot \underline{\alpha}_2 = \frac{\omega^2 \mu \varepsilon_2'' \varepsilon_0}{2} > 0$$

having specified to deal with the case, more interesting for realistic applications,

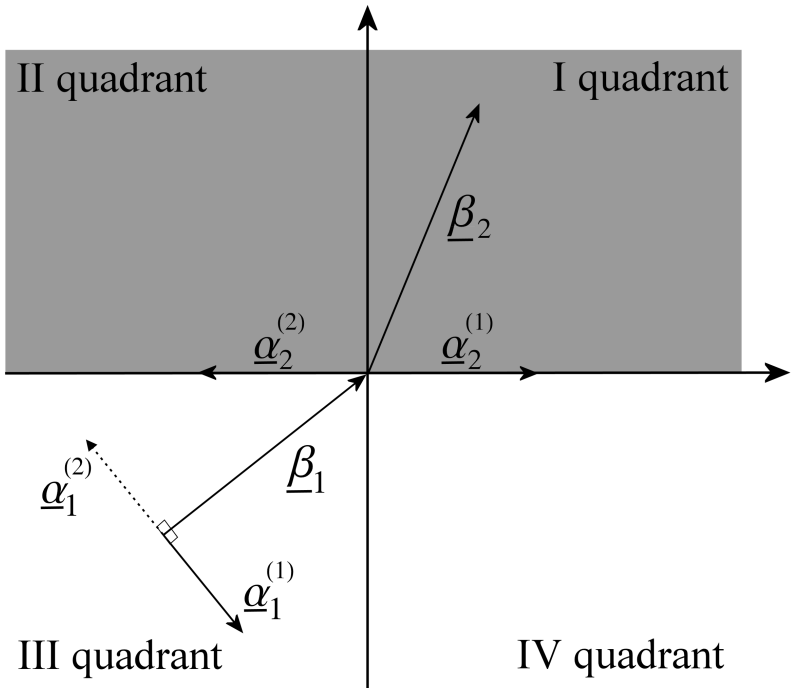

Figure 5.4. Proper and improper inhomogeneous waves at interface between a lossless medium and a lossy medium.

in which $\varepsilon_2'' > 0$, it follows that $\underline{\alpha}_2^{(2)}$ can never be a critical solution of our problem, the only valid solution is represented by $\underline{\alpha}_2^{(1)}$; in other words, the proper solution represented by $\underline{\alpha}_1^{(2)}$ can never allow deep penetration, but it can only admit an attenuated solution with $\underline{\alpha}_2$ laying in the second quadrant (always for the conservation of tangential component); on the opposite, the *growing-wave* solution represented by $\underline{\alpha}_1^{(1)}$ guarantees, as predicted, deep-penetration effect, allowing $\underline{\alpha}_2^{(1)}$ as a valid solution.

A wave behaving in the way described by $\underline{\alpha}_2^{(1)}$, when generated by a finite source, would violate the Sommerfeld condition [11], but, even though the Sommerfeld condition is violated, such a wave can be produced by a finite source in a limited region of space, for example by means of a Leaky-Wave Antenna (LWA), as we have seen in the previous chapters. In particular, if a mono-dimensional planar LWA is used and it is posed on a plane parallel to the separation surface in the medium 1, then radiation by means of leaky waves of the *improper* type must be chosen to allow deep penetration [7].

LWAs are antennas that have already been proposed in the past in many applications, in which deep penetration is also a requirement: from radar imaging applications [63], GPR applications [62] or tracking applications [61], anyway, the choice of this kind of antennas were mainly due to their bandwidth, fidelity factor [89], phase-centre stability and pulse preservation, or for their low-cost ability to perform frequency beam scanning [61]. Here we propose their study for improving penetration, this analysis will be performed in the next chapter.

5.4 Electromagnetic-penetration in the proximity of the minimal deep-penetration condition.

The minimal condition that allows deep penetration is guaranteed by the angle $\zeta_2 = \frac{\pi}{2}$. A stronger penetration can be achieved if the condition:

$$\zeta_2 > \frac{\pi}{2} \tag{5.22}$$

is satisfied. In [81] it was highlighted that the angles ζ_2 and ξ_2 could assume values greater than $\pi/2$ leading to total reflection of attenuation or phase vector, respectively. The study of Roy was limited to lossy media because of the Adler-Chu-Fano equations [15] which are valid only in the lossy scenario. We will confirm here such a finding demonstrating that it is also valid for a medium 1 assumed lossless. In the conventional scenario in which the propagating wave attenuates entering in the lossy medium ($\zeta_2 < \frac{\pi}{2}$) the components normal to the separation surface of both $\underline{\beta}_2$ and $\underline{\alpha}_2$ have the same sign, while Eq. (5.22) shows a case in which those two components must present opposite sign: this means that the wave field increases while propagating in the lossy medium. We are going to demonstrate the validity of the condition in Eq. (5.22) by studying the case in which both incident wave (and in particular its working frequency f_0 and incident angle ξ_c) and medium 1 are maintained constant, while the lossy medium 2 is varied in its ε_2'' value: this is equivalent to consider an inhomogeneous plane wave designed to impinge on a separation surface with

a lossy medium 2 characterised by a permittivity $\varepsilon_2 = \varepsilon_2' - j\varepsilon_2''$, so that $\zeta_2 = \frac{\pi}{2}$ is satisfied; then such a wave is applied, with the same incidents angle, to an interface with a lossy medium $2^{(a)}$ for which $\varepsilon_2^{(a)} = \varepsilon_2^{\prime(a)} - j\varepsilon_2^{\prime\prime(a)} = \varepsilon_2' - j\varepsilon_2^{\prime\prime(a)}$. We note that this scenario has practical applicability, because it describes the common case in which an antenna design is performed and then the antenna is exposed to a medium which does not fully match the one for which the structure was optimised.

Let us now assume that we met the condition of Eq. (5.1) (i.e., $\zeta_2 = \frac{\pi}{2}$) for ε_2 and let us now decrease its imaginary part ε_2'' to a value $\varepsilon_2^{\prime\prime(a)}$, such that $0 < \varepsilon_2^{\prime\prime(a)} < \varepsilon_2''$. This new value of the imaginary permittivity implies different amplitudes and directions for the transmitted phase and attenuation vectors; let us call with β_2' and α_2' the magnitudes of such vectors and with ξ_2' and ζ_2' the new angles formed by those vectors with the normal to the separation surface, respectively. Consequently the new phase vector in medium 2 is indicated with $\underline{k}_2'$ and the wave number with k_2'. From Eq. (5.9), having imposed $\varepsilon_2'' > \varepsilon_2^{\prime\prime(a)}$ (i.e. $0 < \mathrm{Im}(k_2') < \mathrm{Im}(k_2)$), it follows that:

$$\beta_2\alpha_2 \cos\left(\xi_2 - \frac{\pi}{2}\right) > \beta_2'\alpha_2' \cos(\xi_2' - \zeta_2') \tag{5.23}$$

Eq. (5.23) can be rewritten as follows:

$$\beta_2\alpha_2 \sin(\xi_2) > \beta_2'\alpha_2' \cos(\xi_2' - \zeta_2'). \tag{5.24}$$

We considered the hypothesis in which the same wave incoming from a lossless material was applied to two different media with the same incident angle; therefore using Eqs. (5.6) and (5.12) the following system of equation is obtained:

$$\begin{cases} \beta_1 \sin\xi_1 = \beta_2 \sin\xi_2 \\ \alpha_1 \sin\zeta_1 = \alpha_2 \\ \beta_1 \sin\xi_1 = \beta_2' \sin\xi_2' \\ \alpha_1 \sin\zeta_1 = \alpha_2' \sin\zeta' \end{cases} \tag{5.25}$$

Removing β_1 and α_1 from the previous we have:

$$\begin{cases} \beta_2' \sin \xi_2' = \beta_2 \sin \xi_2 \\ \alpha_2' \sin \zeta' = \alpha_2 \end{cases} \tag{5.26}$$

Now, β_2 and α_2 in Eq. (5.24) can be eliminated, finally having:

$$\beta_2' \sin(\xi_2')\alpha_2' \sin(\zeta_2') > \beta_2'\alpha_2' \cdot \\ \cdot \left[\cos(\xi_2')\cos(\zeta_2') + \sin(\xi_2')\sin(\zeta_2')\right].$$

Simplifying it is obtained:

$$\cos(\xi_2')\cos(\zeta_2') < 0. \tag{5.27}$$

With reference to the Fig. 5.4, from Eq. (5.27) it follows that $\underline{\beta}_2'$ and $\underline{\alpha}_2'$ need to be positioned one on the I quadrant and one on the IV quadrant, and in particular they cannot be both in the I quadrant, the latter would be the solution for an attenuated transmitted wave; moreover, no assumption was made on ξ_2, apart from the deep-penetration condition that forces ξ_2 to be in the first quadrant, while it was posed $\zeta_2 = \frac{\pi}{2}$. Hence it follows that it must be $\zeta_2' > \frac{\pi}{2}$ because the attenuation vector $\underline{\alpha}_2'$ needs to be positioned to the right of $\underline{\beta}_2'$, according to the previous discussion (see Fig. 5.4), to allow deep penetration. Eq. (5.27) can be correlated to the critical angle of the phase and attenuation type. In fact when $\xi_1 > \xi_c$, if ξ_c is of the attenuation type, then $\underline{\alpha}_2$ enters in the IV quadrant while $\underline{\beta}_2$ remains in the I quadrant; on the other hand, if ξ_c is of the phase type, then $\underline{\alpha}_2$ remains in the I quadrant, while $\underline{\beta}_2$ enters in the IV quadrant.

Considering $\varepsilon_2''^{(a)} > \varepsilon_2''$ would have caused, on the opposite, $\underline{\alpha}_2'$ and $\underline{\beta}_2'$ both in the I or both in the IV quadrant: in particular, the continuity of the solution would have requested $\zeta_2 < \frac{\pi}{2}$, so both $\underline{\alpha}_2'$ and $\underline{\beta}_2'$ would lie in the first quadrant. This solution corresponds to pure attenuation of the transmitted wave in medium 2. This theoretical expansion permits us to state that, found a β_c value for which Eq. (5.1) is satisfied, the deep-penetration effect stops

occurring for higher ε_2'' values, while the wave penetrates in medium 2 with an increasing electric field module for lower ε_2'' values.

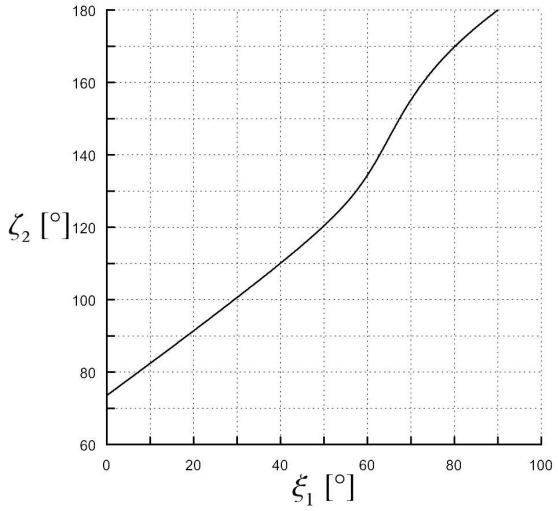

Figure 5.5. Angle ζ_2, in degrees, formed by the attenuation vector inside the lossy medium with the normal to the separation surface, calculated as a function of the angle ξ_1 of the incident phase vector, expressed in degrees. Medium 1 is a vacuum, medium 2 is chosen such that $\varepsilon_2'^{(a)} = 1$ and $\varepsilon_2''^{(a)} = 0.5$. The magnitude of the incident phase vector is the one in Eq. (5.1) when $\varepsilon_2' = 1$ and $\varepsilon_2'' = 0.9$.

A numerical representation of the analytical formulas shown in this study was developed to prove the result just explained. Let us assume a 1.55 μm wavelength, the medium 1 is a vacuum, designing $\beta_1 = \beta_c$ to meet the condition $\zeta_2 = \frac{\pi}{2}$ when the second medium has $\varepsilon_2' = 1$ and $\varepsilon_2'' = 0.9$ with an angle $\xi_{c1} = \frac{\pi}{4}$. Results of the numerical evaluation, obtained through custom code, are available in Figs. 5.5-5.7; in such figures it is shown ζ_2 as a function of ξ_1, when $\varepsilon_2' = 1$ in all cases and $\varepsilon_2''^{(a)}$ assumes values of 0.5, 0.9, and 1.4, respectively. It can be seen in Fig. 5.5 that $\zeta_2(\xi_1) > \frac{\pi}{2}$ for $\xi_1 > \xi_{min}$ for $\varepsilon_2''^{(a)} = 0.5$, while in Fig. 5.6, $\varepsilon_2''^{(a)} = 0.9$ implies $\zeta_2(\xi_1) \leq \frac{\pi}{2}$; in particular, there is only a point in which the angle $\zeta_2(\xi_1) = \frac{\pi}{2}$ that occurs when $\xi_1 = \xi_{c1}$. Finally, in Fig. 5.7, $\varepsilon_2''^{(a)} = 1.4$ implies $\zeta_2(\xi_1) < \frac{\pi}{2}$ for any ξ_1.

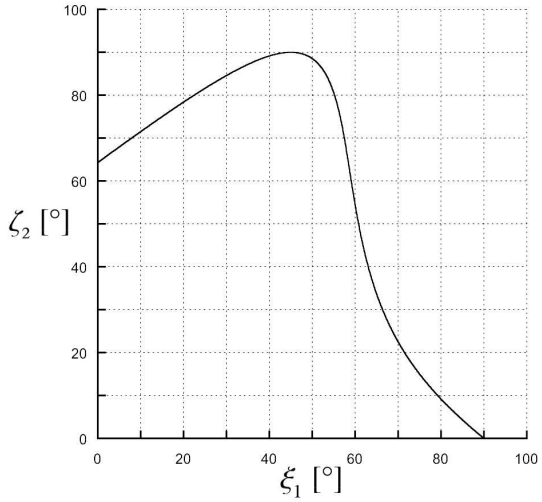

Figure 5.6. Angle ζ_2, in degrees, formed by the attenuation vector inside the lossy medium with the normal to the separation surface, calculated as a function of the angle ξ_1 of the incident phase vector, expressed in degrees. Medium 1 is a vacuum, medium 2 has $\varepsilon_2^{\prime(a)} = 1$ and $\varepsilon_2^{\prime\prime(a)} = 0.9$. The magnitude of the incident phase vector is the critical one in Eq. (5.1) when $\varepsilon_2' = 1$ and $\varepsilon_2'' = 0.9$.

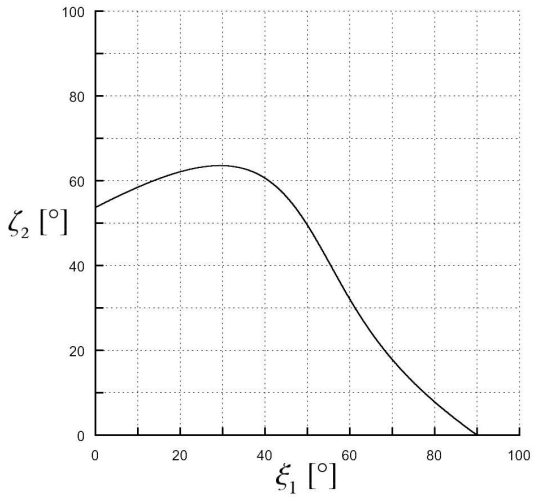

Figure 5.7. Angle ζ_2, in degrees, formed by the attenuation vector inside the lossy medium with the normal to the separation surface, calculated as a function of the angle ξ_1 of the incident phase vector, expressed in degrees. Medium 1 is a vacuum, medium 2 has $\varepsilon_2^{\prime(a)} = 1$ and $\varepsilon_2^{\prime\prime(a)} = 1.4$. The magnitude of the incident phase vector is the critical one in Eq. (5.1) when $\varepsilon_2' = 1$ and $\varepsilon_2'' = 0.9$.

5.5 Conclusions

This chapter presented novel theoretical results concerning the electromagnetic penetration in lossy media by means of inhomogeneous plane waves, in the condition in which the incident wave is incoming from a lossless medium; this represents the most common scenario in antennas simulations, where the antenna is usually placed in a vacuum (that approximates closely the air [11]). This was a fundamental step in order to collect all the theoretical requirements for practical antenna design. It has to be remembered that the analytic demonstration carried out here is strictly related to plane-wave solutions, which are non-physical, and we have also to note that the Sommerfeld condition is usually violated by the deep-penetration requirement. One can expect therefore, that, even when deep-penetration is possible, this can only be allowed for a finite portion of space when physical and not ideal waveform are used.

Part III

Deep-penetration conditions and limits for leaky waves produced by realistic structures, and conclusions

Chapter 6

Deep-penetration through leaky-wave antennas.

The deep-penetration effect, demonstrated in the previous chapter for the ideal case of plane waves, is exploited here by simulating practical, physical, leaky waves (see ch. 2) generated by the mentioned leaky-wave antennas, previously described in Ch. 3. Those antennas are usually designed for an attenuation constant α negligible, this permits to have a very narrow beam, but unfortunately this requirement is not beneficial to deep-penetration achievement, therefore, before approaching the LWA design for deep penetration, the characteristics of the lossy medium will need to be studied, to prepare a test scenario suitable for deep penetration. The medium designed for the simulation will be also used to investigate practical limits of LWAs in terms of penetration. Moreover a horn antenna will be designed to compare the homogeneous and inhomogeneous radiation patterns, the horn designed will be fully described, so that this simulations can be reproduced and new results may be added using different approaches. All the antennas were simulated with the aid of the CST Microwave Studio *commercial tool [90], results were then exported to Matlab [91]-[92] for further analyses and investigations, that will be explained in the present chapter.*

6.1 Requirements for a suitable LWA

Analyzing Eq. (5.1), it is possible to verify how difficult can be the deep-penetration achievement by means of leaky-wave antennas. Therefore a specific lossy medium is considered such that deep-penetration can be practically achieved.

For antenna design, it is better to work with dimensionless, normalized, quantities, therefore we rewrite Eq. (5.1) here as follows:

$$\beta_{cn} = \frac{1}{\sqrt{2}}\sqrt{1+\sqrt{1+4\chi^2}}\,, \tag{6.1}$$

where $\beta_{cn} = \beta_c/k_1$ and $\chi = \varepsilon_2''/\varepsilon = \sigma_2/\omega\varepsilon_1$, depending on the notation adopted (see Ch. 2).

It is immediatly clear that deep penetration cannot be achieved through realistic LWA structures if the lossy medium is a good conductor: we have seen previously that a good conductor is usually defined such that $\sigma_2 >> \omega\varepsilon_2$, but, in real media, the difference of values in conductivity can be several orders of magnitude larger than the difference in the real permittivity, hence, if medium 2 is a good conductor, it is also $\sigma_2 >> \omega\varepsilon_1$ [11], i.e. $\chi >> 1$. Introducing the former condition in Eq. (6.1) it is $\beta_{cn} \approx \sqrt{\chi} >> 1$ that is clearly not achievable by means of a leaky-wave antenna, because, as we have already seen introducing such structures, it must be $\beta_{cn} \approx 1$, instead. By inverting Eq. (6.1) we can obtain a better estimate of how χ relates to β:

$$\chi = \beta_{cn}\sqrt{\beta_{cn}^2 - 1} = \beta_{cn}|\alpha_{cn}| \tag{6.2}$$

where $\alpha_{cn} = \alpha_c/k_1$ was introduced.

The dispersion relation (see Ch. 2) implies $\beta_{cn} \geq 1$. Such a relation does not limit the maximum β_{cn} value, but it make sense to consider only values that may be reasonably achieved: in order to check for a reasonable value we can consider the Menzel antenna [93], whose description is available at Ch. 3. The Menzel antenna, in its original design, radiates only the 65% of the power

accepted and has a beam width $\Delta\theta \approx 30.3^o$[1]. The low efficiency of this antenna is due to the huge value of the longitudinal component of the attenuation vector, and specifically $\alpha_{zn} = \alpha_z/k_0 \approx 0.0378$, where α_z is the longitudinal direction of the attenuation vector $\underline{\alpha}$. The short dimension of the Menzel antenna, just 2.5λ, causes, moreover, an extensive backside lobe in the radiation pattern [73], that can be reduced considerably increasing the microstrip longitudinal length. At best of our knowledge such antenna represents the leaky-wave structure having the higher α_{zn} value reported in literature and therefore we can infer the order of magnitude for the maximum value of β_n (or for β_{cn}) considering the one obtained through the Menzel antenna.

Knowing that the maximum radiation of the Menzel antenna exists at a beam angle $\theta_0 \approx 41^o$, it follows $\alpha_{cn} = \alpha_{zn}/\cos\theta = 0.0507$. This is not the maximum α_{cn} value that can be obtained: for instance, we will be able here to design an antenna, derived from the Menzel antenna, characterized by $\alpha_{cn} \approx 0.075$ at X-band; the existence of antennas capable of higher α_{cn} values cannot be excluded, but we did not find in literature any reference to such structures.

Let us assume that it would be possible to radiate, for example, a leaky wave produced in a vacuum and having amplitude of the attenuation vector $\alpha_{cn} \approx 0.2$: it follows $\beta_{cn} \approx 1.02$, and therefore, $\chi \approx 0.204$. Let us suppose that the LWA radiates in the X-band and specifically at a frequency of 12 GHz and let us pose the lossy medium above the antenna aperture with is edge parallel to the antenna aperture. The maximum value of conductivity of the medium which causes a transmitted wave such that the angle ζ_2 formed by the amplitude vector $\underline{\alpha_2}$ and the normal to the separation surface is 90^o is $\sigma \approx 0.139$ Siemens/meter.

$\chi = \chi(\beta)$ for $\beta_{cn} \in [1; 1.05]$ is shown in Fig. 6.1. The curve monotonically grows from its minimum at $\beta_{cn} = 1$ and it tends to a parabolic curve centered in $(0, 0)$ when $\beta >> 1$, this means that χ grows almost geometrically when

[1]Menzel misured $\Delta\theta \approx 28^o$ in its original work, the value $\Delta\theta \approx 30.3^o$ was estimated after the correction applied by Oliner [73]

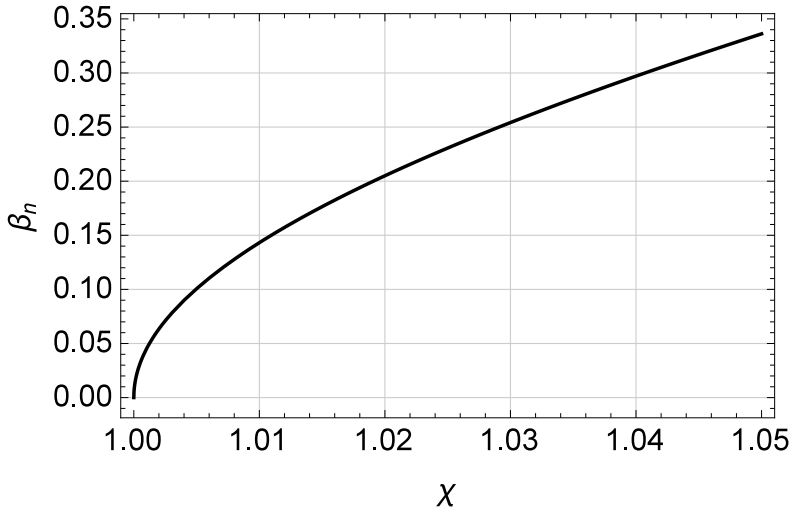

Figure 6.1. Plot of $\chi = \varepsilon_2''/\varepsilon_1$ as a function of $\beta_n = \beta/k_0$ to allow a fast wave at an angle of 45^o.

β_{cn} grows linearly: a small increase in β_{cn} results into a large increase of the χ value and, therefore, of σ. For example, when $\beta_{cn} = 1.05$, which is just the 3% increase in respect to $\beta_{cn} = 1.02$ it is $\chi \approx 0.336$, which at 12 GHz implies $\sigma \approx 0.225$ S/m: this value is more than 60% higher than the conductivity value previously obtained.

The values of conductivity just computed permit us to state that the deep-penetration property exploited by means of LWA may be very challenging in some applications such as air-to-sea communications, where the value of σ, even though it depends on many conditions [94], is generally assumed to be approximatively 5 $\frac{S}{m}$ [95].

The approximated-analytic approach taken in this paragraph strongly suggests to properly design both lossy medium and a LWA to test the feasibility of deep-penetration and its extension (see decay of leaky-wave radiation for a finite mono-dimensional-uniform LWA described in Ch. 3).

6.2 The lossy medium

In the case under study, a vacuum is assumed as medium 1, this approach is quite common in antenna simulations because the vacuum well approximates the air and therefore it is relevant for most of the practical applications (see Ch. 1). The lossy medium 2 is designed here to reduce the reflections that could disturb our "measurements": avoiding reflection is crucial as the presence of the reflected wave can affect the measurement of the field amplitude in proximity of the separation interface. Minimum reflections had to be guaranteed for different angles, because, as we have seen in Chapters 4 and 5, maximum penetration by means of inhomogeneous wave is never permitted by normal incidence, while, on the opposite, for the case of the homogeneous wave generated by a conventional antenna, the normal incidence must be considered, not only because this is the condition that allows maximum penetration for homogeneous waves (see Eqs. (2.17)-(2.19)), but also because it is the only setup that guarantees a constant distance between lossy medium and antenna when the former is posed parallel to the antenna aperture: having a constant distance between lossy medium and antenna aperture is definitely a strong requirement to guarantee an opportune field evaluation especially in near-field simulations, like the one performed here.

To allow low, or better, negligible reflections, in both cases of normal and oblique incidence, and at the same time to make the deep penetration by means of LWAs possible according to the observations reported in the previous paragraph, the lossy medium was designed to meet the following requirements:

$$\begin{cases} \sigma_2 = 0.05\ S/m \\ \varepsilon_2 = \varepsilon_{r2}\varepsilon_0 = \varepsilon_0 \\ \mu_2 = \mu_{r2}\mu_0 = \mu_0 \end{cases} \tag{6.3}$$

where $\varepsilon_0 \approx 8.8542 \cdot 10^{-12}\ F/m$ is the vacuum permittivity and $\mu_0 = 4\pi \cdot 10^{-}7\ N/A^2$ is the vacuum permeability.

With the conditions imposed by Eq. (6.3), Eq. (5.1) becomes:

$$\overline{\beta}_1 = \frac{\beta_{1c}}{k_1} = \frac{1}{\sqrt{2}}\sqrt{1+\sqrt{1+\left[\frac{2\omega\mu_0\sigma_2}{\omega^2\mu_0\varepsilon_0}\right]^2}} \tag{6.4}$$

Assuming to operate at a constant angular frequency $\omega = \omega_0 = 2\pi f_0$ and simplifying the equation above, it is:

$$\overline{\beta}_1 = \frac{\beta_{1c}}{k_1} = \frac{1}{\sqrt{2}}\sqrt{1+\sqrt{1+\left[\frac{\sigma_2}{\pi f_0\varepsilon_0}\right]^2}} \tag{6.5}$$

and for $\overline{\alpha}_1 = \sqrt{\overline{\beta}_1^2 - 1}$ it is:

$$\overline{\alpha}_1 = \frac{\beta_{1c}}{k_1} = \frac{1}{\sqrt{2}}\sqrt{\sqrt{1+\left[\frac{\sigma_2}{\pi f_0\varepsilon_0}\right]^2}-1} \tag{6.6}$$

We have seen in Ch. 3 that $\alpha/k << \beta/k$ is usually assumed for LWAs, it follows $\beta_l/k \approx \cos\theta$, where θ is the angle of maximum radiation and β_l the component of the vector $\underline{\beta}$ in the longitudinal direction of the antenna. The more the condition $\sigma_2 << \pi f_0\varepsilon_0$ is valid (i.e. $\overline{\alpha}_1 \to 0$ in Eq. (6.6)), the more the the approximation on the θ angle applies, and consequently, an LWA that is designed to fit more common requirements, may also apply to deep penetration.

The normalised quantity $\overline{\alpha}_1$ of Eq. (6.6) is plotted in Fig. 6.2 for a frequency range $f \in [1; 12]\ GHz$. It is $0.07 < \overline{\alpha}_1 < 0.08$ when $\sigma_2 = 0.05\ S/m$ and $f_0 = 12\ GHz$; increasing the σ_2 value also $\overline{\alpha}_1$, which is the minimum value of α/k_0 for which deep-penetration is possible, increases.

Given the high amplitude of the $\overline{\alpha}_1$ requested, a choice of a lossy medium such that $\sigma = 0.05\ S/m$ appears almost critical for a LWA operating at a frequency of $12\ GHz$, if $\zeta_2 = \pi/2$ is wished; the frequency $f_0 = 12\ GHz$, chosen in this dissertation, is a further project requirement which goes in addition to the ones presented by Eq. (6.6) for the simulations performed.

The characteristic impedance of medium 1, commonly expressed in literature as ζ_1, is:

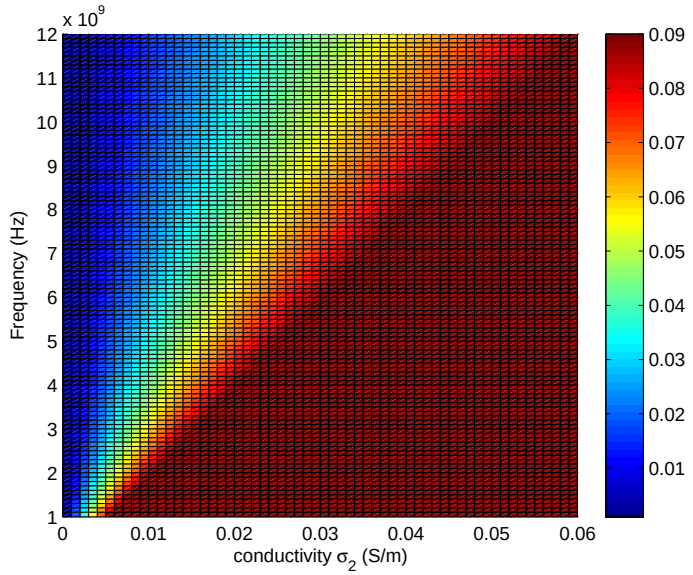

Figure 6.2. $\overline{\alpha}_1$ value requested for deep-penetration at a frequency range of $[1:12]$ GHz and a value of conductivity $\sigma \leq 0.06$ S/m

$$\zeta_1 = \sqrt{\frac{\mu_0}{\varepsilon_0}} \approx 377\ \Omega \tag{6.7}$$

The characteristic impedance ζ_2 of the lossy medium 2 chosen is, instead:

$$\zeta_2 = \sqrt{\frac{j\omega\mu_0}{\sigma_2 + j\omega\varepsilon_0}} \tag{6.8}$$

The complex Fresnel coefficients for p and s-polarized waves at the planar interface with a lossy medium are therefore [96]:

$$\Gamma_s = \frac{\cos\xi_1 - \sqrt{\eta - \sin^2\xi_1}}{\cos\xi_1 + \sqrt{\eta - \sin^2\xi_1}} \tag{6.9}$$

$$\Gamma_p = \frac{\eta\cos\xi_1 - \sqrt{\eta - \sin^2\xi_1}}{\eta\cos\xi_1 + \sqrt{\eta - \sin^2\xi_1}}. \tag{6.10}$$

where:

$$\eta = \left(\frac{\zeta_1}{\zeta_2}\right)^2 = 1 - j\frac{\sigma_2}{\omega\varepsilon_0} = 1 - \varepsilon''_{2r} = 1 - j0.008. \tag{6.11}$$

Reflections always occurr at the interface between medium 1 and medium 2 because the Brewster angle [97], i.e. the angle of total transmission, is only applicable to p-polarized plane waves at the interface between two lossless dielectrics: clearly, if the second medium presents losses, no incident angle can produce a null Fresnel reflection coefficient.

The project parameters imposed here imply $\sigma_2/\omega\varepsilon_0 \approx 0.008$ therefore $\sigma_2 << \omega\varepsilon_0 \Rightarrow \zeta_2 \approx \zeta_1$: the approximation applied appears certainly acceptable considering that the exact solution for the problem studied is very close to the unitary complex circle, and specifically it is $r \approx 0.998$ and $\theta \approx 2^o$, having defined, as usual, r as the radial distance from the origin of axis and θ as the polar angle.

It follows that, even if the pseudo-Brewster angle for Γ_p is verified only for an incident angle $\xi_1 = \pi/4$ (see Fig. 6.4) the reflection may be neglected for any given incident angle: the exact solution for the amplitude of the complex reflection coefficient is shown in Fig. 6.3, where the amplitudes $|\Gamma_p|$ of Γ_p and $|\Gamma_s|$ of Γ_s are shown, such a figure confirms the goodness of the zero-reflection approximation for the given medium.

The reflection coefficients in Fig. 6.3 are particularly negligible when $-\pi/4 \leq \xi_1 \leq \pi/4$: which exactly represents the area of our interest, therefore $|\Gamma_p|$ and $|\Gamma_s|$ for such an interval reported in Fig. 6.4.

We have seen that the common skin-depth formula:

$$\delta_p = \sqrt{\frac{1}{\omega\mu\sigma}} \tag{6.12}$$

is valid only for good conductors (i.e. when $\sigma >> \omega\varepsilon$), in our scenario the homogeneous wave penetration needs to be calculated through the general formula:

$$\delta = \frac{1}{\alpha}, \tag{6.13}$$

where δ is the distance for which the field reduces of a factor $1/e$.

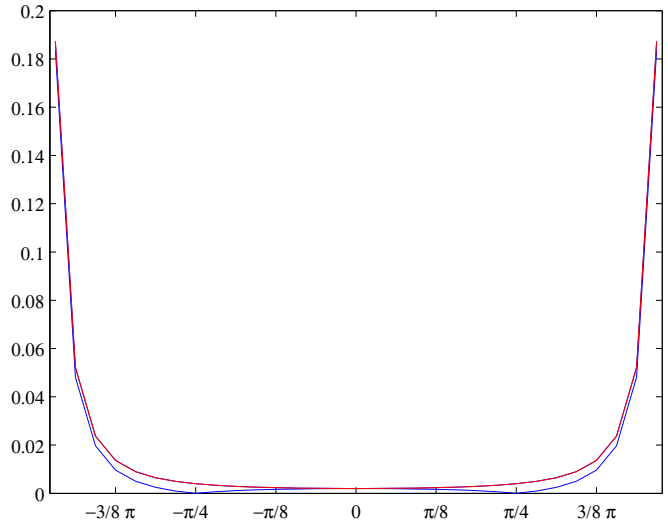

Figure 6.3. Amplitude of the Fresnel coefficients Γ_p (blue), and Γ_s (red) when the condition of Eq. (6.11) is imposed.

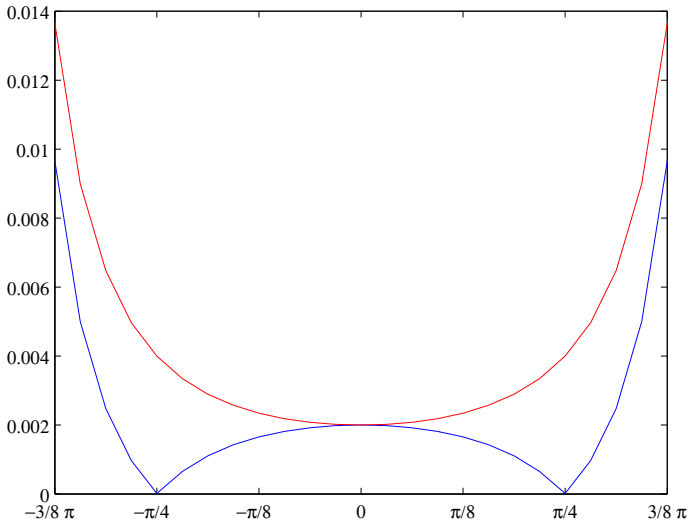

Figure 6.4. Amplitude of the Fresnel coefficients Γ_p (blue), and Γ_s (red) for $\xi \in [-3/8\pi,\ 3/8\pi]$ when the condition of Eq. (6.11) is imposed.

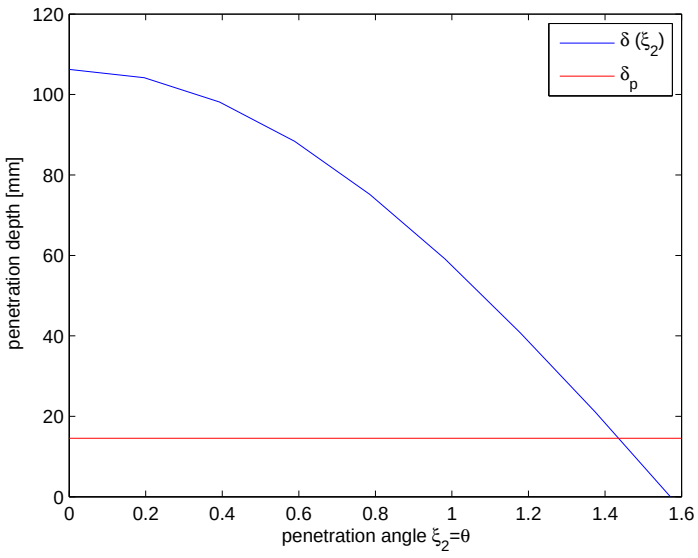

Figure 6.5. Penetration-depth δ of a plane wave in the chosen lossy medium for different angles expressed in radians compared to the penetration-depth δ_p that would have been obtained for a good conductor at the same frequency $f_0 = 12\ GHz$.

The expression of α for this medium can be derived from the Adler-Chu-Fano formula illustrated in Eq. (2.18), where the angle between attenuation and phase vector is, in this instance, the angle ξ_2 that the transmitted vector forms with the normal to the separation surface [2]:

$$\alpha = \pi f_0 \sqrt{2\varepsilon_0 \mu_0} \sqrt{\sqrt{1 + \left(\frac{\sigma}{2\pi f_0 \varepsilon_0 \cos \xi_2} \right)^2} - 1} \tag{6.14}$$

The value $\delta = \delta(\xi_2)$ in Eq. (6.13) is maximum for $\xi_2 = 0$ and then decreases to a minimum value of 0 obtained when $\xi_2 = \pi/2$, (see Fig. 6.5, where both $\delta(\xi_2)$ and δ_p are shown).

As it was anticipated, maximum penetration for a homogeneous incident wave is guaranteed in the case of normal incidence, in particular it is $\delta \approx 106\ mm$ for $\xi_1 = \xi_2 = 0$; more surprisingly, an inhomogeneous wave does never guarantee maximum penetration for normal incidence (see Eq. (5.2)).

[2] Remember that the attenuation vector $\underline{\alpha}$ is always orthogonal to the separation surface when the incident wave is homogeneous

Looking at Fig. 6.5 the difficulty in penetrating a lossy medium in the chosen frequency band is obvious: a medium with modest σ value, like the one that has been chosen, can only be penetrated for few wavelengths (about 4 in our example) by a homogeneous plane-wave (which requires an infinite source). Anyway we must also remember that high frequencies guarantee not only low antenna dimensions, but also high resolution, which is an important factor for many applications, so it is important to increase the penetration at such frequencies.

The medium described above was built and numerically simulated on CST by means of both Finite Integration tecnique (FIT), in time domain, [98]-[99] and Finite Element Method (FEM) [100] in frequency domain (note that FEM can, in theory, also be applied to time domain [101] even though this does not represents the standard approach, and it is not followed by CST which uses FEM in the more common frequency domain configuration); the infinite lossy-medium structure was excited using a plane wave and normal incidence. The boundary conditions were set periodic on the four lateral directions, the bottom side was excited by the plane wave, and PEC was chosen as its boundary; finally, the top layer was set as open boundary, which corresponds to a Perfect Matching Layer (PML) [102]; the medium boundary conditions are shown in Fig. 6.6.

The results obtained through both FIT and FEM simulations are shown in Fig. 6.7 for real and imaginary parts of the field: a very good agreement between the two simulation domains can be noted, but also a slight difference with the result expected analytically, illustrated in Fig. 6.5. The results for the field amplitude, shown in Fig. 6.8, has an excellent agreement also when it is compared to the analytical expected result.

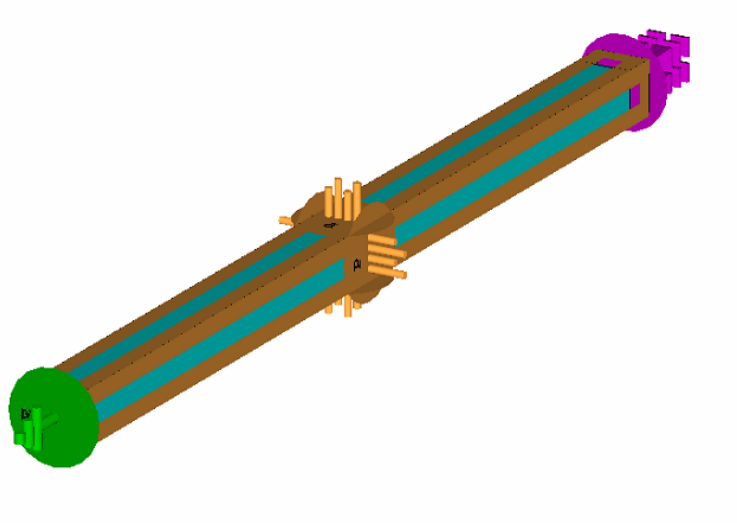

Figure 6.6. Design of the infinite lossy medium used for simulations. Periodic boundary conditions on the lateral edges were imposed to guarantee infinity of the homogeneous medium.

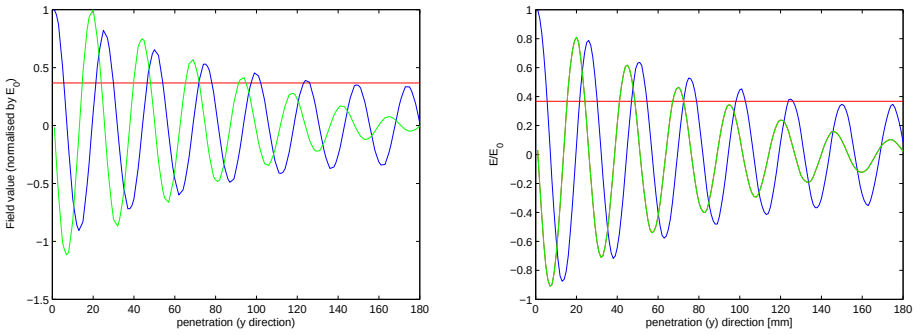

(a) FIT method **(b)** FEM Method

Figure 6.7. FIT and FEM simulations reporting both real (blue) and imaginary (green) values of the electric field, compared with the threshold at $\delta = 1/e$: Results obtained through the two methods are almost equivalent.

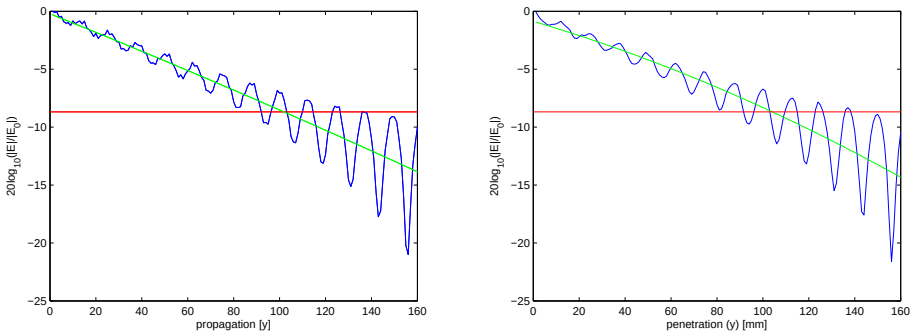

(a) FIT method **(b)** FEM Method

Figure 6.8. FIT and FEM simulations: amplitude of the electric field (Blue) in dB from its maximum value ($20\log_{10}(|E|/|E_0|)$), electric-field average value (green) and threshold at $\delta_{dB} = 20\log_{10}\delta = 20\log_{10}(1/e)$: note that the results obtained through the two methods coincide, moreover, they are also in good agreement with the one theoretically expected.

6.3 Design and simulation of the antennas

A LWA and a pyramidal horn antenna [103] were designed to compare the penetration at a frequency of 12 GHz, the penetration can also be compared with the one obtained through a plane wave impinging normally to the separation surface illustrated in the previous paragraph. The design for the antennas was perfomed in the X-band, mainly because LWAs are several wavelengths long [7] and it was necessary a dimension that would lead to a limited, confortable simulation, for instance, at $12GHz$, that was chosen as operating frequency for our study, a LWA 5λ long would result in 125 mm[3]. Moreoever, the X-band is not an exotic choice, but it represents a suitable frequency for some applications (see for example [104]) in which deep-penetration is an important requirement as shown, for instance, in [105] and in [106]. The design of both antennas is further presented and discussed. In both cases the medium specifically designed for the scope, and described in Par. 6.2, was used, the medium was put at a distance 1.5λ from the antenna aperture, such a short distance justifies the

[3] At the frequency of 1 GHz the same antenna would have been 1.25 meters long

requirement seen at the beginning of this chapter of having the interface with medium 2 parallel to the antenna apertures.

It has to be reminded that the interface between medium 1 and medium 2, assumed infinite in the theoretical studies presented in Ch. 4, Ch. 5, and in the previous paragraph, is not infinite here. Anyway, the approximation of infinite medium 2 still stand if its dimensions are taken reasonably larger than both the wavelength and the antenna aperture (note that the lossy medium does not depend on the beam as the latter is a far-field figure that is not valid in near-field approximation, at least for the horn antenna).

6.3.1 The horn antenna

The horns are medium-directive travelling wave antennas [107] widely used in many fields, and their low Voltage Standing Wave Ratio (VSWR) [103], wide band and easy construction make them very successful especially at the microwave band. A pyramidal horn Antenna was designed and simulated through the commercial tool "Microwave CST", available in the Engineering department of "La Sapienza", the model is illustrated in Fig 6.9. The horn antenna was immersed in a vacuum then, PML was assumed as a boundary in all directions (the option "open and space" of CST achieve both objectives), as it is usually done for antenna design. The simmetry of the electromagnetic field produced by such an antenna permitted to impose a magnetic plane passing by the centre of the antenna and bisecting the larger aperture dimension (blue in figure). This permitted to perform simulation with half of the mesh reducing the computational cost. The antenna was fed through a waveguide port [4]

A time domain simulation, through the *Finite Integration Tecnique* (FIT) method was launched on CST, obtaining a WSVR, illustrated in Fig. ig. 6.10, in line with the value expected from the literature [103].

The far-field radiation pattern [18] obtained is displayed in fig 6.11, such

[4] A waveguide port is a surface perpendicular to a transmission line on which the modes that can propagate along the transmission line are calculated. The field patterns corresponding to these modes are then used as excitation during the simulation [108].

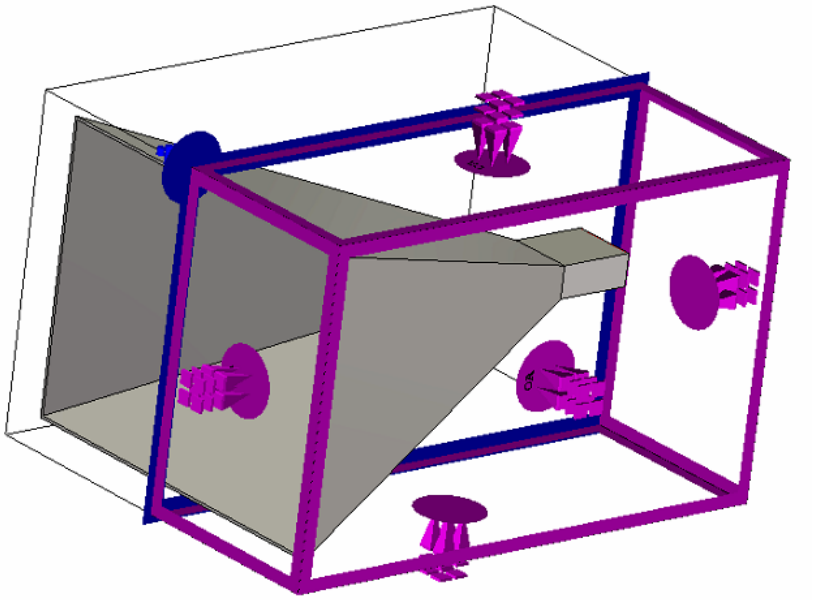

Figure 6.9. Horn antenna design on CST, note the symmetric magnetic plane, in blue, passing for the centre of the antenna structure. PEC was chosen as medium for the antenna structure to allow faster simulations.

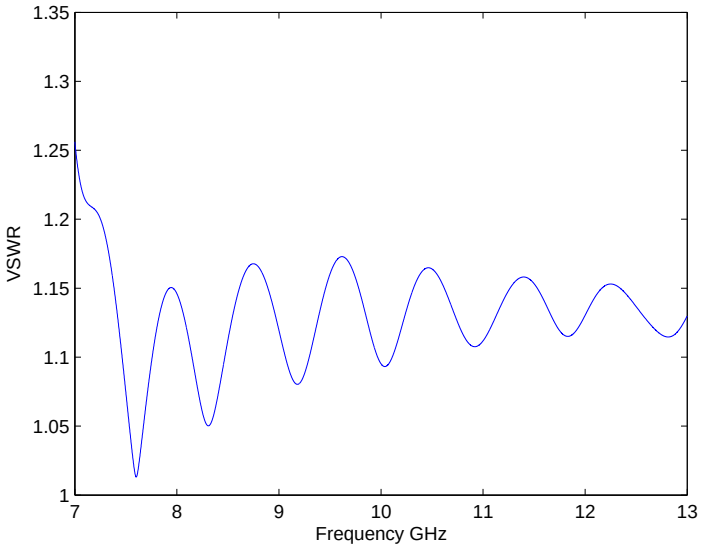

Figure 6.10. Voltage Standing Wave Ratio of the pyramidal horn antenna designed and chosen as a comparison to the LWA.

a radiation pattern is only shown to illustrate the adherence of the modeled antenna to the expected characteristics, and it is not strictly relevant to a near-field application such the simulation performed in this study.

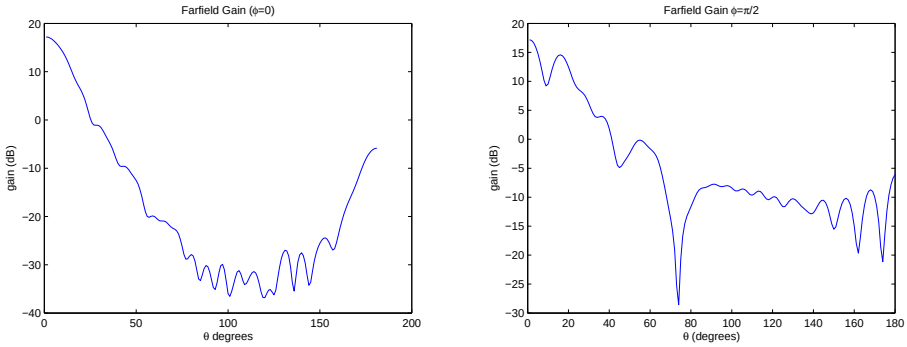

(a) Farfield for $\phi = 0$ **(b)** Farfield for $\phi = \pi/2$

Figure 6.11. Far field diagram generated by the horn antenna for $\theta \in [0; \pi/2]$, both E-plane ($\phi = \pi/2$) and H-plane $\phi = 0$ are shown.

In Fig. 6.12 is, instead, shown the electric-field distribution on the E-plane inside the antenna structure.

It was important to perform our simulation inside the radiating near-field (Fresnel) region and not inside the reactive near-field region: for a horn antenna, the reactive field is usually considered negligible already at a distance $r_0 = \lambda$ from the aperture [109], where the Fresnel region starts. The Fresnel region extends beyond the aperture up to a distance of:

$$r_1 \leq 2D^2/\lambda \ , \tag{6.15}$$

where D is the maximum diameter of the antenna aperture [109], after this distance the antenna is considered radiating in far field. The Fresnel region exists for every antenna such that $D > \lambda$, and the upper boundary reported in Eq. (6.15) is based on a criterion of maximum phase error $\phi_e = \pi/8$ radians [18]. In our case it is $D = 140\ mm$, and the operating frequency is $12\ GHz$, therefore the near-field radiating region extends in $25\ mm \leq r \leq 1.6\ m$. Even though the near field extends for approximately 64λ we performed the simulation putting the lossy medium at the very short distance of $r = 3/2\lambda = 37.5\ mm$.

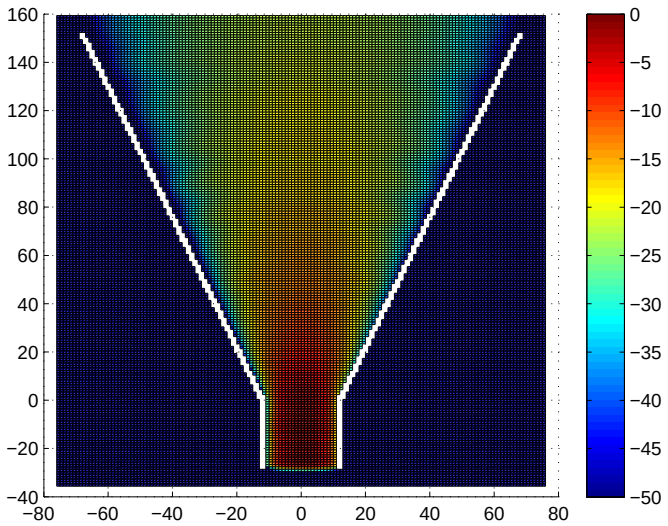

Figure 6.12. Amplitude of the electric-field distribution inside the antenna structure on the E-plane at a frequency of 12 GHz, calculated in dB from the source (Waveguide port)

This distance was chosen such that the requisites for the LWA that will be discussed in the next paragraph, could be satisfied.

As seen in the previous paragraph, and in particular through Fig. 6.5, maximum penetration for homogeneous waves is obtained for normal incidence, therefore posing the lossy medium with its base parallel to the antenna aperture as shown in Fig. 6.13 guarantees an optimum propagation-condition for the chosen antenna. The base of the lossy parallelepiped was chosen as large as the antenna aperture, so that the infinite planar separation surface requested by the theoretical approach would still be acceptable. The assumption of a lossy medium larger than the antenna aperture is relevant in many practical near-field applications, e.g. hyperthermia or Ground Penetrating Radar (GPR) [110]: in both described cases the lossy medium to be heated and explored, respectively, can be many times wider than the antenna used for the task.

In order to verify the penetration achievable by the designed horn antenna, the electric-field monitor option of CST was activated on the $x = 0$ plane with reference to the Fig. 6.13. The penetration of the electric field produced by

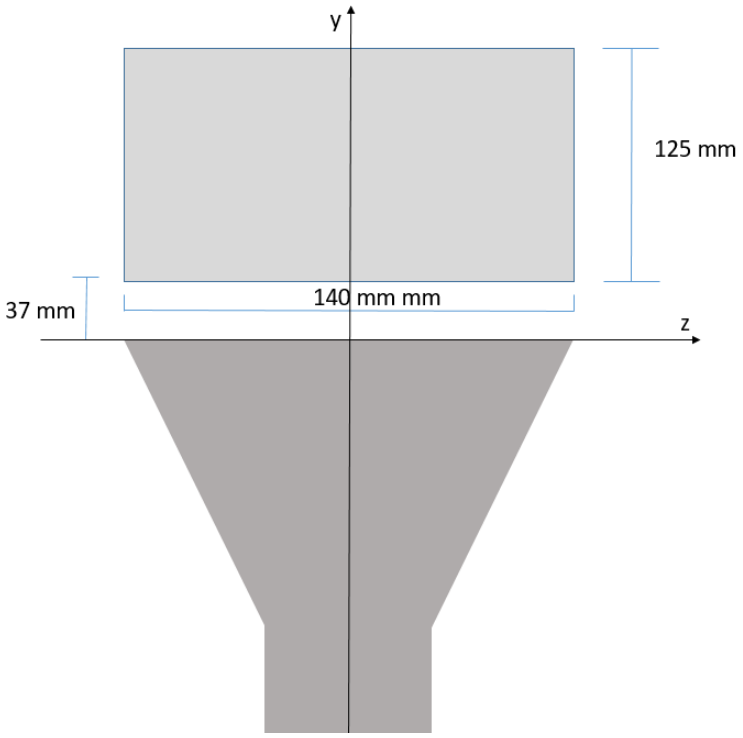

Figure 6.13. Simulation setup, penetration was verified on the $x = 0$ plane.

the horn antenna can be obtained by finding the points $p = p(0, y, z)$ laying on $x = 0$ plane such that the amplitude of the electric field inside the lossy medium ($E_x = |\underline{E}_x(0, y, z)|$), normalised by the maximum of the electric field at the interface between the two media (the field at the interface is expressed by $E_x^{if} = |\underline{E}_x(0, y_{if}, z)|$) is equal to $1/e$: this is an indirect measure of the penetration-depth δ as defined by Eq. (2.24).

The electric-field distribution inside the lossy medium obtained is shown in Fig. 6.14 in dB, and its amplitude is established by the following equation:

$$\begin{aligned} \overline{E}(0, y, z) &= 20 \log_{10} \left\{ \frac{E(0, y, z)}{Max_z \left[E(0, y_{if}, z) \right]} \right\} \\ &= 20 \log_{10} \left[\frac{E(0, y, z)}{E(0, y_{if}, 0)} \right] \forall y > y_{if} \ , \end{aligned} \tag{6.16}$$

where, as usual, E represents the amplitude of the electric vector field $\underline{E}$, i.e. $E = |\underline{E}|$ and where $y_{if} = 1.5\lambda = 37.5\ mm$.

It should be noted that the attenuation was calculated as the quota on

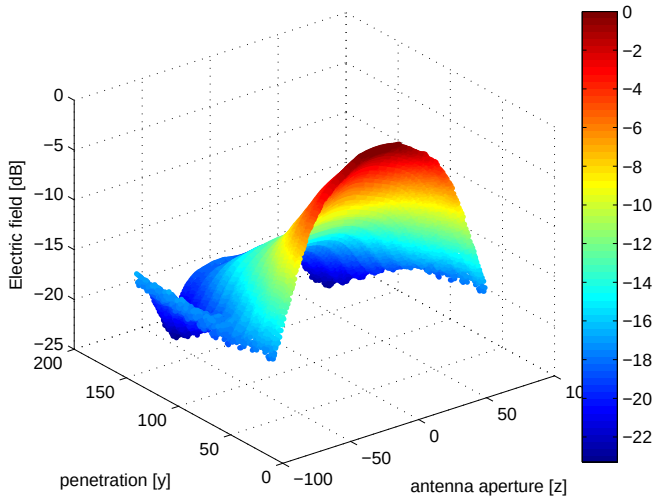

(a) 3D view of the electric-field distribution inside the lossy medium

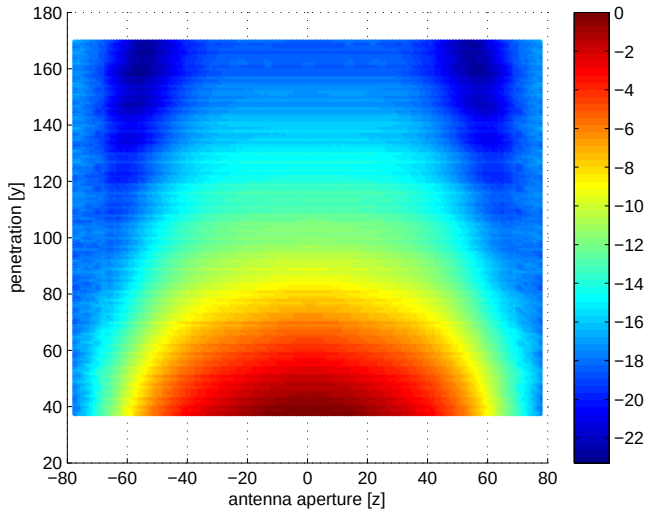

(b) 2D view of the electric- field distribution inside the lossy medium

Figure 6.14. Electric field in the lossy medium produced by the horn antenna, computed in dB from the maximum amplitude of the field at the interface ($x = 0, z = 0$): the origin of axis is posed at the antenna aperture, and the interface with the lossy medium is at $y = 37.5\ mm$.

the y axis for which the signal decreases of a $1/e$ factor from its maximum at y_{if}. Being the Fig. 6.14 expressed in dB from the maximum, we can verify that the penetration depth is given by the y value for which $n = 20\log_{10}(1/e) = -8.86\ dB$, this happens at about $y = 80\ mm$ in Fig 6.14: this means approximately 3.5λ from the aperture, that corresponds to a penetration of about 2λ inside the lossy medium (having subtracted $y_{if} = 1.5\lambda$).

The penetration is lower than the one achieved by means of the plane wave, described by Eq. 2.11, because, in near-field radiating condition, the field decreases intrinsically of a $1/r^2$ factor [5], the field reduction due to this factor accumulates on top of the losses introduced by the designed lossy medium.

6.3.2 Choice of the leaky-wave antenna

The leaky-wave antenna was designed to prove that it is possible to improve penetration by means of inhomogeneous waves. LWAs are naturally near-field operating antennas, anyway, conventional definitions related either to the attenuation in near field or to the boundaries of the near-field region do not apply to those structures, because, for instance, the field may increase, in the near-field region, when the distance r from the antenna aperture grows, as typically happen for an uniform mono-dimensional LWA (see Ch. 3), while, for conventional antennas, a decay going either as $1/r^2$ or $1/r^3$, would be expected.

A uniform, non-periodic, and planar LWA structure was designed to achieve the objective of deep penetration in regards to the medium described in the previous paragraph. Let us discuss this choice.

We have seen that inhomogeneous waves can be created by different kind of structures, for instance, a lateral inhomogeneous wave can be created by means of a dipole, but LWAs are the only kind of structure known, at best of our knowledge, that can artificially create a leaky wave, i.e. a non-uniform wave that radiates away from the source and is not bounded to the interface

[5] Do not confuse this region with the near-field reactive region, for which the field decreases intrinsically of a factor $1/r^3$.

with the lossy medium, where different kind of inhomogeneous waves, such as surface or lateral waves, are instead confined (see Ch. 2).

Planar LWAs have been chosen for this test because they have important advantages: they are easy to be simulated, protyped first and then mass produced, they are cheaper than traditional LWAs, they have a high quality factor, and low losses [111]-[112], all those characteristics made them very attractive in view of a possible experimental verification.

We have seen in Ch. 3 that the main disadvantage of planar structures, when compared to LWAs derived by waveguide three-dimensional structures, is the reduced amount of power that the planar structures are able to handle; anyway, this feature is not important from an experimental point of view.

Established that a planar structure was convenient for all the reasons mentioned above, choices could have been periodical against uniform, or quasi-uniform structures and two-dimensional (2-D) against mono-dimensional (1-D). In a periodic LWA, the periodical modulation creates a guided wave consisting of an infinite number of space harmonics, said Floquet waves [59, 36]. In a 1-D periodic antenna, the fundamental mode does not radiate while usually the radiation occurs through the -1 order mode; at this point the beam of the 1-D periodic leaky-wave antenna can point in either the backward or the forward direction, allowing both $\beta_{-1} < 0$ and $\beta_1 > 0$, and in particular a proper wave is produced when $\beta_{-1} < 0$, while an improper wave is radiated when $\beta_1 > 0$ [7]. We already demonstrated that, by choosing a lossy medium laying at a constant distance from the antenna aperture the required mode for deep-penetration needs to be improper, this makes the dual-direction scanning property just mentioned useless and therefore periodic 1-D antennas do not constitute the most straightforward choice for testing deep-penetration.

The planar leaky-wave antenna with 1-D periodicity presents a natural stop-band at broadside, and many techniques were used in literature to overcome to this problem, for instance see [113]-[114]; anyway, a two-dimensional periodic antenna permits to overcome the difficulty of radiating a broadside

permitting a pencil beam at broadside and of conical shape when the frequency increases (together with the scanning angle), moreover this kind of antenna permits a frequency scan in both E-plane and H-plane. A typical planar and two-dimensional antenna structure is characterised by a top PRS (Partially Reflective Screen) that can be achieved either through a substrate/superstrate structure or through metal patches: it is possible to demonstrate the equivalence [115] between these two different geometries.

Even though it was previously demonstrated that deep-penetration never occurs for normal incidence ($\zeta_2 < 90^o \ \forall \xi_1 \in [0, 90^o[\ U \ \beta \in \mathbb{R}$), it was interesting to test the penetration of a LWA radiating at broadside because this configuration allows a direct and simple comparison with a typical traditional antenna, and because it is beneficial in many applications in which broadside radiation is a requirement.

In the broadside leaky-wave radiation, when present, the existence of the tangential component α_t of the attenuation vector must necessarily be conserved, therefore it was worth to verify whether α_t presence was a sufficient condition for a deeper penetration.

6.3.3 The two-dimensional LWA

In [116]-[117] we designed the two-dimensional metal-patch antenna first proposed by Zhao et al. in [55] whose layout design is illustrated in Fig. 6.15

The original design was based on a substrate having $\varepsilon_r = 1$ but we chose to design two prototypes, the first using RT5870 ($\varepsilon_r = 2.2$) as dielectric and the second using RO4003 ($\varepsilon_r = 3.55$). Only the former antenna design is described here, the interested reader may refer to [116] for the full details of both antenna projects. The choice of RT5870 resulted in different antenna dimensions from the ones reported in [55] (where $\varepsilon_r = 1$ was assumed), and in particular, with reference to Fig. 6.15, the following parameters were set: $h = 8.4$ mm, $L = 12.5$ mm, $w = 1$ mm, $a = 13.5$ mm, $b = 2$ mm. The feeding was initially realized through a $\lambda/2$ dipole [18] posed at a distance $h/2$ from

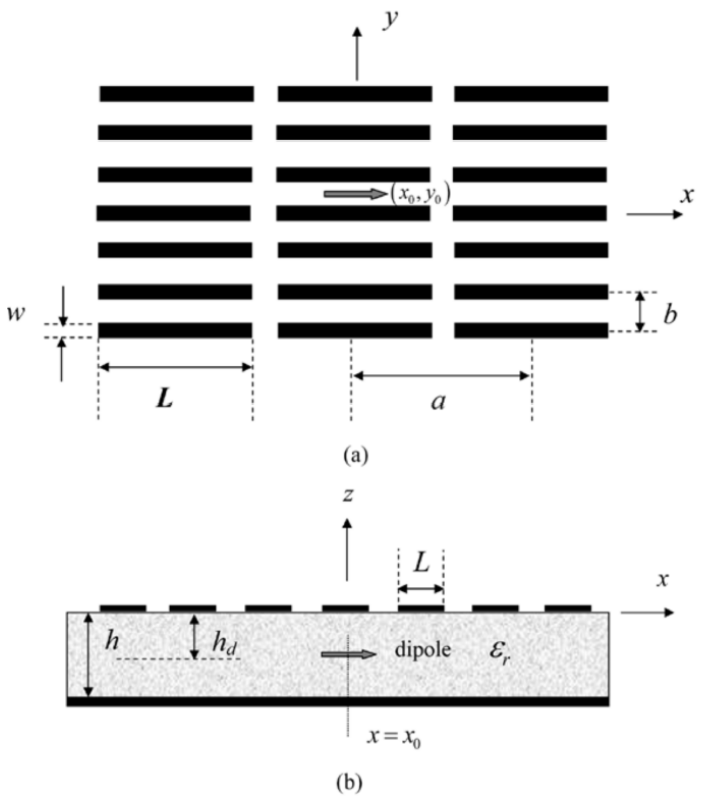

Figure 6.15. Geometry of the Zhao antenna, (a) top view and (b) front view.

the groundplane in the dielectric and fed through a discrete port; in a second moment, a microstrip slot [118]-[119] was taken into consideration to achieve a more realistic feeding mechanism.

This antenna structure behaves as a "leaky parallel-plate waveguide", operating in its first mode, this means that the field varies of half wavelength between the patch plane and the ground plane. The PRS permits to radiate at an angle θ_p which is easy to calculate from the parallel guide approximation, it is:

$$k_{z1}h = (k_1 cos\theta_d) = n\pi \ , \tag{6.17}$$

θ_d is the radiation-angle of the leaky mode in the substrate and n represents the mode, i.e. $n = 1$ for the first mode; θ_d is related to θ_p through the Snell law, therefore we can write:

$$\frac{h}{\lambda_0} = \frac{n}{2\sqrt{\epsilon_r - \sin^2\theta_p}}, \tag{6.18}$$

If the broadside radiation is the only wished, then relative permittivity ε_r of the substrate can be arbitrary. If, instead, a scanning angle $\theta_p > 0$ is requested, then ε_r is no longer arbitrary and if its amplitude is chosen too low, higher order modes of the parallel-plates guide may be encountered, disturbing the leaky mode and reducing the effective value of the possible scanning angle obtainable. In order to achieve a scanning angle $0 \leq \theta_p \leq \theta_0$ it is required that the mode $n = 1$ would arrive to θ_0 before the mode $n = 2$ would appear at broadside.

The maximum value for the scanning angle that can be reached through the mode $n = 1$ without disturbs incoming from the mode $n = 2$ is therefore represented by:

$$\theta_0 = \theta_p^{max} = \arcsin(\sqrt{3\epsilon_r}/2) \tag{6.19}$$

Using the formulas above, and fully described in [55, 120], we designed the LWA for a maximum scan angle of 60^o. Note that the E-plane scan is

not suitable for this antenna because of the presence of the TM_0 surface-wave mode, therefore the eventual frequency scanning was designed to operate on the H-plane.

To avoid grating lobes it is necessary that the $p = -1$ Floquet mode is at backward endfire, i.e. $\sqrt{k_1^2 - (\pi/h)^2} = k_0$ when, at maximum, the $p = 0$ Floquet mode is forward endfire, i.e. $\sqrt{k_1^2 - (\pi/h)^2} - 2\pi/a = -k_0$. Imposing the two, it is:

$$\frac{a}{\lambda_0} \leq 0.5 \tag{6.20}$$

Note that some grating lobes, even if this condition is met, necessarily appear when the antenna has finite dimensions because of the border effects.

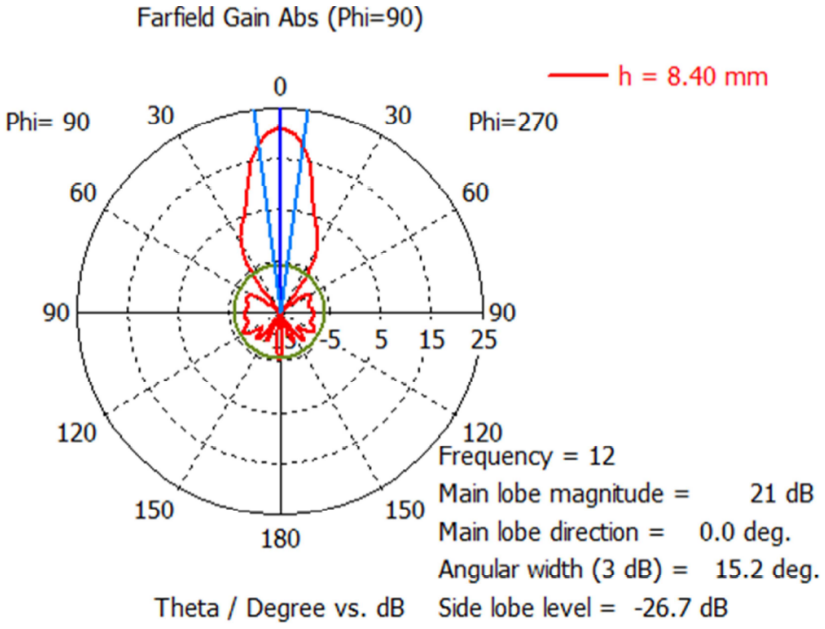

Figure 6.16. Radiation pattern at broadside obtained for the two-dimensional periodic LWA (H-plane) having a RT5870 substrate.

The antenna designed was simulated in CST Microwave Studio (using FIT mainly because of it results usually in quicker processing time). The H-plane radiation pattern and the three-dimensional radiation pattern at broadfield obtained are shown in Fig. 6.16 and Fig. 6.17.

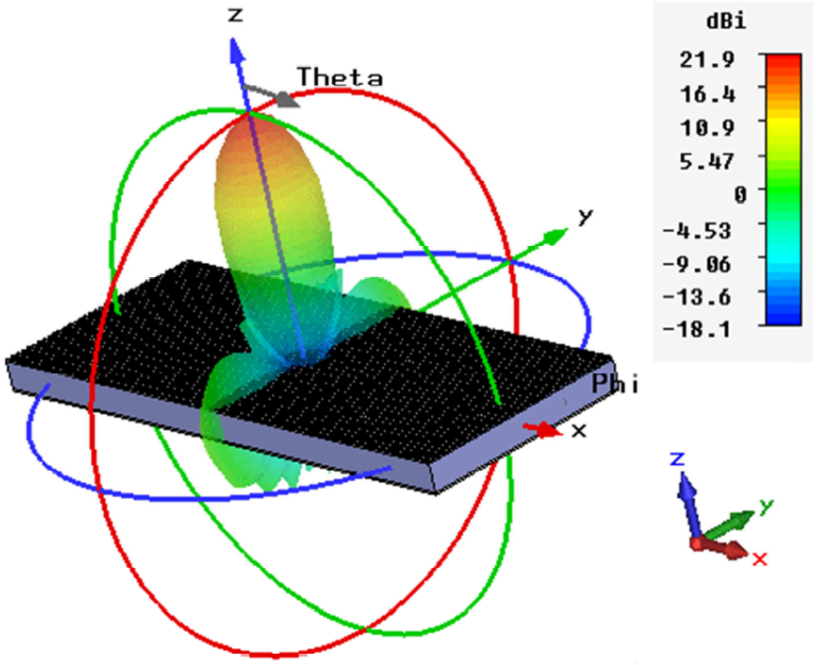

Figure 6.17. two-dimensional LWA antenna design and three-dimensional radiation pattern (RT5870 substrate).

To verify the penetration produced by this antenna into a lossy medium posed parallel to the separation surface, a horn antenna with circular aperture was used and optimized for a frequency of 12 GHz using the parameter sweep option of CST. The antenna is shown in Fig. 6.18 and its three-dimensional farfield is shown in 6.19.

While the first comparisons seemed to indicate comforting results, subsequent simulations verified no significant differences between the penetration produced by the two antenna on media such that $\sigma > 0.005$ Siemens/meter, therefore a higher value of the attenuation constant α was required for broadside radiation, or a radiation angle greater then 0^o. The conflict between results in this antenna simulations are under investigation and they seem to be mostly due to the resilience of the Leaky field from small disturbance, i.e., even when the field is calculated through E-field monitor on the central line passing by the axis of symmetry of the antenna, the lossy solid cannot be taken smaller than the antenna aperture, otherwise contributions coming from

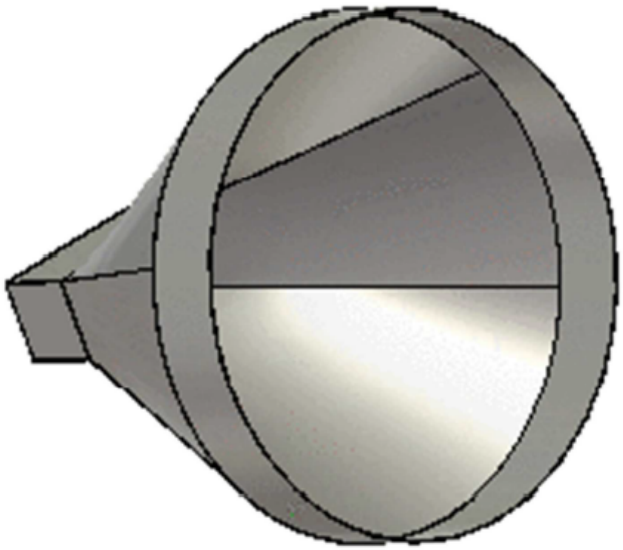

Figure 6.18. Design of a circular-aperture broadband horn antenna optimised for 12GHz radiation.

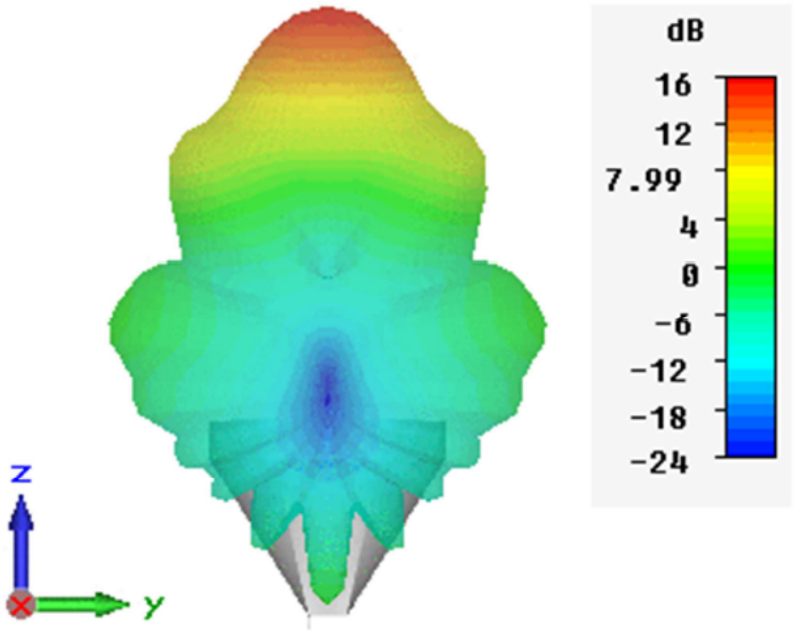

Figure 6.19. Farfield produced by a circular-aperture broadband horn antenna optimised for 12GHz radiation.

patches lateral to the lossy medium and entering in the medium from its lateral edges participate to the field internal to the medium, giving the impression of higher penetration, moreover those simulations were performed when the theoretical expansion was not completed, therefore will be reviewed analysed in the near future, again.

Note that in the metal-plate two-dimensional antenna, h and ϵ_r do not influence α, but they influence the scan angle. This is true under the assumption that the metal patch are very close each other, so that the reflection coefficient of the PRS is very close to -1. It is the space and the shape of the patches that influences α, but the reflection coefficient needs to be close to -1, this reduces the applicability of this antenna for deep-penetration purposes. The distance between the patches (and therefore α) is very sensible and its variation may lead to the radiation of unwanted modes [120].

In Fig. 6.20 we show the penetration achieved modifying the aforementioned distance between patches. As we can see, initially the penetration increases, but then, above a certain critical value of the parameter "a", it starts decreasing again, confirming what was explained above. Moreover, it is evident that the increase of penetration with this strategy is very modest.

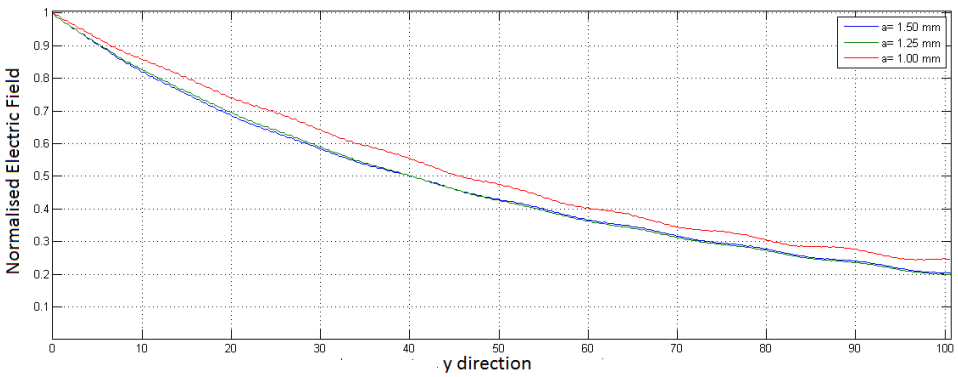

Figure 6.20. Penetration obtained modifying the distance "a" between the patches. The $y = 0$ direction in abscissa represents the interface between lossless and lossy media in figure.

Having verified that a broadcast radiation did not achieved the wished

result, the two-dimensional periodical structure became unnecessary, because, to verify the formulas reported in Chapters 4-5 it is sufficient to create a LWA radiating at a specific angle, best chosen to be 45^o, which is the value that minimizes the phase vector amplitude β_1.

It is therefore clear that the additional complexity implied by periodical antennas does not result in an advantage from a deep-penetration prospective, therefore uniform mono-dimensional LWAs represented the best choice.

6.3.4 The microstrip leaky-wave antenna

A typical problem of LWA technology is the presence of the surface wave, whose radiation mode may overlap with the leaky-wave radiation mode. It was important either to reduce such a disturbing wave or, better, removing it, so that we could compute exactly the contribute of the leaky mode to the penetration, without the influence of the unwanted surface waves; we therefore chose a planar, mono-dimensional and non-periodic structure, derived from the Menzel [93] antenna, which consists of a simple uniform microstrip line and does not present surface wave in the leaky radiating region, the antenna is shown in Fig. 6.21, and it was extensively described in the Ch. 3.

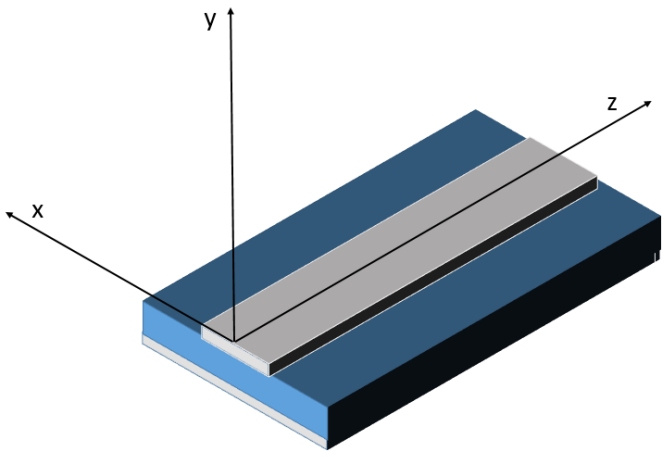

Figure 6.21. Geometry of the microstrip Menzel antenna: a simple uniform microstrip line.

Here, a well established full-wave numerical approach [121] based on a mixed-potential integral equation in a unit-cell environment solved by the Method of Moments (MoM) in the spatial domain through a triangular Delaunay mesh[6] [122]-[123] was employed; such a technique is suitable for the study of both periodic and uniform mono-dimensional structures: when a uniform stripline is considered then it is regarded as a periodic structure along its longitudinal direction (see Fig. 6.21), a similar approach is also described in [124]. The antenna was designed to allow deep-penetration at an incident angle[7] $\xi_1 = \pi/4$, so that β_{1c} in Eq. (5.1) assumes its minimum value, it is:

$$\frac{\beta_{1c}}{k_1} = \frac{1}{\sqrt{2}}\sqrt{1+\sqrt{1+\left[\frac{2\cdot 0.05}{2\pi\cdot 12\cdot 10^9\cdot 8.85\cdot 10^{-12}}\right]^2}} \approx 1.0027879\ , \qquad (6.21)$$

and consequently, for α_{1c}/k_1:

$$\frac{\alpha_{1c}}{k_1} = \sqrt{\left[\frac{\beta_{1c}}{k_1}\right]^2 - 1} \approx \sqrt{1.0027879^2 - 1} \approx 0.0747234 \qquad (6.22)$$

where $k_1 = k_0$ was imposed, having assumed a LWA radiating into a vacuum.

Uniform LWAs are usually designed to meet certain requirements in terms of the longitudinal components of phase and attenuation vectors, i.e. β_z/k_0 and α_z/k_0, respectively. Those components are directly related to the amplitude of phase and attenuation vectors, respectively, when the maximum radiation angle is known. In the represented case, such an angle is $\theta_0 = \pi/4$ radians, therefore:

$$\frac{\beta_z}{k_1} = \approx 1.0027879\frac{\sqrt{2}}{2} \approx 0.711 \qquad (6.23)$$

[6]Delaunay triangulation is a geometric structure possessed of mathematical properties uniquely well suited to creating good triangular and tetrahedral meshes. Delaunay triangulation in the plane is that no vertex of the triangulation lies in the interior of any triangle's circumscribing disk - the unique circular disk whose boundary touches the triangle's three vertices. In three dimensions, no vertex is enclosed by any tetrahedron's circumscribing sphere.

[7]Lossy medium separation surface and antenna aperture are parallel, therefore the incident and the angle of radiation always share the same value

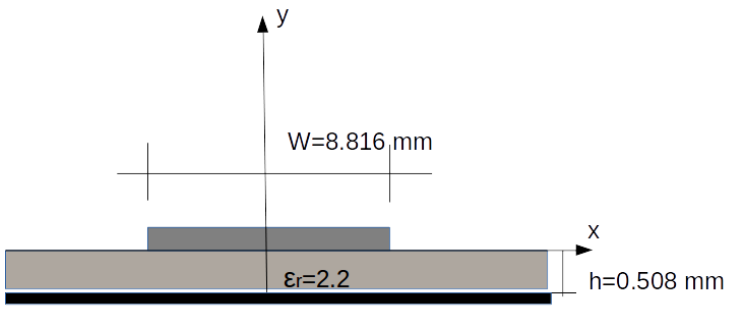

Figure 6.22. Microstrip leaky-wave antenna dimensions, note that both the metal strip and the ground-plane are considered PEC ($\sigma \to \infty$ and that the substrate losses are neglected, i.e. the substrate conductivity is $\sigma = 0$

$$\frac{\alpha_{1c}}{k_1} \approx 0.0747234\frac{\sqrt{2}}{2} \approx 0.0528 \tag{6.24}$$

Using a fortran MoM code that implemented the method described above an antenna having microstrip-width dimension of 8.816 mm, substrate tickness of 0.507 mm and substrate relative dielectric constant $\varepsilon_r = 2.2$ (the substrate was considered non lossy, i.e. $\sigma = 0$) was designed; the antenna dimensions are reported in 6.22 for simplicity. This code assumed infinite transversal section, and infinite ground-plane approximation.

The values obtained through the MoM code for both β_z/k_0 and α_z/k_0 well approximated the ones requested by Eqs. (6.23)-(6.24), and specifically the following values were found:

$$\begin{cases} \frac{\beta_z}{k_0} = 0.7088 \\ \frac{\alpha_z}{k_0} = 0.05234 \end{cases} \tag{6.25}$$

The code employed did not exactly indicate which high-order mode was related to the dispersion diagram shown, but it highlighted the existence of such high-order mode, with the given dispersion diagram. The code employed also highlighted that such a mode had to be odd in respect to the waveguide port feeding the microstrip LWA. The dispersion diagram obtained by means of the MoM analysis performed by the code is shown in Fig. 6.23.

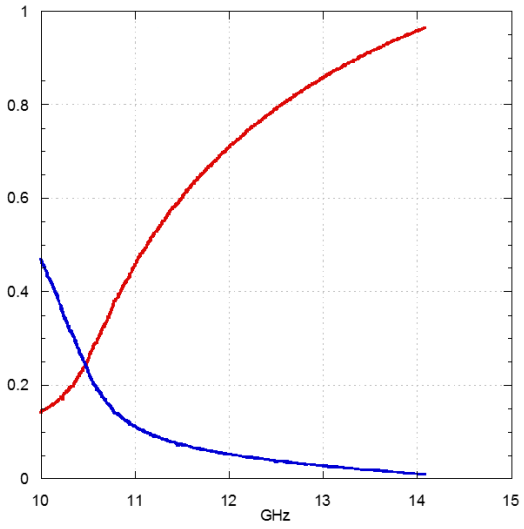

Figure 6.23. Dispersion diagram computed in the LWA design phase: β_z/k_0 (in red) and α_z/k_0 (in blue) are shown

The antenna was then reproduced in the commercial CST Microwave Studio, and it was designed to radiate the 94% of the power accepted, this set the longitudinal length on the z axis to approximately $L = 5\lambda = 125\ mm$, such a length was decided through simulations, but its value resulted about $\lambda/2$ longer than the value obtained by theoretical equation defined in [7] and reported in Eq. (3.10), that in this specific case results into:

$$L = -\frac{\lambda}{4\pi\alpha_z/k_0} ln\left[\frac{P(L)}{P(0)}\right] \approx\ 106\ mm \tag{6.26}$$

The LWA was fed through a waveguide port at one extreme, an identical waveguide port was placed at the opposite longitudinal termination of the antenna to act as a load so that the 6% of non-radiated power could be absorbed. The three-dimensional radiation pattern of the second higher-order odd mode, according to the full-wave FIT and FEM simulations performed is shown in Fig. 6.24 and the radiation pattern in the $\phi = 0$ plane, which was shown in Ch. 3 for an ideal infinite antenna, is shown in 6.25 and it is consistent with the results expected from the custom code employed.

CST permits to select and analyze a single mode at the time, while a

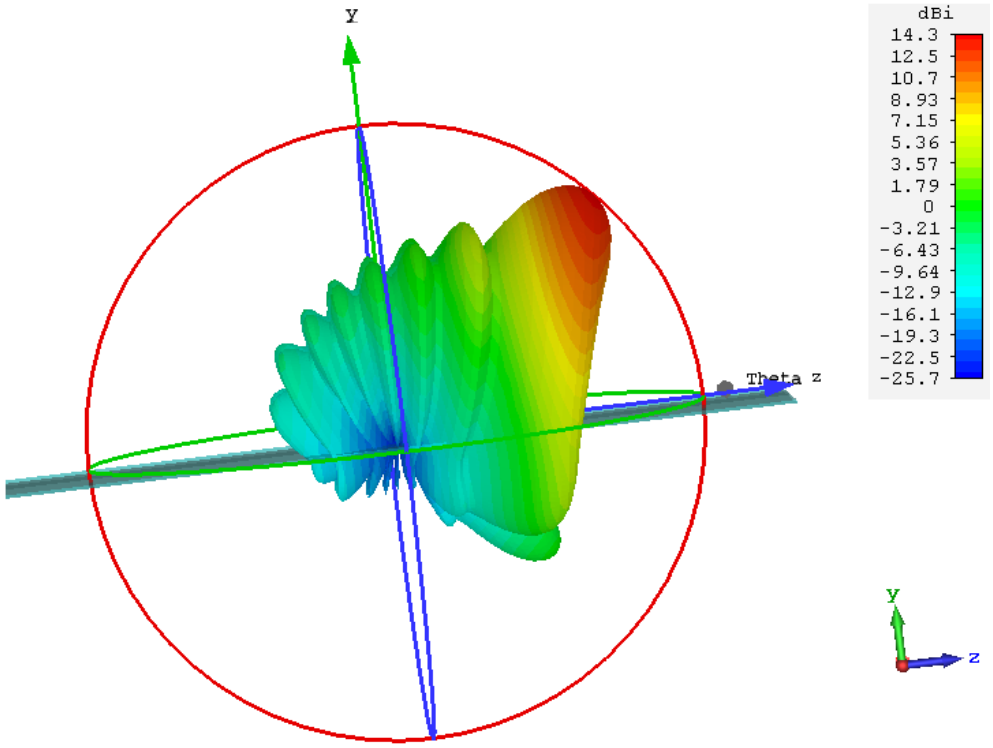

Figure 6.24. Microstrip leaky-wave antenna 3D radiation pattern, it can be noted the absence of back lobes due to the waveguide port posed as a load, the tipical conical shape and the presence of grating lobes.

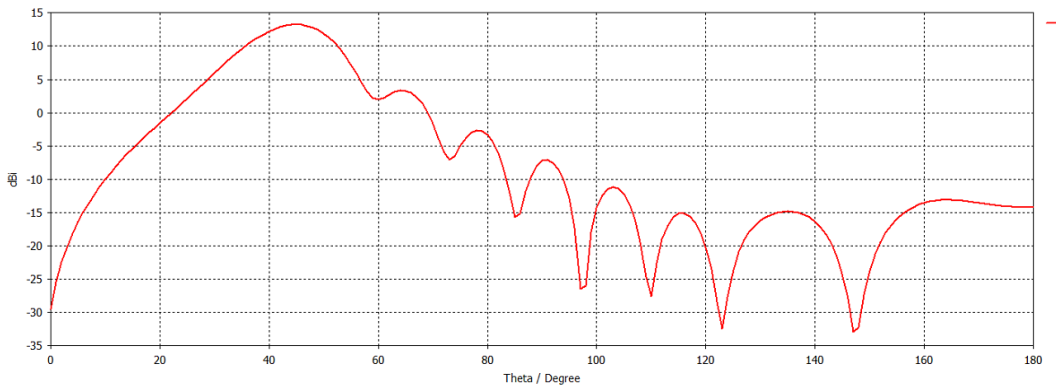

Figure 6.25. Microstrip leaky-wave antenna radiation pattern (in the $\phi = 0$ plane) at a frequency of 12 GHz. The beam-width at $3dB$ is 16.6^o, the radiation angle is 45^o. Note that grading lobes, which are expected for a finite-length antenna, are present, such lobes can be reduced, but not fully eliminated, by imposing TE as boundary condition for the lowest y value.

prototype would require the suppression of undesired modes. In this particular case, the dominant mode can be suppressed by exciting the upper conductor of the microstrip line in antisymmetric fashion using a pair of stubs fed from below [69]. Another way is to use an asymmetric feed arrangement together with a sequence of transverse slits on the center line of the antenna [93], finally, the suppression of the fundamental mode can be obtained through a vertical via connecting the central axis of the Microstrip with the groundplane [125], such a design is equivalent to considering just half of the Menzel antenna (see Fig. 6.26) whose LWA radiation pattern is approximates very well the one of the full Menzel Antenna.

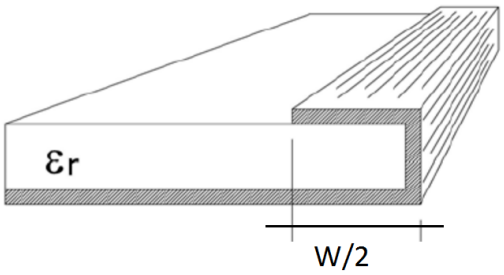

Figure 6.26. Half Menzel Antenna, this antenna approximates the full Menzel antenna and suppresses the fundamental mode.

Here, in order to kill the Q-TEM mode and all the even modes, a PEC symmetry plane passing for the longitudinal symmetry axis[8], i.e. $x = 0$ plane, was imposed on CST as illustrated in Fig. 6.27, this PEC plane was then removed for the final simulation where the electric field at the symmetry axis of the structure had to be evaluated.

To evaluate the penetration, the electric field was sampled on the antenna-simmetry plan at $x = 0$ (see Fig. 6.22), through the E-field monitor option of CST.

As seen, all theoretical results found in Ch. 5, which are strictly valid only for a plane-wave approximation, can be only verified in a limited region

[8]This was not required for CST, for which a single mode can be isolated, but it resulted in a quicker simulation as only half structure needs to be simulated.

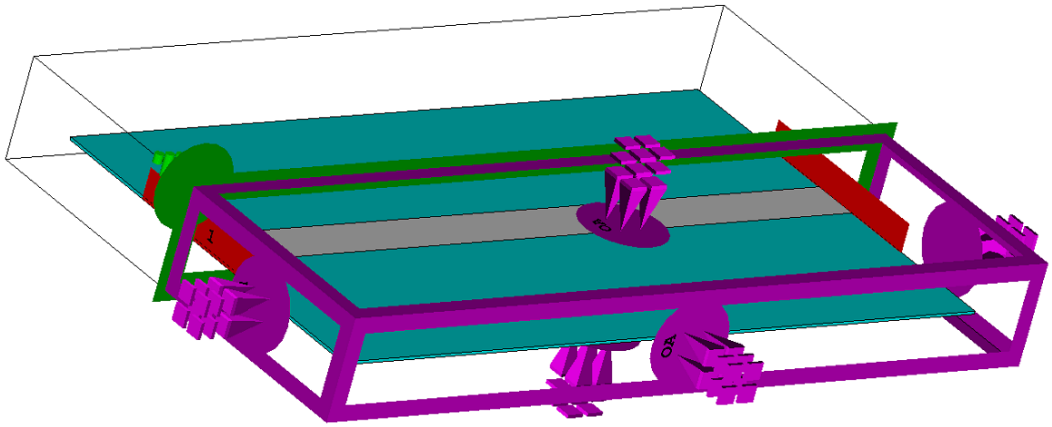

Figure 6.27. LWA geometry, note the PEC symmetry plane imposed on the symmetry-axis of the LWA structure. Two waveguide ports (in red) are present at the two longitudinal extremes of the LWA.

of space by a realistic LWA, because of the Sommerfeld condition, and, in particular the Silver-Müller equations reported in Eqs. (2.26).

In order to obtain a perfect inhomogeneous plane-wave behaviour, the mono-dimensional uniform LWA must present uniform and continuous leakage of power all along the aperture, moreover its longitudinal dimension has to be infinite and so needs to be the radiated power. When the source is finite, the electromagnetic field leaked by the LWA must exponentially decay along the longitudinal antenna aperture from its maximum, at feeding point, as explained in Par. 3.1.2, and illustrated in Fig. 3.2: in our case the maximum power along the aperture is found on the origin of the z axis, where the waveguide port is set. In this, practical, scenario, we need to find a region in which the improper-wave behaviour exists at the interface with the lossy medium, in other terms, the interface with the lossy medium needs to be outside the shadow cone in which the radiation decays (see Ch. 3).

The broadside direction, in the antenna design, corresponds to the y direction; we can indicate with y_{if} the position in which the interface with the lossy medium is expected, experimentally posed at 37.5 $mm = 1.5\lambda$ from the antenna aperture. If the antenna is electrically long enough, a value of z_c on

the longitudinal direction exists such that y_{if} meets exactly the shadow cone. For $z < z_c$ an attenuated wave is found at $y \geq y_{if}$, reducing further the z value the field at y_{if} may result negligible; finally, the radiation at $y = y_{if}$ behaves as an improper leaky wave for $z > z_c$: the curve described by the amplitude of the electric field at $y = y_{if}$ is illustrated by the green curve shown in Fig. 6.30, it has to be noticed, in such a figure, that the field at y_{if} quickly grows, stays almost constant, and then decreases with an high slope, this behaviour is direct effect of the finite electric-field radiation: at first contributes to the field due to the electric field leaked in previous sections of the antenna aperture need to start summing up to a maximum, then, increasing the distance from the feeder, those high-energy contributes move on the vertical for $y > y_{if}$, and new contributes have to sum to create field at y_{if}, but the latter have less energy because of the exponential decay of the field along the aperture. Regardless to the value that the field on the aperture assume, for higher values along the z longitudinal direction, more points move outside the shadow cone and inside the leaky region, as it can visualized looking at Fig. 3.2.

To verify the exposed behaviour for the designed LWA, we evaluated numerically the electric field on the $x = 0$ symmetry plane through the CST E-field monitor option. Let us take N samples on the z axis, i.e. $z \in [0, N-1]$ where $z = 0$ is the plane passing from the feeder and $z = L - 1$ corresponds to the plane passing from the load. In general, it must be assumed $N > L - 1$ because of the radiation angle; in particular, in order to test the penetration $N = L + 5\lambda - 1$ was chosen at a given sampling rate of 1 mm. According to such a sampling rate, z_k represents a plane passing by the k^{th} point on the longitudinal direction, distant k mm from the plane $z = 0$ and parallel to such a plane. The amplitude of the electric field for a generic value of y is $|\underline{E}\,(0, y, z_k)\,|$, this value is normalised by the amplitude of the electric field evaluated at $y = y_{if}$, obtaining the following dimensionless quantity:

$$\overline{E}(y)_{|z_k} = \frac{|\underline{E}\,(0, y, z_k)\,|}{|\underline{E}\,(0, y_{if}, z_k)\,|}, \tag{6.27}$$

Curves describing $\overline{E}(y)_{|z_k}$, for different $z = z_k$ values, whose full analysis is reported in [126], are illustrated in Fig. 6.28: it is possible to verify that the electromagnetic wave generated by the LWA attenuates when $z_k < 100\ mm$, while the improper-wave behaviour start appearing for $z_k \geq 100\ mm$, which is only one wavelength prior the antenna termination ($L = 125\ mm$).

By reducing the distance y_{if}, that represents the distance between lossy medium and the antenna when the lossy medium is present in the simulation domain, the leaky-wave behaviour would have been experienced for $z_i < z_k$, but, at the same time, having the medium too close to the antenna could pose it in the reactive region, where the lossy medium becomes part of the antenna itself, changing completely the nature of our problem: $y_{if} = 1.5\lambda$ was demonstrated to be a good compromise between the two, opposite, requirements[9].

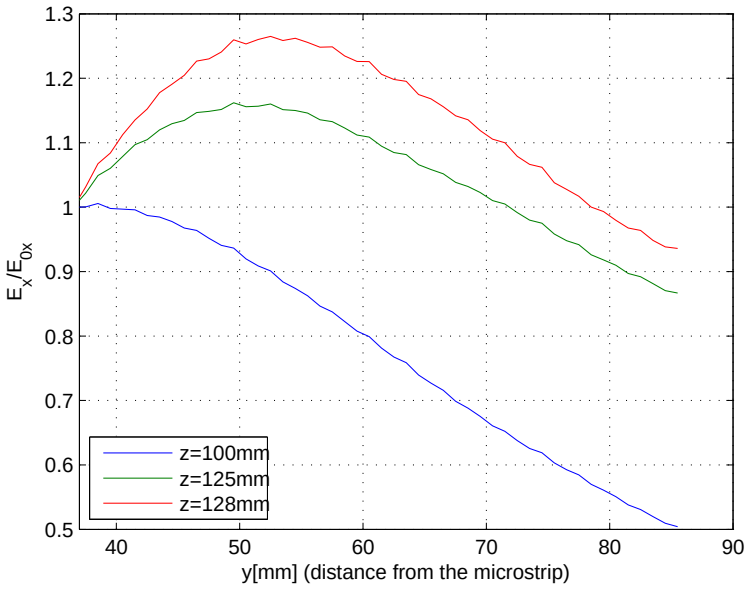

Figure 6.28. Amplitude of the electric field $\overline{E}(y)$ produced in a vacuum and sampled at a point $p_0 = p\,(0, y_j, z_k)$ normalised by the value of the electric-field amplitude calculated at $p_{if} = p\,(0, y_{if}, z_k)$; being $z_k > 0$ and $y_j > y_{if} = 1.5\lambda$

.

[9] we need to rememember that we need to guarantee to be in radiating near-field region not only for the LWA but for all antennas used to compare against the LWA itself.

As seen previously, the microstrip LWA is designed to radiate in a medium characterized by $\sigma_2 = 0.05\ S/m$, $\mu = \mu_0$ and $\varepsilon = \varepsilon_0$ and for which the angle ζ_2, as represented in Fig. 5.1, assumes a $\pi/2$ radians value: it is therefore expected, in the plane-wave approximation, that the inhomogeneous wave amplitude value remains constant propagating into the medium, while, from Eq. (5.27) and Figs. 5.5-5.7, it follows that, maintaining constant permettivity ε_0 and permeability μ_0, the inhomogeneous wave is expected to attenuate ($\zeta_2 < \pi/2$) if the medium conductivity is $\sigma_2'' > 0.05\ S/m$ and to amplify ($\zeta_2 > \pi/2$) if the medium conductivity is $\sigma_2'' < 0.05\ S/m$; the expected behaviour was confirmed also for non-plane waves through the numerical simulation, the amplitude of the normalised E-field monitor as a function of the quota y is shown for $z_k = 125\ mm = 5\lambda$ in Fig. 6.29:

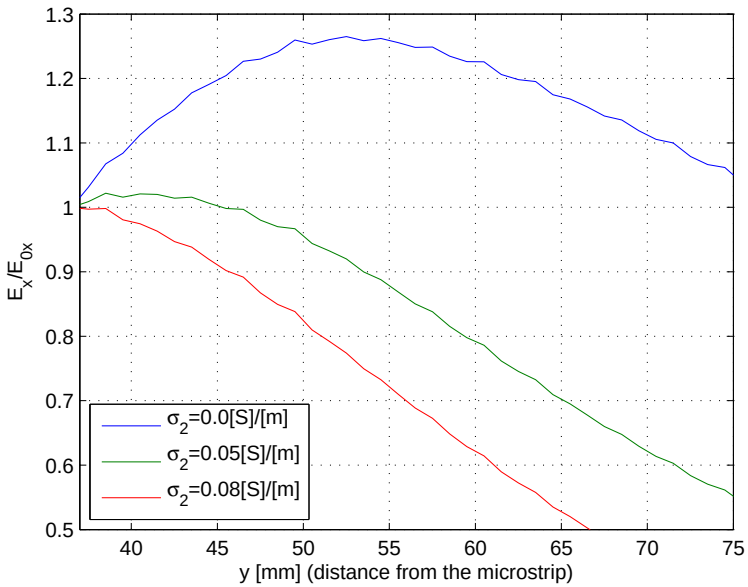

Figure 6.29. Amplitude of the electric field $\overline{E}$ for $z = 5\lambda$ in three different media, having conductivity $\sigma = 0.08\ S/m$ (red curve), $\sigma = 0.05\ S/m$ (green curve) and $\sigma = 0\ S/m$ (blue curve). Permittivity and permeability are $\varepsilon = \varepsilon_0$ and $\mu = \mu_0$ for all three media.The LWA was designed such that the attenuation vector would have been parallel to the separation surface for $\sigma = 0.05\ S/m$, $\mu = \mu_0$, and $\varepsilon = \varepsilon_0$.

The representation of the electric field illustrated in Figs. 6.28-6.29 gives a

good intuitive description of the electric field produced by the LWA, anyway, such a description permits only to compare such a LWA against a LWA having similar radiation pattern, and specifically same radiation angle, but it is not suitable for a comparison between antennas having different radiation characteristics because, for the uniform LWA considered, the electric-field amplitude at y_{if} decreases when the distance from the source on the longitudinal direction increases, as shown in Fig. 6.30 (green curve), this causes a divergence of the quantity $\overline{E}(y)_{|z_k}$ that may tend to infinite when z_k increase beyond the antenna termination, it is in fact, in this case, $y_{if} \to 0$, therefore even a small residual field for $y > y_{if}$ causes $\overline{E}(y)_{|z_k} \to \infty$.

To obtain a fair comparison between this LWA and a generic antenna creating a beam orthogonal to the antenna aperture, one could expect to simply rotate either the lossy medium or the antenna in one of the two simulations, so that the two simulations would share to same incidence angle with the respective lossy medium. This choice is not suitable unfortunately, mainly because a medium non-parallel to the antenna aperture, considering the very short distance between antenna and lossy medium, could lead to problems in determining the field: either a portion of the lossy medium could enter in the near-field-reactive region, or, in the worst case scenario, antenna and medium could collide.

A better comparison can be achieved avoiding rotations and considering, for instance, the field at the interface with the lossy medium opportunely averaged as follows:

$$\overline{\overline{E}}(y)_{|z_k} = \frac{|\underline{E}(0, y, z_k)|}{\sum_{j=0}^{j=k} |\underline{E}(0, y_{if}, z_j)| / (k+1)} \tag{6.28}$$

where evidently, at denominator, all the samples on the z axis preceding the $k^{th} + 1$ sample z_k are taken into account because they are assumed to contribute to the electric-field amplitude $E(0, y, z_k) = |\underline{E}(0, y, z_k)|$ for $y > y_{if}$. The curve describing the mediated electric-field amplitude at the interface between lossy medium and vacuum (which is the denominator of Eq. (6.28))

is displayed in blue in 6.30. It has to be noted that the average considered at denominator of Eq. (6.28) is just an approximation: the samples taken on the interface should not strictly depend only on z_k but on y, too; the condition considered is therefore approximated.

The approach taken through Eq. (6.28), whose numerical simulation results are shown Fig. 6.31 , resolves the problem of having a normalised electric field diverging to infinity.

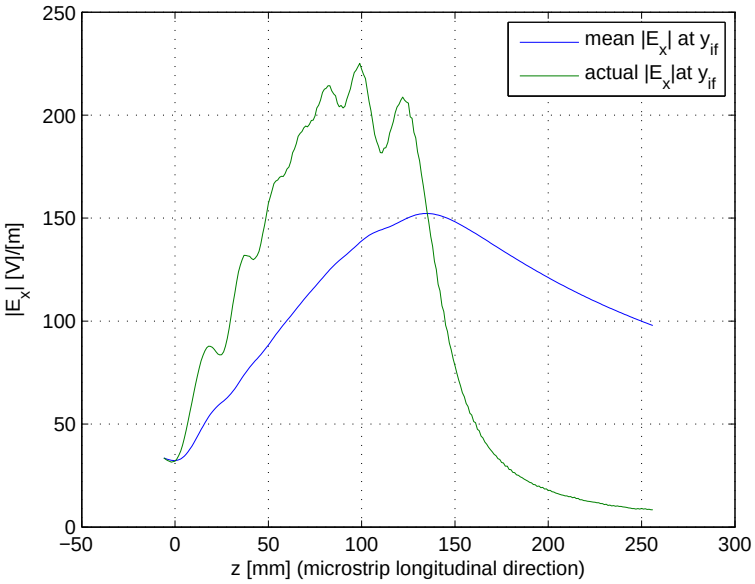

Figure 6.30. Amplitude of the electric field at the separation interface posed at the distance 1.5λ from the antenna aperture, the actual field value (E_x) is shown in green, while the averaged value is shown in blue

.

Fig.(6.31) shows $\overline{\overline{E}}(y)_{|z_k}$ curves for some z_k values compared against the penetration factor δ (Eq. (2.24)) represented by the blue-horizontal line in the figure. The LWA shows a penetration similar to the one obtained by the pyramidal-horn antenna (blue curve) for $z \approx 80\ mm$, while for higher z_k values, the penetration results higher. When $z = 220\ mm$ the penetration reaches a value of $y \approx 5.5\lambda$ ($y \approx 142.5$ mm from the interface with the lossy medium and $y \approx 180mm$ from the antenna aperture), anyway the maximum field value

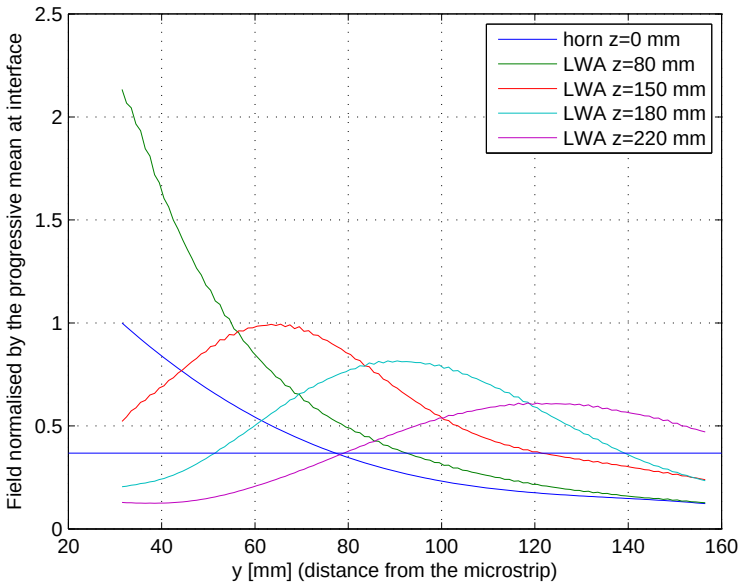

Figure 6.31. Comparison between pyramidal-horn antenna penetration and LWA penetration according to Eq. (6.28), the horizontal line represents the value $1/e$.

.

for $z = 220$ mm is just above $1/e$ for every value of y_k, therefore this result is probably difficult to reproduce in real-case testing scenarios, and it would be safer to assume the value obtained for $z = 180$ mm (light-blue curve in the figure) which gives a penetration of $y \approx 4\lambda$.

Note that the value of the field normalised by the the average at the interface may well assume values greater than 1, this is due to the improper nature of the leakeage, for which, for instance, after the first samples on the z longitudinal direction, the average of the electric-field amplitude at the interface is less then the amplitude of the field at around the interface itself: this is clear comparing Fig. 6.30 with Fig. 6.31 for $z \leq 80\ mm$).

Another good choice, for comparing the penetration caused in the chosen lossy medium by the electric field produced by means of both pyramidal horn and microstrip LWA antennas, is to normalise the amplitude of the electric field at any point inside the medium by the maximum amplitude of the electric field at the interface between lossy and lossless medium as it was done for the

pyramidal-horn antenna in Fig. 6.13, i.e. in dB from the maximum value at the interface (see also Par. 6.2 for the lossy medium chosen):

The electric field at any point inside the lossy medium is evaluated according to Eq. (6.16), as it was done for the pyramidal-horn antenna, obtaining the results available in Fig. 6.32.

Again, the electric field was evaluated using the E field-monitor option of CST and then the data was ported to Matlab to obtain both a three-dimensional and a two-dimensional views of the average value electric-field penetration.

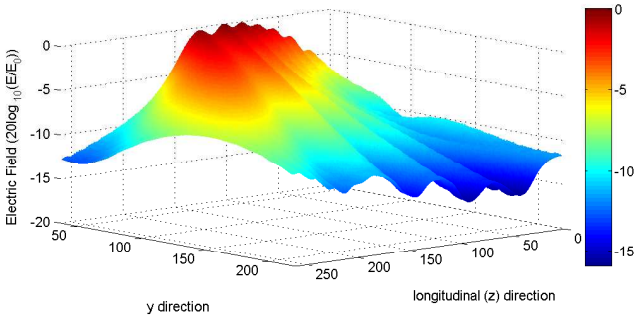

(a) 3D view of the electric field distribution inside the lossy medium

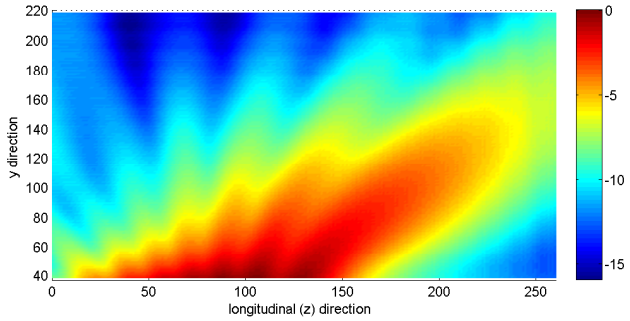

(b) 2D view of the electric field distribution inside the lossy medium

Figure 6.32. Electric field in the lossy medium produced by the LWA *Menzel* antenna, computed in dB from the highest amplitude of the field at the interface, note that the origin of axis is posed at the antenna aperture, the interface with the lossy medium is at $y = 37.5\ mm$.

The comparison between Fig. 6.32 and 6.14) shows that the LWA penetra-

tion is sensibly higher than the one reached by means of the pyramidal-horn antenna, this is especially verified for high values of z_k. In particular, the penetration reached by the LWA is even higher than the one reached with the ideal homogeneous plane wave. The value of penetration reached applying this method is analogous to the one computed by means of Eq. (6.28), for instance, when $z = 220\ mm$ then $\delta \approx 142.5$ mm.

The penetration evaluated in the way described above give us certainly a comforting result, and this is probably the most opportune way to evaluate the penetration in many applications, in which the maximum power at the interface is given as a requirement.

Anyway, a comparison between the average fields inside the lossy medium chosen is also important; this kind of "measurement" give us a broader indication on the penetration of the two structures as a global effect. It is easy to compute an electric-field average for the pyramidal-horn antenna, because it is certainly sufficient to compute the average of all samples on a direction parallel to the antenna aperture ($z \in [0; 140]\ mm$) for every y_j on the y direction, with $y_j > y_{if}$, i.e.:

$$\overline{E}(y_j) = \frac{\sum_{k=0}^{k=N-1} |\underline{E}(0, y_j, z_k)|}{N};\ \forall y_j > y_{if}$$

having considered N samples $\{z_0, z_1, .., z_{N-1}\}$ on the z axis parallel to the antenna aperture. Unfortunately for the LWA this average is not so immediate, because the field is propagating at an angle of 45 *degrees*. Therefore an algorithm had to be developed, independent from the specific radiating angle. Let us describe the produced algorithm: at first, it was verified the field at the termination of the LWA aperture, obtaining:

$$\frac{|\underline{E}(0, 0, L)|}{|\underline{E}(0, 0, 0)|} = 0.24$$

such a value, obtained through the simulation, was in good agreement with the design expectations (power at the termination was expected to be, i.e.: $P_L/P_0 = (0.24)^2 \Rightarrow P_L/P_0 = P(0, 0, L)/P(0, 0, 0) \approx 0.06$.

At this point N_{LWA} samples with a sampling rate of 1 mm were chosen between $(0, 0, 0)$ and $(0, 0, 125)$. For the pyramidal-horn antenna, N_{HORN} samples, at a sampling rate of 1 mm, where chosen on the z axis on the aperture in a symmetrical position from the center of the pyramidal-horn antenna aperture (posed at $z = 0$). Those samples were chosen such that the minimal electric field was, again, inside the 24% of the maximum electric field obtained at $z = 0$, i.e. $(E_{MAX}^{HORN} = |\underline{E}_{HORN}(0, 0, 0)|)$. The described approach permitted to homogenize the amplitude of the energy radiated along the aperture by those, different, antennas, permitting a direct comparison, that could not be achieved otherwise.

For every y_i, being $y_i > y_{if}$, the electric-field amplitude was then mediated taking N samples z direction, where $N = N_{LWA}$ for the microstrip-LWA antenna and $N = N_{HORN}$ for the pyramidal-horn antenna.

For every $y_i \geq y_{if}$, the algorithm employed searches the maximum amplitude of the electric field on the z direction, i.e. the algorithm looks for a value z_M such that:

$$E_{yi}(0, y_i, z_M) > E_{yi}(0, y_i, z_i) \; \forall z_i \in [0; N] - z_M$$

After z_M is found, then samples around z_M with the largest amplitude of the electric field are selected such that they result consecutive, i.e. every sample is distant exactly 1 mm from the surrounding ones; this step of the algorithm terminates when all the N requested samples are found.

The process is repeated for every $y_{i+1} = y_i + 1$ mm in the simulation domain. The computed averaged value is then normalized for the sum calculated at the first step, i.e. at the separation surface y_{if} :

$$\overline{E}(y_i) = \frac{\sum_{k=n^{(i)}}^{k=N+n^{(i)}} |\underline{E}(0, y_i, z_k)|}{\sum_{j=m}^{j=m+N} |\underline{E}(0, y_{if}, z_j)|} \; \forall y_i \geq y_{if} \tag{6.29}$$

This time, differently from the case indicated by Eq. (6.28), a single curve is found rather than a family of curves.

The implemented algorithm, clearly, does not assume any field symmetry around the maximum value of the amplitude of the electric field resulting in a more accurate estimation than the one that could be achieved just assuming the field moving with an angle of $\pi/4$ with the normal of the separation surface for the LWA and normally to the separation surface for the horn antenna. In particular, the samples on the z axis are not in general aligned for $y_i \neq y_j$, i.e., $z_{n^{(i)}} \neq z_{n^{(j)}}$, this observation is always true for the LWA unless the radiation at broadside is considered (we know that this can only be obtained through dual-feeding).

The described algorithm was implemented using Matlab, the samples chosen by the Matlab routine for both microstrip-LWA and pyramidal-horn antennas are shown in Fig. 6.33.

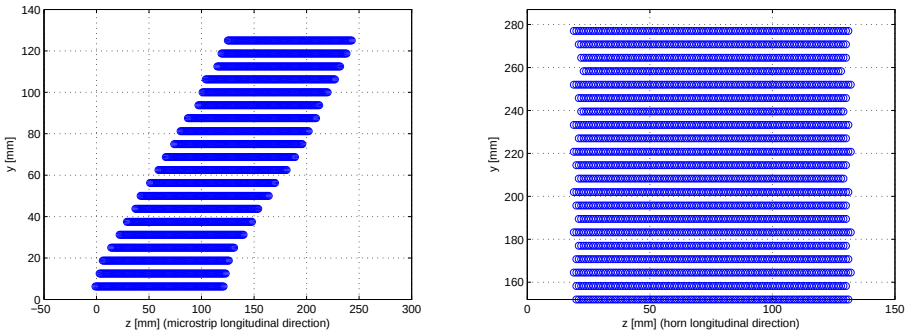

(a) Chosen samples for the LWA microstrip antenna

(b) Chosen samples for the pyramidal horn antenna

Figure 6.33. Samples chosen for horn and LWA Microstrip in order to compute the average penetration for both antenna structures, samples were chosen according to the radiation diagram in a vacuum.

The normalised field calculated by the Matlab routine are shown instead in Fig. 6.34.

This, last, comparison gives a very clear indication in terms of electric-field penetration for both antennas from a more global point of view, even though it hides the improper behavior of the wave generated by the LWA, that get lost averaging the amplitude of the field on different samples.

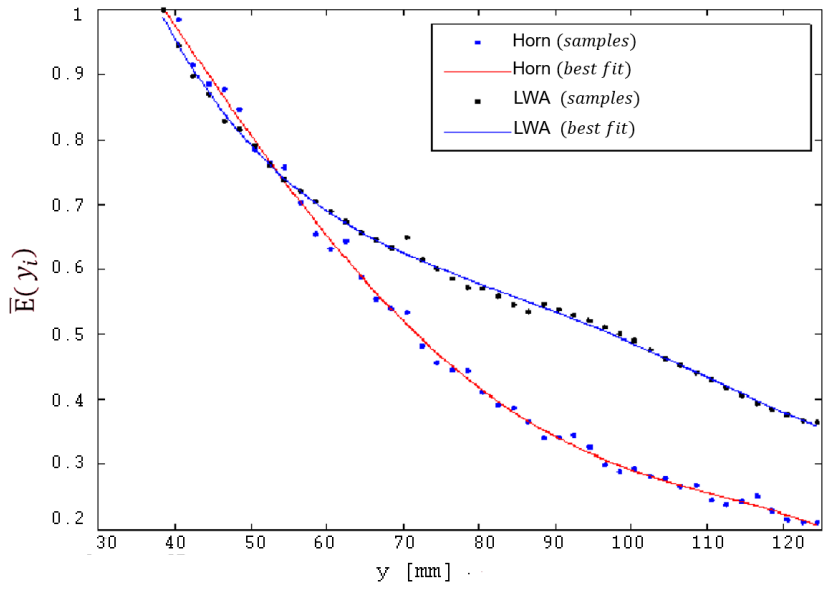

Figure 6.34. Comparison between horn and LWA penetration averaged according to Eq. (6.29) in a lossy medium for which $\sigma = 0.05\ S/m$, $\mu_r = 1$ and $\varepsilon_r = 1$.

Again, coherently with the results obtained by the previous diagrams shown, Fig. 6.34 illustrated that the penetration obtained by means of the horn antenna is higher than the one obtained by means of the LWA radiation for low z values, which also correspond to low y values as it can be verified in Fig. 6.33; then, for greater z values, the leaky-wave improper behavior starts appearing, reducing the slope of the attenuation curve for the LWA, that finally results constantly above the one described by the horn radiation.

6.4 Conclusions

A LWA was designed and simulated to investigate the possibility of obtaining a deep-penetration behaviour in a realistic scenario. It has been demonstrated that, also in this case, in which the power radiated by the antenna is limited, it is possible to achieve a growing field inside the lossy medium in a limited space region. The obtained results proved the applicability of the theory explained in the first part of this dissertation.

It needs to be highlighted, however, how the high amplitude α_z required may constitute an obstacle to the project of LWA antennas that may allow deep penetration in media of practical interest, in facts, we limited the study to a lossy medium characterised by a conductivity $\sigma = 0.05\ S/m$. Increasing such a conductivity value inevitably leads to a reduction of the antenna longitudinal direction and, consequently, to an earlier decay of the leaky wave produced, causing a further reduction of the penetration: we must note that the antenna design proposed is already critical from this point of view. To demonstrate the importance of the antenna length for deep-penetration purposes, a comparison between two microstrip-LWA layouts, designed to reach the $\zeta_2 = 90^o$ condition for different σ values, was exposed in [127]: it was verified through full-wave simulation on CST that an antenna having longer dimension would maintain the deep-penetration condition for an higher number of wavelengths, but at the same time would permit the $\zeta_2 = 90^o$ condition on a medium having lower amplitude of the conductivity σ. The layout of the two antennas and their results in term of penetration are reported in Figs. 6.35 and 6.36, both antennas were designed to radiate a 45^o beam at 12 GHz, and in particular the first one (Fig. 6.35) was designed to radiate on a medium such that $\sigma = 0.015\ S/m$ resulting in a longitudinal length of 10λ and the second one (Fig. 6.35) was the antenna, analysed up to now, designed to radiate on a medium such that $\sigma = 0.05\ S/m$ resulting in a longitudinal length of 5λ.

In all studies approached in this chapter, in order to neglect reflections, the lossy medium was accurately chosen such that its permittivity ε_2 resulted equal to the vacuum permittivity ε_0: future studies will need to take into account the effects introduced from a lossy medium charectiresd by a permittivity $\varepsilon_2 \neq \varepsilon_0$.

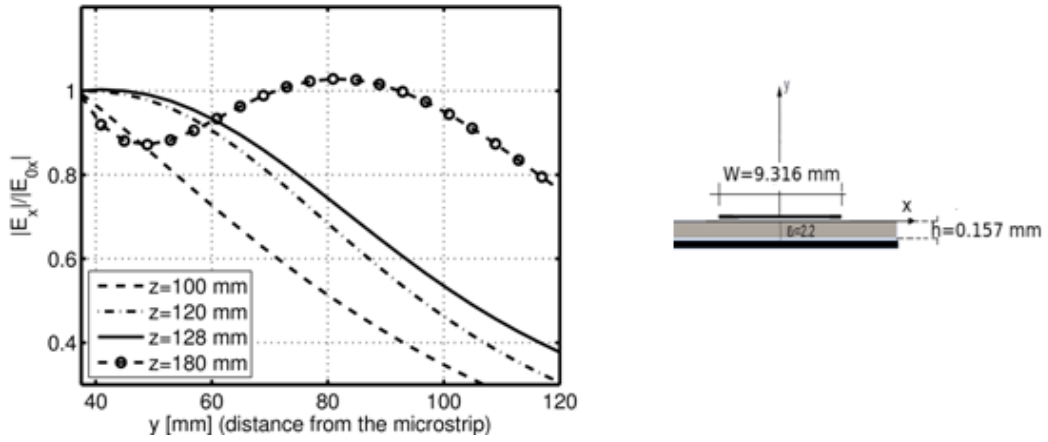

Figure 6.35. Layout of the microstrip LWA designed to penetrate with critical condition ($< \zeta_2 = 90^0 | \xi_{1c} >$) on a medium such that $\sigma = 0.015$ S/m, $\mu_r = 1$ and $\varepsilon_r = 1$. The penetration on such a medium is shown for an antenna length of 10λ

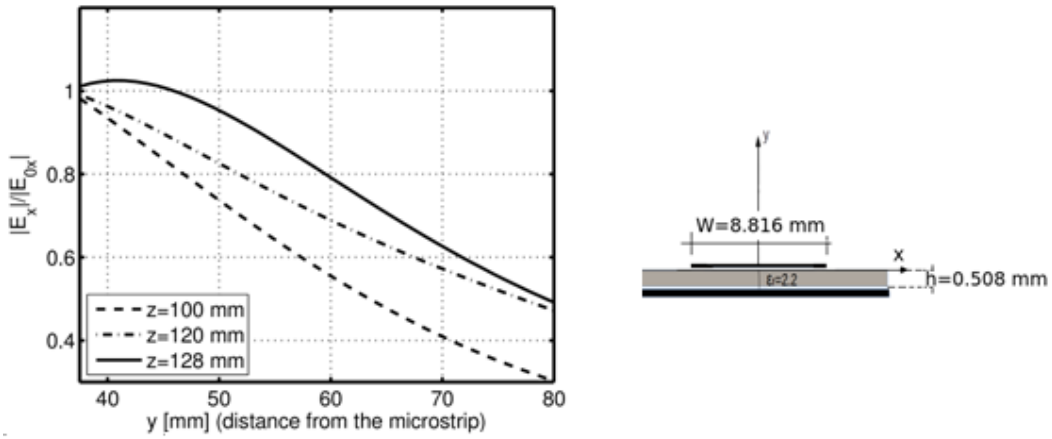

Figure 6.36. Layout of the microstrip LWA designed to penetrate with critical condition ($< \zeta_2 = 90^0 | \xi_{1c} >$) on a medium such that $\sigma = 0.05$ S/m, $\mu_r = 1$ and $\varepsilon_r = 1$. The penetration on such a medium is shown for an antenna length of 5λ.

Chapter 7

Ongoing Research: the Lossy Prism

7.1 Abstract

In the previous chapters we introduced the deep-penetration properties of inhomogeneous waves at the interface between a lossless and a lossy medium. It was shown that such waves can be generated by means of leaky-wave antenna structures, anyway it was also demonstrated that conventional LWAs might not provide a phase vector whose amplitude is large enough to guarantee deep-penetration in lossy media having a conductivity value interesting for practical application, and, even when they penetrate with a proper incidence of the attenuation vector, the field may decay too early. Here, a solution to the limits imposed by conventional LWAs is proposed through a complete different approach based on the use of a lossy prism that can be designed to create an inhomogeneous wave by exploiting the property for which the tangential components of the electromagnetic field need to conserve. The approach taken here is purely theoretical, and it does not take into account all the design variables, but it aims to be a first input to an innovative LWA design.

7.2 Working principles of the lossy prism

Historically, at best of our knowledge, leaky waves artificially generated were exclusively produced by means of leaky-wave antennas, but recent papers tried to exploit the inhomogeneous-wave generation that can be obtained by irradiating a two-dimensional lossy dielectric structure with a homogeneous wave. Such a two-dimensional structure was first named in [128] lossy prism, and presents two non-parallel, planar and infinite interfaces; a possible geometry for the lossy prism is shown in Fig. 7.1 where a section of the lossy prism on $z = K$ plane is shown, being $K \in \mathbb{R}$ a generic constant; in other words the structure is invariant to all the planes taken orthogonal to the z longitudinal axis.

The lossy prism is a structure simply based on the conservation of the tangential component. Let us assume a stratified medium as illustrated in Fig. 7.2, in which medium 1 and medium 3 are lossless and medium 2 is a lossy region. Let us take then a homogeneous wave incoming from medium 1 and impinging on the lossy medium with an incident angle ξ_1, this wave, characterised by a phase vector $\underline{\beta}_1 = \underline{k}$ produces a transmitted wave in the medium 2 that must have attenuation vector $\underline{\alpha}_2$ (see Eqs. (4.4)-(4.9)) forming an angle $\zeta_2' = 0$ with the normal to the separation interface, because there is no tangential component of the attenuation vector $\underline{\alpha}_1$ of the incident wave that can be conserved. The wave travelling inside the lossy prism is characterised by a phase vector $\underline{\beta}_2$ that forms an angle ξ_2' with the normal to the separation surface whose amplitude depends on both the media involved and the incident angle ξ_1 (Snell law).

Let us now imagine that such an inhomogeneous wave, travelling inside the lossy medium 2, reaches the other side of the lossy medium impinging to the separation surface with medium 3. Let us call with ξ_2'' and ζ_2'' the angles that the phase vector $\underline{\beta}_2$ and the attenuation vector $\underline{\alpha}_2$ respectively form with the normal to the separation surface with medium 3: this time, assuming that such a separation interface is not parallel to the opposite one, it must be $\xi_2'' \neq \xi_2'$

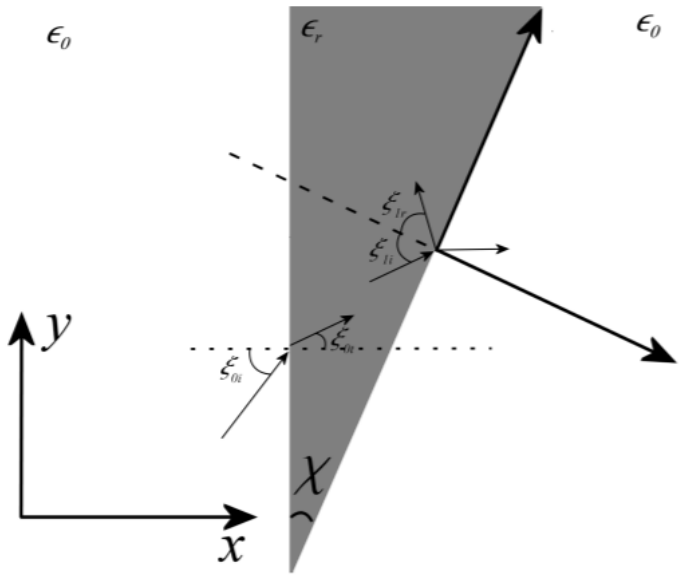

Figure 7.1. Planar section of the lossy prism considered: a possible geometry.

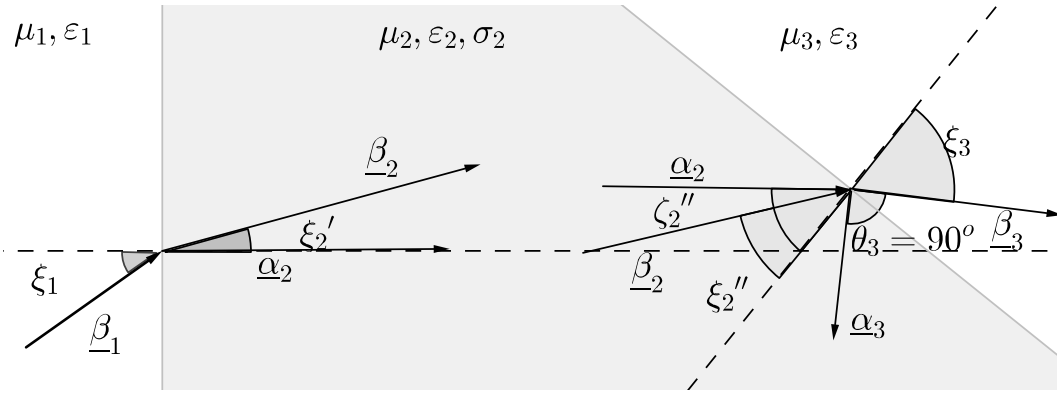

Figure 7.2. Propagation in a stratified medium, in which the first and the third medium are lossless and the inner medium is lossy, the two interfaces are not parallel, but they are planar and infinite.

and $\zeta_2'' \neq 0$. In particular, the condition the $\zeta_2'' \neq 0$ is caused by the existence of a tangential component for the incident attenuation vector at the interface that needs to be conserved; as a result, the transmitted wave in the lossless medium 3 must be, this time, inhomogeneous. Said θ the angle formed by $\underline{\beta}_3$ and $\underline{\alpha}_3$, it must be $\theta_3 = \pi/2$ radians, i.e. having indicated with ξ_3 and ζ_3 the angles that phase and attenuation vectors form with the normal to the separation surface needs to be: $\xi_3 \pm \pi/2 = \zeta_3$.

For the considered applications, the lossy prism is imagined immersed in a lossless homogeneous and isotropic medium, therefore medium 3 and medium 1 coincide into a medium having real permittivity ε_1 and null-conductivity value: such a medium may be assumed as a vacuum to fit most of the simulation environments.

A first consideration that needs to be exposed when comparing the lossy prism to conventional leaky-wave antennas is that in the former losses are present in the material, while in the latter losses are mainly due to radiation (LWAs do not require a lossy medium), and only a small quantity of energy ($< 10\%$) is actually dissipated, usually by a load posed at the end of the antenna; hence, the inhomogeneous-wave radiation by a lossy prism comes at the price of loss of energy, i.e. the total efficiency e_0 of the antenna, and in particular the dielectric efficiency e_d, is reduced [18].

Anyway, often, the power limit is not dictated by the amount of power that can be provided to the antenna, but by the power that can be radiated by the antenna, either for regulations or for the sensitivity of the surfaces exposed to radiation. In all those cases, the dissipation in the lossy medium is not a major concern, as it can be recovered providing more power to the antenna structure.

Despite to its relative simplicity, the lossy prism presents some difficult implementations challenges, first of which the interaction between the electromagnetic field and the prism wedge: it is important to find a configuration that prevents this interaction. A second challenge is represented by the handling of multiple reflections that may arise at the two boundaries of the considered

prism. Finally the effects of a finite prism must be taken into account, while here the prism was considered infinite.

7.2.1 A first proposed geometry

Let us look at Fig. 7.2 The angle $\xi_2'' = \xi_2' + \chi$ and $\zeta_2'' = \chi$, where χ is the prism wedge drawn in Fig. 7.1 and omitted in Fig. 7.2. The values for β_2 and α_2 can be found through the equation illustrated in Chs. 4-5, similar approach can be applied to the second interface obtaining:

$$\beta_3 = \frac{1}{\sqrt{2}}\sqrt{|\mathbb{I}m(k_{2\|}'')|^2 + \mathbb{R}e(k_3^2) + |k_{2\|}''^2 - k_3^2|} \tag{7.1}$$

and:

$$\alpha_3 = \frac{1}{\sqrt{2}}\sqrt{|\mathbb{I}m(k_{2\|}'')|^2 - \mathbb{R}e(k_3^2) + |k_{2\|}''^2 - k_3^2|} \tag{7.2}$$

Where $\mathbb{I}m(k_{2\|}'')$ represents the component of the imaginary part of the wave vector in medium 2 parallel to the interface between media 2 and 3.

For the direction of the phase and attenuation vectors the followings are valid:

$$\zeta_3 = \arcsin\left(\frac{\alpha_2}{\alpha_3}\sin\zeta_2''\right) \ , \tag{7.3}$$

and:

$$\xi_3 = \arcsin\left(\frac{\beta_2}{\beta_3}\sin\xi_2''\right) \tag{7.4}$$

From Eqs. (7.1)-(7.4) it follows that both the β_3 amplitude and the ξ_3 angle can be controlled by opportunely manipulating the parameters typical of the prism which allow us several degree of freedom, being:

$$\begin{cases} \beta_3 = f(\chi, \xi_1, \varepsilon_2', \tan\delta) \\ \xi_3 = g(\chi, \xi_1, \varepsilon_2', \tan\delta) \end{cases} , \tag{7.5}$$

where the notation $\varepsilon = \varepsilon' - j\varepsilon''$ was used for the permittivity and where δ represents, as usual, the loss tangent[1]

Let us assume $\chi < 90^o$ and let us consider a narrow-beam in the optical approximation impinging with a generic angle ξ_1 on the vertical edge of the prism (on the left-hand side of Fig. 7.1). Such a lossy-prism geometry requires the handling of the first reflection from the second interface that is always present and it may return to the illuminated edge, and, consequently, can reach again the interface which separates media 2 and 3, causing multiple reflections. Let us consider the direct wave inside the lossy prism: its incidence angle on the separation surface between media 2 and 3 is given by $\xi_2'' = \chi \pm \xi_2'$ where the sign '+' for χ is chosen if β_2 forms an angle η greater than 90^o with the vertical edge and '-' is chosen instead if such an angle is smaller or equal than 90^o having assigned the positive direction as the one directed toward the prism wedge. Let us investigate the condition $\eta < 90^o$, in this case is $\xi_2'' = \chi + \xi_2'$.

The angle formed by the reflected ray with the normal to the separation surface between media 2 and 3 must necessarily have the same amplitude of the direct one. This means that the reflected wave would hit the illuminated edge if $\pi/2 - \chi - \xi_2' > \chi$, i.e. $\xi_2' < \pi/2 - 2\chi$. In the particular case of normal incidence ($\xi_1 = 0$), such a reflected wave necessarily hits the illuminated interface for $\chi < \pi/4$.

A similar demonstration can be carried for the upward direction, in this case the reflected wave comes back to the illuminated edge if the amplitude of the angle of incidence is $\xi_2' > \pi/2 - 2\chi$: also in this circumstance, for normal incidence ($\xi_1 = \xi_2' = 0$), it must be $\chi > \pi/4$, as one would expect.

So, for any incidence angle there are always values of $\chi < 90^o$ such that reflections hit again the illuminated interface; those unwanted reflection can be avoided increasing the conductivity value σ_2 of the lossy medium considered,

[1]The logical steps for those conclusions were not reported here, and they descend from a combination of Snell law, geometrical construction and dispersion relation. A full demonstration, analogous to the one requested to obtain the results shown here, will be reported later in this chapter for a different geometry.

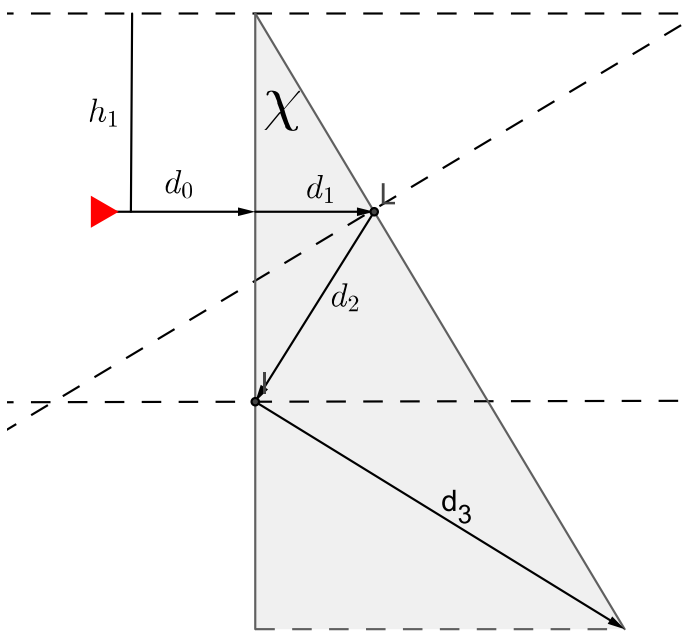

Figure 7.3. Lossy prism: paths followed by direct ad reflected waves when $\chi < 90^o$ is the prism wedge.

anyway this solution is not suitable for some applications such as radar, because if the reflection from the edge of the prism cannot come back to the antenna, a wave reflected beyond the end of the prism will very unlikely reach the antenna as well. Another way to reduce the effects of reflection is to increase the angle χ, in particular, if χ is large enough reflection do not go back to the illuminated interface, while if it is not, it may come back to the illuminated interface but it could go beyond the illuminating antenna aperture, that would be also acceptable in realistic scenarios.

In view of a numerical simulation, the case of normal incidence on the separation surface between media 1 and 2 can be considered, as in Fig. 7.3

In such a configuration, given an incident beam treated in the optical approximation and assumed behaving like a plane wave, it is easy to determine the path followed by said reflections through simple geometrical considerations.

In the case of normal incidence, the transmitted wave is always normal to the separation surface [11], therefore is $\xi_1 = \xi_2' = 0$. Hence, calling with d_1

the path followed by the direct-transmitted wave from the first to the second interface, and with d_2 the path followed by the first reflection, it is:

$$d_1 = h_1 \tan\chi \tag{7.6}$$

$$d_2 = \frac{d_1}{\cos 2\chi} \tag{7.7}$$

where h_1 indicates the distance between the wedge of the prism and the center of the incident beam.

When $\chi \geq \pi/4$, d_2 never returns back to the illuminated edge, but, when $\chi < \pi/4$, also the second reflection, indicated by the d_3 path in in Fig. 7.3 exists, and it returns back to the oblique interface if $\chi < \pi/6$: in this case, its length can be computed analyzing the triangle formed by d_2 and d_3:

$$d_3 = d_2 \frac{\cos\chi}{\cos 3\chi} = \frac{[h_1 + d_1 \tan(2\chi)]\sin\chi}{\cos 3\chi} \tag{7.8}$$

In Fig. 7.4 the normalised quantities d_1/h_1, d_2/h_1, and d_3/h_1 are shown for $\chi \in]0, \pi/8[$.

An early numerical verification of the shown geometry for the lossy prism was first presented in [129]. In such a paper a finite beam was considered and the prism was studied through a full-wave FIT simulation performed through the commercial CST software suite. A tapered pyramidal horn antenna radiating at 10.6 GHz was first designed. The far-field radiation was then exported and used to illuminate normally the vertical edge of the prism directed along the y axis in Fig. 7.1.

The FR4 material, having permittivity $\epsilon_r = 4.3$ and loss tangent $\tan\delta = 0.025$ (see Eq. (2.7)), was chosen as medium for the prism, and the angle χ was designed to be 5^o.

It is first of all interesting to note the distortion introduced by the lossy prism to the radiation pattern of the horn antenna, such a diagram is illustrated in Fig. 7.5. There are three effects introduced by the prism, the first is an attenuation of the front lobe, the second is a strong back lobe due to the

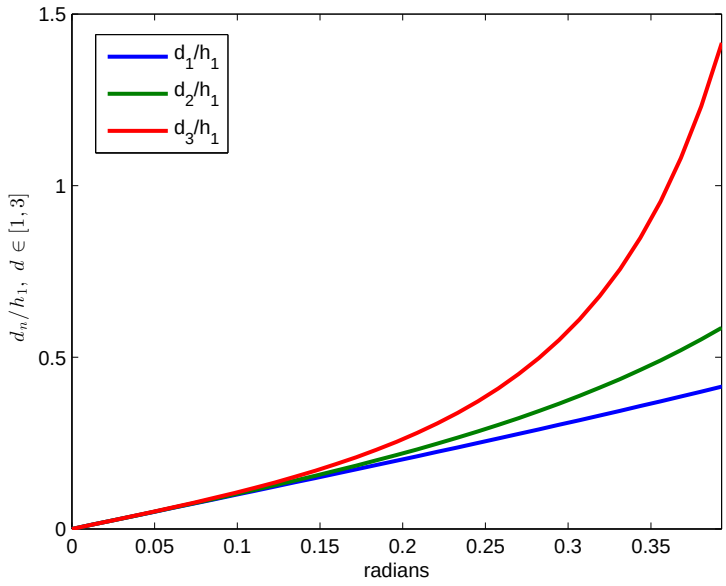

Figure 7.4. Lossy prism: normalised direct wave path (d_1/h_1), normalised first-reflection path (d_2/h_1), and normalised second-reflection path (d_3/h_1) for $\chi \in [0,\ \pi/8]$.

reflections caused by the prism boundaries, and the third is a field rotation, that is expected and due to the angle $\chi \neq 0$.

A better view of the effects of the reflections on the field produced on both the prism edges is obtained by using the E-field monitor option present on CST. The E-field on the vertical side of the prism is shown in Fig. 7.6, and the electric field on the oblique side of the prism is shown in Fig. 7.7. In both figures two field peaks are visible, a top one, due to the reflection, and a bottom one, due to the direct wave. The simulation confirms the predicted behavior, according to which reflected paths up to d_3, at least, had to be expected, and in particular $d_1/h_1 \approx 0.0875$, $d_2/h_1 \approx 0.0888$, and $d_3/h_1 \approx 0.0916$.

This preliminary attempt of designing a lossy prism highlighted the possibility of generating a leaky wave through a structure alternative to the conventional leaky-wave antennas, anyway disturbing multiple-reflection effects were discovered. For this reason our focus moved on a different geometry of the lossy prism, described in the following paragraph of this dissertation, in which we mostly focus on the amplitude of attenuation and phase vectors that can

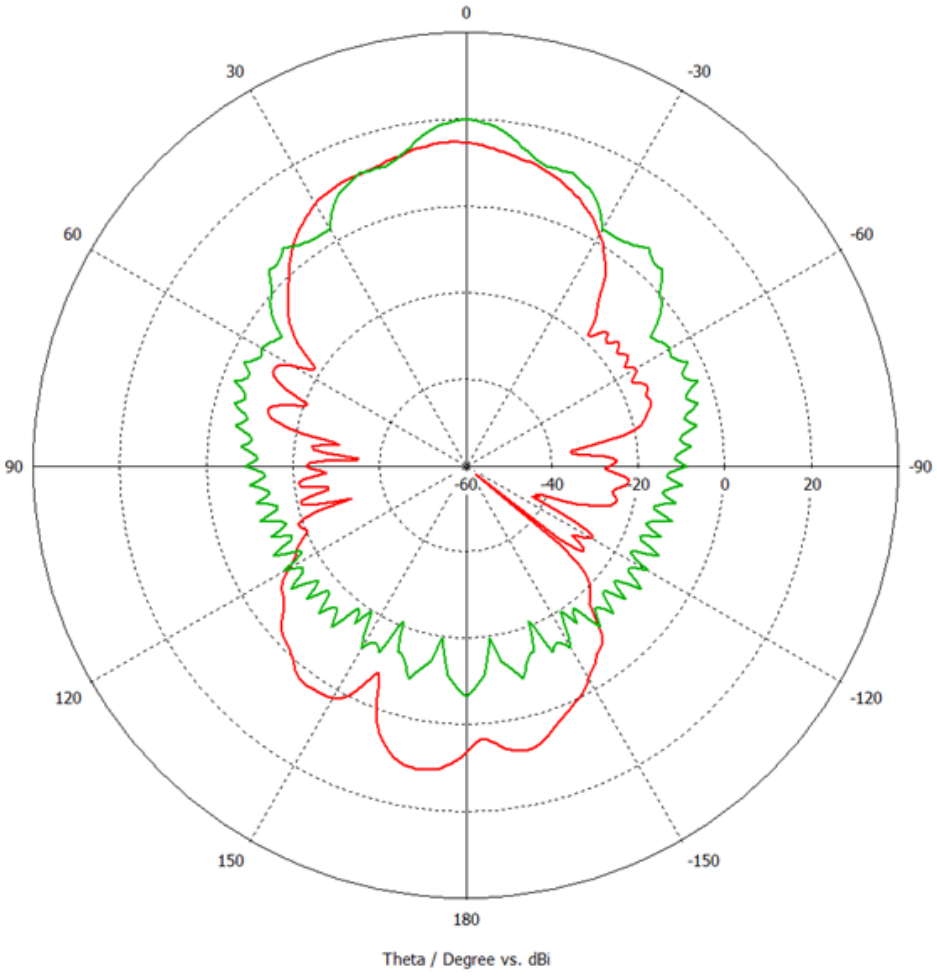

Figure 7.5. Far-field radiation pattern produced by a horn antenna illuminating the prism (green) and the radiation pattern produced by the lossy prism (red): a strong back lobe is visible in the case of the prism.

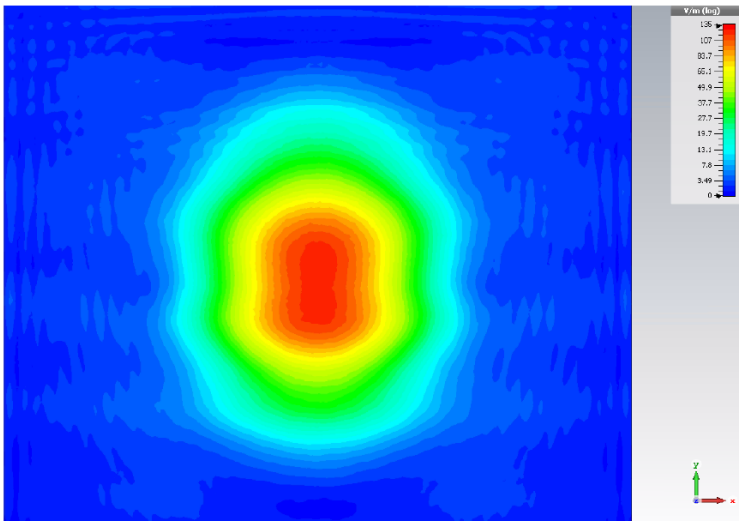

Figure 7.6. CST Simulation: electric field at the lossy prism (FR-4 medium) vertical interface illuminated normally by a far-field radiation produced by means of a pyramidal-horn antenna at 10.6 GHz. The top peak is due to reflections in the lossy prism.

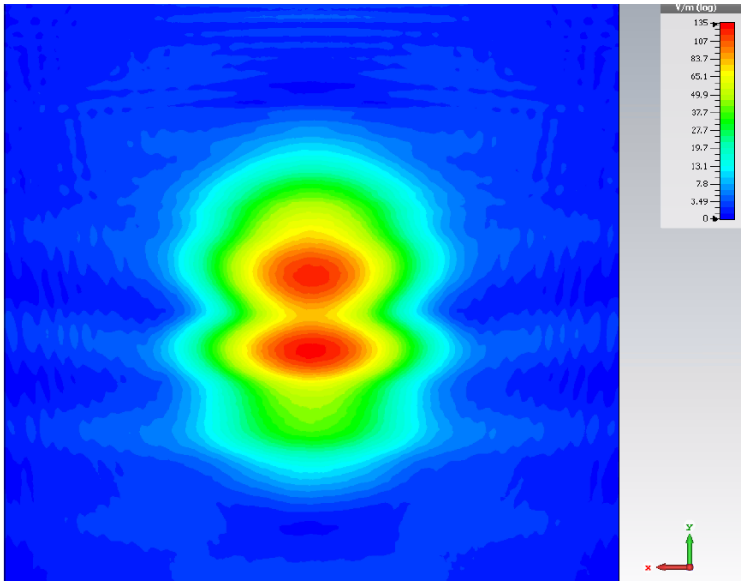

Figure 7.7. CST Simulation: electric field at the lossy prism (FR-4 medium) oblique interface when the vertical interface is illuminated normally by a far-field radiation produced by means of a pyramidal-horn antenna at 10.6 GHz. The top peak is due to reflections in the lossy prism.

be achieved by means of such a structure, in comparison with the amplitudes of those vectors obtained by the conventional leaky-wave antennas.

In the first part of the next paragraph the evaluation of the amplitude of phase and attenuation vectors shown in Fig. 7.2 will be studied considering exclusively the direct wave, while effects due to reflections will be analysed at the end of the chapter, where, in particular, it will be shown that, in the proposed configuration, reflections can be neglected, moreover, effects of the prism wedge will be neglected, mostly because near-field applications are targeted and, in this case, in practical scenarios, it is usually sufficient that the lossy prism is chosen larger than the illuminating antenna aperture to allow an infinite-length prism approximation.

7.3 Analisys of a different lossy-prism setup.

When the two faces of the lossy prism are parallel, then the incident wave in medium 1 and the transmitted wave in medium 3 are both homogeneous, because the attenuation vector $\underline{\alpha}_2$ is purely normal to both separation surfaces: in this case the amplitude of the attenuation vector $\underline{\alpha}_2$ produced by means of the lossy medium is completely lost. On the opposite, if the two faces form an angle of 90^o, then $\underline{\alpha}_2$, being normal to the first face, needs to be parallel to the second face: therefore its amplitude is fully conserved. This is the case in which we fully exploit the $\underline{\alpha}_2$ vector generated in medium 2, and therefore this is the case which results, according to our analysis, the most interesting for deep-penetration studies. The lossy prism, according to what discussed, needs to be modelled as reported in Fig. 7.8.

In Fig. 7.8, the wedge is drawn for clarity, but in an eventual near-field simulation carried to verify the effect, the radiating aperture should not see the wedge, so that wedge effects can be avoided.

Let us simply apply the generalised Snell law:

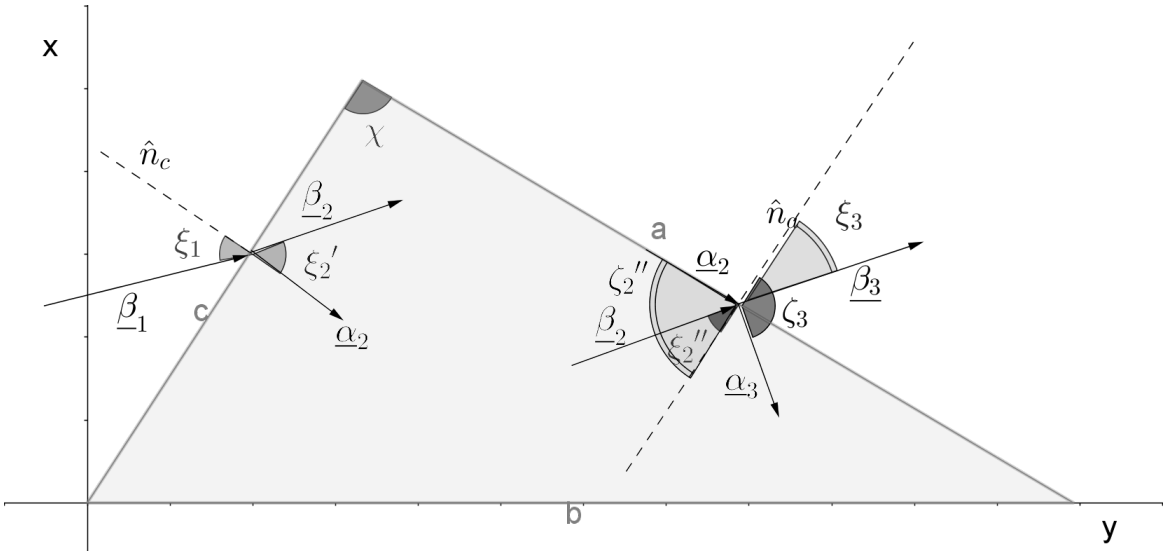

Figure 7.8. Propagation in a prism in which $\chi = 90^o$: the wedge is shown here only to give evidence of the structure, anyway it is considered far from the source in the real scenario, the c and a sides are assumed infinite (reasonably larger than the antenna aperture).

$$\begin{cases} \beta_1 \sin\xi_1 = \beta_2 \sin\xi_2' \\ \beta_2 \sin\xi_2'' = \beta_3 \sin\xi_3 \\ \alpha_2 \sin\zeta_2'' = \alpha_3 \sin\zeta_3 \end{cases} \tag{7.9}$$

From the conservation of the tangential component, and from $\chi = 90^o$, it follows:

$$\begin{cases} \zeta_2' = 0 \\ \zeta_2'' = \pi/2 \\ \xi_2'' = \pi/2 - \xi_2' \\ \zeta_3 + \xi_3 = \pi/2 \end{cases} \tag{7.10}$$

Substituting the values of Eqs. (7.10) in Eqs. (7.9), it is:

$$\begin{cases} \beta_1 \sin\xi_1 = \beta_2 \sin\xi_2' \\ \beta_2 \cos\xi_2' = \beta_3 \sin\xi_3 \\ \alpha_2 = \alpha_3 \cos\xi_3 \end{cases} \tag{7.11}$$

Applying the dispersion relation to the media of interest [11]:

$$\begin{cases} \beta_1^2 = k_0^2 = \omega^2 \epsilon_0 \mu_0 \\ \beta_3^2 - \alpha_3^2 = \omega^2 \epsilon_0 \mu_0 \\ \beta_2^2 - \alpha_2^2 = \omega^2 \mu_2 \epsilon_2 \\ \beta_2 \alpha_2 \cos\xi_2' = \omega \mu \sigma_2 / 2 \end{cases} \tag{7.12}$$

Now, we can put the second and the third of Eqs. (7.11) in the fourth of (7.12), obtaining:

$$\beta_3 \alpha_3 \sin 2\xi_3 = \omega \mu_2 \sigma_2 \ , \tag{7.13}$$

this gives us the following requirement in terms of the angle ξ_3:

$$\xi_3 = \frac{1}{2} \arcsin\left(\frac{\omega \mu_2 \sigma_2}{\alpha_3 \beta_3}\right) \tag{7.14}$$

and, imposing the second of Eqs. (7.12) in Eq. (7.13), the values of β_3 and α_3 can be found as a function of ξ_3 and the conductivity of the medium 2. For β_3 it is:

$$\frac{\beta_3}{k_0} = \frac{1}{\sqrt{2}} \sqrt{1 + \sqrt{1 + \left[\frac{2\sigma_2}{\omega \epsilon_0 \sin(2\xi_3)}\right]^2}} \tag{7.15}$$

having assumed $\mu_2 = \mu_0$ (non-magnetic medium). These equations are the complementary of the equations (12)-(13) presented in [6]: in that paper the incidence from homogeneous to inhomogeneous media was presented, here the opposite.

The value for α_3/k_0 simply follows from the second of Eqs. (7.12):

$$\frac{\alpha_3}{k_0} = \frac{1}{\sqrt{2}}\sqrt{1+\sqrt{\left[\frac{2\sigma_2}{\omega\epsilon_0\sin(2\xi_3)}\right]^2}-1} \tag{7.16}$$

The inhomogeneous wave generated in the 3^{rd} region of the stratified medium has stronger β_3 and α_3 values for higher σ_2 values: therefore, in principle, if there is enough power provided to the lossy prism, it is sufficient to increase the σ_2 value to obtain the wished β_3 amplitude.

In particular, we can compare the results obtained through this lossy prism configuration against the antenna presented in the previous paragraph. The minimal value of β is the one for which $\sin 2\xi_3 = 1$, i.e. $\xi_3 = \pi/4$. In this condition, putting $\sigma_2 = 0.008$ $[S]/[m]$ at a frequency of 12 GHz we obtain $\beta_{3n} = \beta_3/k_0 \geq 1.0028174$: larger values can be obtained either increasing the angle ξ_3 (by means of suitably impinging with the angle ξ_1), or increasing the σ value.

This small amplitude of σ already provides a larger phase vector amplitude than the one obtained with the microstrip leaky-wave antenna optimised for deep-penetration seen in the previous chapter.

Finally, the angle ξ_1 can be analytically determined as a function only of the quantities in the region 3. Squaring the first and the second of Eqs. (7.11) and summing them together yields:

$$\beta_1^2 \sin^2\xi_1 + \beta_3^2 \sin^2\xi_3 = \beta_2^2$$

but $\beta_1^2 = k_0^2$ and $\beta_2^2 = \omega^2\mu_2\epsilon_2 + \alpha_3^2\cos^2\xi_3$, so, in the case in which 3 is non-magnetic:

$$\xi_1 = \arcsin\left[\sqrt{\epsilon_{r2} + \beta_{3n}^2\cos(2\xi_3) - \cos^2\xi_3}\right], \tag{7.17}$$

having introduced the normalised quantity β_{3n} defined as $\beta_{3n} = \beta_3/k_3 = \beta_3/k_0$.

For the illustrated scenario, where $\xi_3 = \pi/4$ is wished, it is:

$$\xi_1 = \arcsin\left(\sqrt{\epsilon_{r2} - 1/2}\right) \tag{7.18}$$

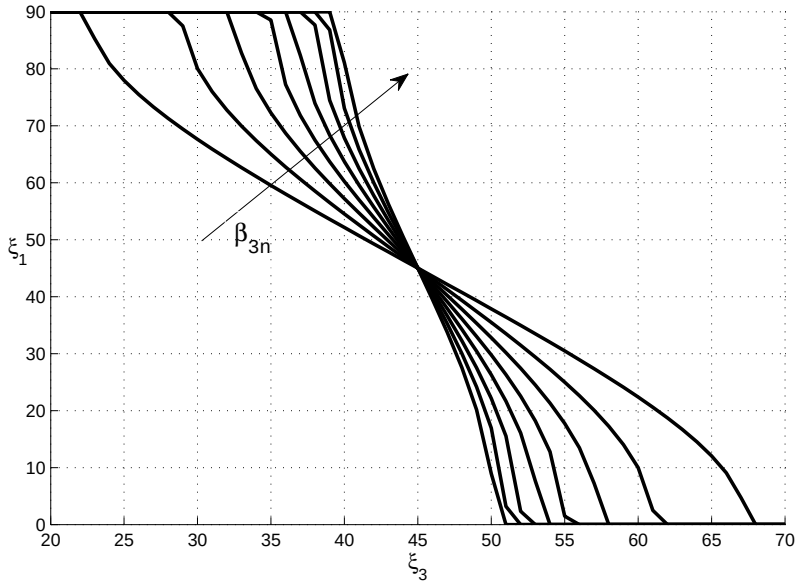

Figure 7.9. Curves described by ξ_3 when ξ_1 varies from 0^o to 90^o and $\beta_{3n} \in [1.1; 1.8]$, being $\epsilon_{r2} = 1$.

the above condition makes sense for every ϵ_{r2} such that $\epsilon_{r2} > 1/2$. In particular, if $\epsilon_{r2} = 1$, the incident angle is $\xi_1 = \pi/4$ as it should be expected due to the continuity of the dielectric constant in this scenario.

In Fig. 7.9 it is illustrated how the radiation angle is dependent on the normalised amplitude of the attenuation vector $\beta_{3n} \in [1.1, 1.8]$ when $\epsilon_{r2} = 1$: the angle ξ_3 becomes more and more independent of ξ_1 and the curve as a function of ξ_1 tends to its average value (which is 45^o for $\epsilon_r = 1$) when β_{3n} increases.

The condition $3/2 \geq \epsilon_{r2} \geq 1/2$ can be certainly satisfied choosing properly the material: we can conclude therefore that $\xi_3 = 45^o$ does not represent an issue, and can be always found. This condition represents, according to [6], the incident angle that guarantees maximum penetration in a lossy medium, therefore we can pose a lossy medium parallel to the separation surface between medium 2 and 3 and expect maximum penetration condition, reproducing the configuration that we proposed through the microstrip leaky-wave antenna introduced in [126] and presented in the previous chapter; this setup represents,

in fact, the easiest scenario for experimenting the deep penetration through numerical simulations.

As said, for some applications, the condition $\xi_3 = 0$ may be wished, then imposing such a condition into Eq. (7.15), the following is obtained:

$$\begin{aligned} \xi_1 &= \arcsin\left(\sqrt{\epsilon_{r2} + \beta_{3n}^2 - 1}\right) \\ &= \arcsin\left(\sqrt{\epsilon_{r2} + \alpha_{3n}^2}\right) \end{aligned} \tag{7.19}$$

From Eq. (7.19), we can see that the ξ_1 angle is real only for materials such that $\varepsilon_{r2} \leq 1 - \alpha_{3n}^2$, and achievable only with metamaterials ($0 < \varepsilon_{r2} \leq 1$): the larger is the α_{3n} value, the smaller needs to be the ε_{r2} value; anyway, the former equation is valid only as a limit and $\xi_3 = 0^o$ does not strictly represent a valid solution for Eqs. (7.15)-(7.17) because such condition would come from a multiplication by 0 in Eqs. (7.11) and (7.13). $\xi_3 = 0$ can be studied, instead, imposing $\alpha_3 = \alpha_2$ (for the conservation of the tangential component): from the second of Eqs. (7.11), it follows $\xi_2'' = 0$, and therefore, $\xi_2' = \pi/2$, which is possible when ξ_1 is the critical angle for total reflection: therefore such a wave does not penetrate the prism.

In Fig. 7.10, different curves are shown for $\varepsilon_2 \in [0.2,\ 2]$ and $\beta_{3n} = 1.2$: for $\varepsilon < 1$, ξ_3 tends to 0 while for $\varepsilon > 1$, ξ_3 tends to 90^o, in particular we can see that the smaller is ε_{r2}, the closer ξ_3 is to broadside radiation, as stated by Eq. (7.19).

Let us finally study the effects of the reflections produced at the interface between medium 2 and medium 3: the incident angle at such interface is $\xi_2'' = \pi/2 - \xi_2'$; consequently, because of the Snell law, the reflected angle is equal, again, to $\pi/2 - \xi_2'$. It follows that the angle formed by the incident and reflected waves is $\theta = \pi - 2\xi_2'$. The reflected wave hits again the interface between media 1 and 2 only when $\theta + \xi_2' < \pi/2$, therefore $\pi - \xi_2' < \pi/2$, i.e. $\xi_2' > \pi/2$. It is possible therefore to confirm that with this configuration the reflected wave does not return back to the illuminated interface; moreover, in the assumption of infinite edges, the reflected wave never hits the edge b of Fig.

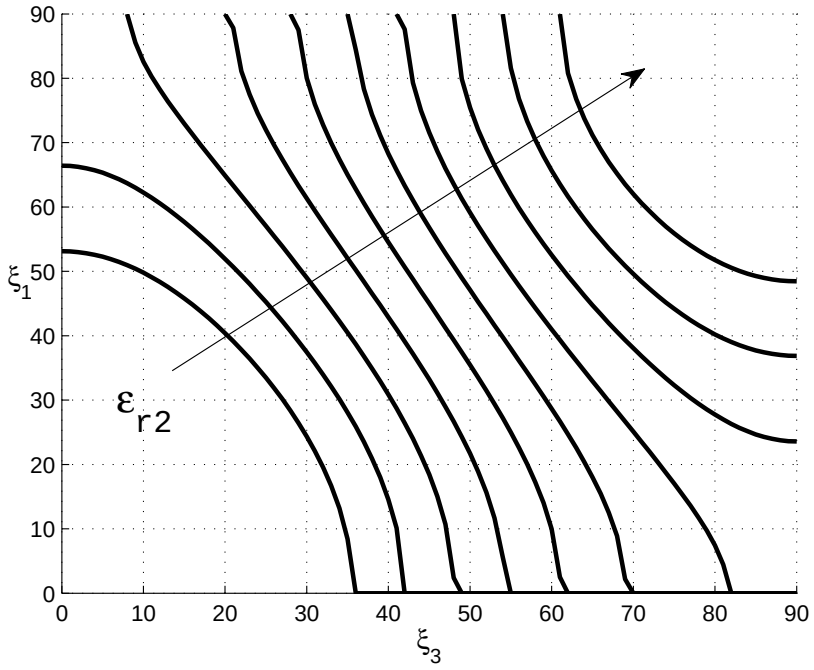

Figure 7.10. Curves described by ξ_3 when ξ_1 varies from 0^o to 90^o and $\varepsilon_{r2} \in [0.2,\ 2]$, being $\beta_{r2} = 1.2$.

7.8, so the edge a of Fig. 7.8 experiences only the presence of the direct wave. In normal scenarios, the edges a and c will need to be chosen long enough to avoid that the reflection occurring on b would reach the edge a again.

7.4 Conclusions

An innovative approach, based on the use of a prism lossy medium for increasing the penetration of electromagnetic waves in lossy media, was presented. This approach promises to guarantee deeper penetration than the one obtained through a LWA. In particular α and β values can be controlled not only acting on the angle, but also on the prism conductivity: this promises to obtain good penetration conditions even for values close to the normal incidence (note, anyway, that the attenuation vector in the lossy medium to be penetrated hardly will be parallel to the separation surface in this case).

In this preliminary study, a finite wave behaving as a plane wave was

assumed as excitation, while a realistic feeding or guiding structure should be considered. In [129] the lossy prism was illuminated through a far-field radiation, while a near-field structure, more representative of practical scenarios, will be modelled in the next studies.

The lossy medium, as presented here, produces also losses whose effects may conflict with the deep-penetration property of the generated wave, but in many scenarios the limit is imposed by the maximum power at the separation surface between the two media: in all those circumstances the power lost inside the antenna is not a fundamental issue; a greater issue, in practical design, would be the dissipation of the lost energy.

Chapter 8

General Conclusions

8.1 Abstract

In this brief chapter all the results obtained and previously presented in this dissertation are summarised, showing both the promising breakthrough and limits of the actual approach; moreover the ongoing studies and future tasks that are going to be performed to increase the applicability of this deep-penetration technique will be announced.

8.2 Results and Future Research

This dissertation presented new developments around the argument of deep penetration of electromagnetic fields in lossy media.

At first, a pure analytical study was elaborated, finding requirements and constraints to the deep penetration achievable by means of inhomogeneous-plane waves incoming from a lossless medium and impinging on an infinite and planar separation interface with a lossy medium, where both media were assumed homogeneous and isotropic.

After the study of such theoretical conditions, the dissertation moved to the feasibility of deep penetration through more realistic waveforms generated by suitable structures, known as leaky-wave antennas. Full wave simulations were performed to demonstrate that a realistic leaky-wave antenna structure

can be exploited to practically achieve deep penetration in lossy media, but not an infinite penetration, because in this case, in which the source is finite, the Sommerfeld condition must be verified. All diagrams and comparisons presented demonstrated that the deep penetration is achievable by means of a LWAs.

Analysing the results obtained, we also determined the limits of the proposed approach: all LWAs guarantee deep penetration only when the amplitude α of the attenuation vector $\underline{\alpha}$ is "large enough": this requirement, for the mono-dimensional LWA, translates into a requirement on the antenna electric length, which needs to be shorter than a critical value; for instance, the length of the Menzel antenna proposed to achieve deep penetration in a medium having $\sigma = 0.05\ S/m$ was found to be approximately 5λ; the resulting improper wave was sustained for a distance of 5λ from the antenna at a maximum radiation angle of $\pi/4\ radians$. The low number of wavelengths for which the improper behaviour was valid, resulted in a limit on the position of the interface with the lossy medium that, in fact, could not be too far from the antenna aperture (this was the primary constraint for which the interface with the lossy medium was posed at a distance 1.5 λ from the antenna aperture). A shorter Menzel antenna would have allowed deep penetration on a medium having higher conductivity value, but the leaky wave generated by such an antenna would have decayed earlier reducing, on the opposite, the penetration.

In order to allow deep-penetration on media having higher conductivity value an innovative design, consisting of a lossy prism, was finally considered. It was demonstrated that the inhomogeneous wave generated by a lossy prism could result into an higher amplitude of the attenuation vector then the one achieved by means of LWAs. Anyway, such a high amplitude of the attenuation vector comes at the cost of energy dissipation in the dielectric that constitutes the prism, this may reduce the applicability of this kind of solution. A particular prism configuration that maximises the amplitude of attenuation and phase vectors and reduces effects of reflections was also taken into account.

The future research will focus on the design of a realistic antenna structure based on the lossy-prism concept here demonstrated. At the same time, the deep penetration through more conventional LWAs will continue to be explored.

List of Figures

Bibliography

[1] S. Curto, P. McEvoy, X. Bao, and M. J. Ammann, "Compact patch antenna for electromagnetic interaction with human tissue at 434 mhz," *IEEE Transactions on Antennas and Propagation*, vol. 57, pp. 2564–2571, September 2009.

[2] M. Skolnik, *Radar Handbook, Third Edition.* McGraw-Hill Education, 2008.

[3] D. G. Smith and H. M. Jol, "Ground penetrating radar: antenna frequencies and maximum probable depths of penetration in quaternary sediments," *Journal of Applied Geophysics*, vol. 33, no. 1, pp. 93–100, 1995.

[4] A. Annan and J. Davis, "Radar range analysis for geological materials," *Geological Survey of Canada*, vol. 77, pp. 117–124, 1977.

[5] O. F. Howlader and T. P. Sattar, "Miniaturization of dipole antenna for low frequency ground penetrating radar," *Progress In Electromagnetics Research C*, vol. 61, pp. 161–170, 2016.

[6] F. Frezza and N. Tedeschi, "Deeply penetrating waves in lossy media," *Optics letters*, vol. 37, no. 13, pp. 2616–8, 2012.

[7] D. R. Jackson and A. A. Oliner, "Leaky-wave antennas," in *Modern Antenna Handbook* (C. Balanis, ed.), pp. 325–367, New York: Wiley, 2008.

[8] A. A. Oliner and D. R. Jackson., *John Volakis,Antenna Engineering Handbook*. McGraw Hill Professional, 4th ed., 2015.

[9] R. F. Harrington, *Time-Harmonic Electromagnetic Fields*. Wiley-IEEE Press, 2001.

[10] J. . Balmain, *Electromagnetic Waves & Radiating Systems*. Pearson India, 2015.

[11] F. Frezza, *A Primer on Electromagnetic Fields*. Springer, 2015.

[12] K. Yee, "Numerical solution of initial boundary value problems involving maxwell's equations in isotropic media," *IEEE Transactions on Antennas and Propagation*, vol. 14, pp. 302–307, May 1966.

[13] A. Taflove, "Application of the finite-difference time-domain method to sinusoidal steady-state electromagnetic-penetration problems," *IEEE Transactions on Electromagnetic Compatibility*, vol. EMC-22, pp. 191–202, August 1980.

[14] M. Hazewinkel, *Encyclopaedia of Mathematics (set)*. Springer, 1994.

[15] R. B. Adler, L. J. Chu, and R. M. Fano, *Electromagnetic Energy Transmission and Radiation*. MIT Press, November 1968.

[16] S. V. Yuferev and N. Ida, *Surface Impedance Boundary Conditions: A Comprehensive Approach*. CRC Press, September 2009.

[17] D. G. Swanson and W. J. R. Hoefer, *Microwave Circuit Modeling Using Electromagnetic Field Simulation*. Artech House Publishers, June 2003.

[18] C. A. Balanis, *Antenna Theory: Analysis and Design*. Wiley, iv ed., 2016.

[19] G. Gerosa and P. Lampariello, *Lezioni di Campi elettromagnetici)*. Ed. Ingegneria 2000, Rome, 2^{nd} ed., 2006.

[20] W. Keenan and P. Schumann, "Pseudo-brewster angle determination of carrier concentration," *Journal of The Electrochemical Society*, vol. 118, no. 12, pp. 2010–2014, 1971.

[21] F. Frezza and N. Tedeschi, "Electromagnetic inhomogeneous waves at planar boundaries: tutorial," *J. Opt. Soc. Am. A*, vol. 32, pp. 1485–1501, August 2015.

[22] E. Becker, "L. m. brekhovskikh, waves in layered media (applied mathematics and mechanics, vol. 6). translated from the russian. new york/london 1960. academic press.," *ZAMM - Journal of Applied Mathematics and Mechanics Zeitschrift für Angewandte Mathematik und Mechanik*, vol. 42, no. 3, pp. 129–129, 1962.

[23] G. Goubau, "Surface waves and their application to transmission lines," *J. Appl. Phys.*, vol. 21, no. 11, p. 1119, 1950.

[24] J. Zenneck, "Über die fortpflanzung ebener elektromagnetischer wellen längs einer ebenen leiterfläche und ihre beziehung zur drahtlosen telegraphie," *Annalen der Physik*, vol. 328, no. 10, pp. 846–866, 1907.

[25] A. Sommerfeld, "Über die ausbreitung der wellen in der drahtlosen telegraphie," *Annalen der Physik*, vol. 333, no. 4, pp. 665–736, 1909.

[26] W. Hansen, "Radiating electromagnetic wave guide," June 1946. US Patent 2,402,622.

[27] N. Marcuvitz, "On field representations in terms of leaky modes or eigenmodes," *IRE Trans. Antennas Propag.*, vol. 4, pp. 192–194, July 1956.

[28] L. Goldstone and A. Oliner, "Leaky-wave antennas i: Rectangular waveguides," *IRE Trans. Antennas Propag.*, vol. 7, pp. 307–319, October 1959.

[29] L. Goldstone and A. Oliner, "Leaky wave antennas II: Circular waveguides," *IRE Trans. Antennas Propag.*, vol. 9, pp. 280–290, May 1961.

[30] E. Becker, "L. m. brekhovskikh, waves in layered media (applied mathematics and mechanics, vol. 6). translated from the russian. new york/london 1960. academic press. preis geb. $ 16.00," *ZAMM - Zeitschrift für Angewandte Mathematik und Mechanik*, vol. 42, no. 3, pp. 129–129, 1962.

[31] T. T. W. a. Ronold W. P. King, Margaret Owens, *Lateral Electromagnetic Waves: Theory and Applications to Communications, Geophysical Exploration, and Remote Sensing*. Springer-Verlag New York, 1 ed., 1992.

[32] J. M. Dunn, *Electromagnetic lateral waves in layered media*. PhD thesis, Harvard Univ., Cambridge, MA., 1984.

[33] T. Tamir, "Inhomogeneous waves types at planar structures: I. the lateral wave," *Optik*, no. 36, p. 209–232, 1972.

[34] M. Born and E. Wolf, *Principles of optics: electromagnetic theory of propagation, interference and diffraction of light*. CUP Archive, 2000.

[35] M. Belger, R. Schimming, and V. Wünsch, "A survey on huygens' principle," *Zeitschrift für Analysis und ihre Anwendungen*, vol. 16, no. 1, pp. 9–36, 1997.

[36] T. Tamir, "Leaky-wave antennas," in *Antenna Theory, Part 2* (R. E. Collin and F. J. Zucker, eds.), ch. 20, McGraw-Hill, 1969.

[37] R. King, "Lateral electromagnetic waves from a horizontal antenna for remote sensing in the ocean," *IEEE transactions on antennas and propagation*, vol. 37, no. 10, pp. 1250–1255, 1989.

[38] R. W. King, "Scattering of lateral waves by buried or submerged objects. i. the incident lateral-wave field," *Journal of applied physics*, vol. 57, no. 5, pp. 1453–1459, 1985.

[39] A. A. Boryssenko, "The lateral wave phenomena of ground penetrating radar survey," in *Geoscience and Remote Sensing Symposium, 1999. IGARSS'99 Proceedings. IEEE 1999 International*, vol. 5, pp. 2684–2686, IEEE, 1999.

[40] A. D. Boardman, *Electromagnetic surface modes*. John Wiley & Sons, 1982.

[41] L. B. Felsen, "Lateral waves," Tech. Rep. PIBMRI-1303-65, Polytechnic Institute of Brooklyn, New York, Microwave Research Institute, 1965.

[42] F. Zucker, "Theory and applications of surface waves," *Il Nuovo Cimento (1943-1954)*, vol. 9, pp. 450–473, 1952.

[43] G. Goubau, "Surface waves and their application to transmission lines," *Journal of Applied Physics*, vol. 21, no. 11, pp. 1119–1128, 1950.

[44] H. M. Barlow and J. Brown, *Radio surface waves*. Clarendon Press, 1962.

[45] C. A. Balanis, *Advanced engineering electromagnetics*. John Wiley & Sons, 2012.

[46] S. Maci, G. Minatti, M. Casaletti, and M. Bosiljevac, "Metasurfing: Addressing waves on impenetrable metasurfaces," *IEEE Antennas and Wireless Propagation Letters*, vol. 10, pp. 1499–1502, 2011.

[47] W. L. Barnes, "Surface plasmon–polariton length scales: a route to sub-wavelength optics," *Journal of optics A: pure and applied optics*, vol. 8, no. 4, p. S87, 2006.

[48] L. Li, Q. Chen, Q. Yuan, C. Liang, and K. Sawaya, "Surface-wave suppression band gap and plane-wave reflection phase band of mushroomlike photonic band gap structures," *Journal of Applied Physics*, vol. 103, no. 2, p. 023513, 2008.

[49] R. Li, G. DeJean, M. M. Tentzeris, J. Papapolymerou, and J. Laskar, "Radiation-pattern improvement of patch antennas on a large-size substrate using a compact soft-surface structure and its realization on ltcc multilayer technology," *IEEE Transactions on antennas and propagation*, vol. 53, no. 1, pp. 200–208, 2005.

[50] L. H. Weng, Y.-C. Guo, X.-W. Shi, and X.-Q. Chen, "An overview on defected ground structure," *Progress In Electromagnetics Research B*, vol. 7, pp. 173–189, 2008.

[51] P. Baccarelli, P. Burghignoli, G. Lovat, and S. Paulotto, "A novel printed leaky-wave'bull-eye'antenna with suppressed surface-wave excitation," in *Antennas and Propagation Society International Symposium, 2004. IEEE*, vol. 1, pp. 1078–1081, IEEE, 2004.

[52] M. Guglielmi and D. Jackson, "Broadside radiation from periodic leaky-wave antennas," *IEEE transactions on antennas and propagation*, vol. 41, no. 1, pp. 31–37, 1993.

[53] T. Tamir and A. A. Oliner, "Guided complex waves. Part 1: Fields at an interface," *Proceedings of the Institution of Electrical Engineers*, vol. 110, no. 2, p. 310, 1963.

[54] T. Tamir and A. Oliner, "Guided complex waves. Part 2: Relation to radiation patterns," *Proceedings of the Institution of Electrical Engineers*, vol. 110, no. 2, p. 325, 1963.

[55] T. Zhao, D. R. Jackson, J. T. Williams, H. Y. D. Yang, and A. A. Oliner, "2-d periodic leaky-wave antennas-part i: metal patch design," *IEEE Transactions on Antennas and Propagation*, vol. 53, pp. 3505–3514, November 2005.

[56] T. Zhao, D. R. Jackson, and J. T. Williams, "2-d periodic leaky-wave antennas-part ii: slot design," *IEEE Transactions on Antennas and Propagation*, vol. 53, pp. 3515–3524, November 2005.

[57] A. Sommerfeld, *Partial Differential Equations in Physics (Pure and Applied Mathematics: A Series of Monographs and Textbooks, Vol. 1)*. Academic Press, 1949.

[58] S. H. Schot, "Eighty years of sommerfeld's radiation condition," *Historia mathematica*, vol. 19, no. 4, pp. 385–401, 1992.

[59] A. Hessel, "General characteristics of traveling-wave antennas," in *Antenna Theory, Part 2* (R. E. Collin and F. J. Zucker, eds.), ch. 19, McGraw-Hill, 1969.

[60] L. B. Felsen and N. Marcuvitz, *Radiation and Scattering of Waves (IEEE Press Series on Electromagnetic Wave Theory)*. Wiley-IEEE Press, 1994.

[61] S.-T. Yang and H. Ling, "Application of a microstrip leaky wave antenna for range–azimuth tracking of humans," *IEEE Geoscience and Remote Sensing Letters*, vol. 10, no. 6, pp. 1384–1388, 2013.

[62] D. Deiana, F. Nennie, and S. Monni, "Detection of ieds with leaky wave antennas," in *Advanced Ground Penetrating Radar (IWAGPR), 2015 8th International Workshop on*, pp. 1–4, IEEE, 2015.

[63] K. Vaddagiri, S. Monni, A. Neto, F. Nennie, and W. v. Rossum, "A ultrawideband leaky slot antenna for microwave radar imaging," in *7th European Conference on Antennas and Propagation (EUCAP 2013)*, EurAAP, 2013.

[64] M. Ettorre, R. Sauleau, L. Le Coq, and F. Bodereau, "Single-folded leaky-wave antennas for automotive radars at 77 ghz," *IEEE Antennas and Wireless Propagation Letters*, vol. 9, pp. 859–862, 2010.

[65] C. Luxey and J. Laheurte, "Effect of reactive loading in microstrip leaky wave antennas," *Electronics Letters*, vol. 36, no. 15, p. 1, 2000.

[66] F. Frezza, "Lezioni di campi elettromagnetici ii," *Sapienza Università di Roma*, pp. 1–3, 2010.

[67] D. D. Grieg and H. F. Engelmann, "Microstrip — a new transmission technique for the kilomegacycle range," in *Proceedings of IRE*, vol. 40, December 1952.

[68] G. Deschamps, "Microstrip microwave antennas," in *USAF Symposium on Antennas*, vol. 40, 1953.

[69] F. Schwering, A. A. O. (auth.), Y. T. Lo, and S. W. L. (eds.), *Antenna Handbook: Volume III Applications*, vol. 3. Springer US, 1 ed., 1994.

[70] M. Ettore, *Analysis and design of efficient planar leaky-wave antennas*. Siena: Universita Degli Studi di Siena, 2008.

[71] H. Ermert, "Guided modes and radiation characteristics of covered microstrip lines," *Arch. Elektron. Uebertraegungstech.*, vol. 30, pp. 65–70, 1976.

[72] H. Ermert, "Guiding and radiation characteristics of planar waveguides," *Microwaves, Optics and Acoustics*, vol. 3, pp. 59–62, March 1979.

[73] A. Oliner and K. Lee, "Microstrip leaky wave strip antennas," in *Antennas and Propagation Society International Symposium, 1986*, vol. 24, pp. 443–446, IEEE, 1986.

[74] A. A. Oliner, "Leakage from higher modes on microstrip line with application to antennas," *Radio Science*, vol. 22, no. 6, pp. 907–912, 1987.

[75] D. C. Chang and E. F. Kuester, "Total and partial reflection from the end of a parallel-plate waveguide with an extended dielectric loading," *Radio Science*, vol. 16, January 1981.

[76] B. Riemann, *Gesammelte mathematische Werke und wissenschaftlicher Nachlass*, vol. 1. BG Teubner, 1876.

[77] M. Avriel, *Nonlinear Programming: Analysis and Methods (Dover Books on Computer Science)*. Dover Publications, 2003.

[78] J. Snyman, *Practical Mathematical Optimization: An Introduction to Basic Optimization Theory and Classical and New Gradient-Based Algorithms (Applied Optimization)*. Springer, 2005.

[79] J. S. Bagby, C.-H. Lee, D. P. Nyquist, and Y. Yuan, "Identification of propagation regimes on integrated microstrip transmission lines," *IEEE transactions on microwave theory and techniques*, vol. 41, no. 11, pp. 1887–1894, 1993.

[80] G. Franceschetti, *Campi elettromagnetici*. Boringhieri, 1988.

[81] J. Roy, "New results for the effective propagation constants of nonuniform plane waves at the planar interface of two lossy media," *Transaction on Antennas and Propagation*, vol. 51, pp. 1206–1215, 2003.

[82] J. Holmes and C. Balanis, "Refraction of a uniform plane wave incident on a plane boundary between two lossy media," *IEEE Transactions on Antennas and Propagation*, vol. 26, pp. 738–741, September 1978.

[83] R. D. Radcliff and C. A. Balanis, "Modified propagation constants for nonuniform plane wave transmission through conducting media," *IEEE Trans. Geosci. Remote Sensing*, vol. vol. GE-20, pp. 1206–1215, July 1982.

[84] P. Lorrain and D. Corson, "Electromagnetic fields and waves," 1970.

[85] F. Frezza and N. Tedeschi, "Electromagnetic inhomogeneous waves at planar boundaries," *Journal of the Optical Society of America A*, vol. 32, no. 8, pp. 1485–1501, 2015.

[86] F. Frezza and N. Tedeschi, "Total transmission of inhomogeneous electromagnetic waves at planar interfaces," *Physical Review A*, vol. 92, p. 6, 2015.

[87] V. M. Shalaev, "Optical negative-index metamaterials," *Nature photonics*, vol. 1, no. 1, pp. 41–48, 2007.

[88] P. A. Dirac, "A new notation for quantum mechanics," in *Mathematical Proceedings of the Cambridge Philosophical Society*, vol. 35, pp. 416–418, Cambridge Univ Press, 1939.

[89] O. E. Allen, D. A. Hill, and A. R. Ondrejka, "Time-domain antenna characterizations," *IEEE Transactions on Electromagnetic Compatibility*, vol. 35, pp. 339–346, August 1993.

[90] C. M. Studio, "3d em simulation software," *Computer Simulation Technology*, 2014.

[91] D. Hanselman and B. C. Littlefield, *Mastering MATLAB 5: A comprehensive tutorial and reference*. Prentice Hall PTR, 1997.

[92] S. J. Chapman, *MATLAB programming for engineers*. Nelson Education, 2015.

[93] W. Menzel, "A new travelling wave antenna in microstrip," in *8th European Microwave Conference, 1978*, no. 2, pp. 302–306, 1978.

[94] L. Klein and C. Swift, "An improved model for the dielectric constant of sea water at microwave frequencies," *IEEE Transactions on Antennas and Propagation*, vol. 25, no. 1, pp. 104–111, 1977.

[95] B. D. Thomas, T. G. Thompson, and C. L. Utterback, "The electrical conductivity of sea water," *Journal du Conseil*, vol. 9, no. 1, pp. 28–34, 1934.

[96] M. Born and E. Wolf, *Principles of Optics*. Cambridge University Press, 7 ed., 1999.

[97] D. Brewster, "On the laws which regulate the polarization of light by reflection from transparent bodies," in *D Philosophical Transactions of the Royal Society of London*, p. 105–125, 1815.

[98] T. Weiland, "A discretization method for the solution of maxwell's equations for six-component fields," in *Electronics and Communications AEUE*, vol. 31, 1977.

[99] M. C. T. Weiland, "Discrete electromagnetism with the finite integration technique," *Progress In Electromagnetics Research*, vol. 32, pp. 65–87, 2001.

[100] J.-M. Jin, *The finite element method in electromagnetics*. John Wiley & Sons, 2014.

[101] D. Soares and W. Mansur, "A time domain fem approach based on implicit green's functions for non-linear dynamic analysis," *International Journal for Numerical Methods in Engineering*, vol. 62, no. 5, pp. 664–681, 2005.

[102] J.-P. Bérenger, "Perfectly matched layer (PML) for computational electromagnetics," *Synthesis Lectures on Computational Electromagnetics*, vol. 2, pp. 1–117, January 2007.

[103] J. Carr and G. Hippisley, *Practical Antenna Handbook 5/e*. McGraw-Hill Education TAB, 2011.

[104] M. Pieraccini, D. Mecatti, M. Fratini, C. Atzeni, and M. Seracini, "A high frequency gpr application to the cultural heritage survey: the search of the "battle of anghiari" by leonardo da vinci," in *Proceedings of the Tenth International Conference on Grounds Penetrating Radar, 2004. GPR 2004.*, vol. 1, pp. 391–394, June 2004.

[105] O. Boric-Lubecke, P. W. Ong, and V. M. Lubecke, "10 ghz doppler radar sensing of respiration and heart movement," in *Proc. of the IEEE 28th Ann. Northeast Bioeng*, p. 55–56, 2002.

[106] A. S. Turk, K. A. Hocaoglu, and A. A. Vertiy, *Subsurface Sensing*. Wiley, 2011.

[107] V. Rodriguez, "A brief history of horns," *In Compliance Magazine*, November 2010.

[108] T. Weiland, M. Timm, and I. Munteanu, "A practical guide to 3-d simulation," *IEEE Microwave Magazine*, vol. 9, pp. 62–75, December 2008.

[109] A. D. Olver, P. Clarricoats, A. Kishk, and L. Shafai, *Microwave Horns and Feeds (Iee Electromagnetic Waves Series)*. The Institution of Engineering and Technology, 1994.

[110] D. Daniels, "Ground penetrating radar," 2004.

[111] J. R. James and P. S. Hall, *Handbook of Microstrip Antennas*. Peter Peregrinus Ltd. for IEE, 1989.

[112] D. M. Pozar and D. H. Schauber, *Microstrip Antennas*. IEEE Press, 1995.

[113] S. Paulotto, P. Baccarelli, F. Frezza, and D. Jackson, "A novel technique to eliminate the open stopband in 1-d periodic printed leaky-wave antennas," in *Antennas and Propagation, 2007. EuCAP 2007. The Second European Conference on*, pp. 1–5, IET, 2007.

[114] J. T. Williams, P. Baccarelli, S. Paulotto, and D. R. Jackson, "1-d combline leaky-wave antenna with the open-stopband suppressed: Design considerations and comparisons with measurements," *IEEE Transactions on Antennas and Propagation*, vol. 61, no. 9, pp. 4484–4492, 2013.

[115] M. Ettore, *Analysis and design of efficient planar leaky-wave antennas*. Siena: Universita Degli Studi di Siena, 2008.

[116] S. Leo, *Progetto di Antenne a Onda Leaky Planari Periodiche in Banda X*. PhD thesis, Ingegneria Elettronica, The address of the publisher, 2015.

[117] F. Frezza, S. Leo, F. Mangini, N. Tedeschi, and P. Simeoni, "Deep penetration in lossy media through non uniform electromagnetic waves," in *Proceedings of the Third Action General Meeting*, COST TU1208, Aracne, March 2015.

[118] I. J. Bahl and P. Bhartia, *Microstrip antennas*. Artech house, 1980.

[119] D. Mitra, D. Das, and S. R. Bhadra Chaudhuri, "Bandwidth enhancement of microstrip line and cpw-fed asymmetrical slot antennas," *Progress In Electromagnetics Research Letters*, vol. 32, pp. 69–79, 2012.

[120] T. Zhao, D. Jackson, J. Williams, and A. Oliner, "General formulas for 2-d leaky-wave antennas," *IEEE Trans. Antennas Propag.*, no. 53, p. 3525–3533, 2005.

[121] P. Baccarell, C. D. Nallo, S. Paulotto, and D. R. Jackson, "A full-wave numerical approach for modal analysis of 1-D periodic microstrip structures," *IEEE Transactions on Microwave Theory and Techniques*, vol. 54, no. 4, pp. 1350–1362, 2006.

[122] C. Frederick, Y. Wong, and F. Edge, "Two-dimensional automatic mesh generation for structural analysis," *International Journal for Numerical Methods in Engineering*, vol. 2, no. 1, pp. 133–144, 1970.

[123] S.-W. Cheng, T. K. Dey, and J. Shewchuk, *Delaunay mesh generation*. CRC Press, 2012.

[124] D.Yau, N.V.Shuley, and L.O.McMillan, "Total and partial reflection from the end of a parallel-plate waveguide with an extended dielectric loading," in *IEE Proceedings - Microwaves Antennas and Propagation*, vol. 146, November 1999.

[125] G. Zelinski, M. Hastriter, M. Havrilla, J. Radcliffe, A. Terzuoli, and G. Theile, "Fdtd analysis of a new leaky traveling wave antenna," in *IEEE/ACES International Conference on Wireless Communications and Applied Computational Electromagnetics, 2005.*, pp. 152–155, IEEE, 2005.

[126] P. Baccarelli, F. Frezza, P. Simeoni, and N. Tedeschi, "Inhomogeneous wave penetration in lossy media," in *URSI International Symposium on Electromagnetic Theory (EMTS)*, pp. 797–799, IEEE, 2016.

[127] P. Baccarelli, F. Frezza, P. Simeoni, and N. Tedeschi, "Deep penetration properties of inhomogeneous waves," in *XXI Riunione Nazionale di Elettromagnetismo*, RINEM, September 2016.

[128] N. Tedeschi and F. Frezza, "An analysis of the inhomogeneous wave interaction with plane interfaces," in *General Assembly and Scientific Symposium (URSI GASS), 2014 XXXI URSI*, pp. 109–112, IEEE, 2014.

[129] N. Tedeschi, V. Pascale, F. Pelorossi, and F. Frezza, "Generation of inhomogeneous electromagnetic waves by a lossy prism," in *URSI International Symposium on Electromagnetic Theory (EMTS)*, pp. 838–841, IEEE, 2016.